DISSERTATION

THERMOPLASTIC ELECTRODES FOR DETECTION OF BIOMARKERS

Submitted by:

Cynthia P. McCord

Department of Chemistry

In partial fulfillment of the requirements

For the Degree of Doctor of Philosophy

Colorado State University

Fort Collins, Colorado

Fall 2021

Doctoral Committee:

Advisor: Charles S. Henry

Melissa M. Reynolds
James R Neilson
David L. Bark Jr.

Copyright by Cynthia Phipps McCord 2021

All Rights Reserved

ABSTRACT

THERMOPLASTIC ELECTRODES FOR DETECTION OF BIOMARKERS

Biomarkers are indicators of biological processes, pathogenic processes, or exposures that impact an organism. Therefore, detection of biomarkers is vital to understanding and monitoring health. Yet, commonly used laboratory-based methods can be lengthy, costly, and inaccessible in resource limited settings. Electrochemical detection of biomarkers has many advantages including fast measurement times, low-cost portable instrumentation, and lack of interference from sample turbidity. For electrochemical detection, it is valuable to have high quality electrode materials with tunable surface chemistry that can be easily molded and incorporated into array or fluidic devices. This work utilizes a new class of inexpensive and easily moldable carbon composite electrode materials, called thermoplastic electrodes (TPEs). TPEs are made from thermopolymers blended with conductive carbon and have excellent electrochemical properties comparable or superior to that of traditional electrode materials. This thesis focuses on developing TPE materials and sensors for detection of protein and small molecule biomarkers. To this end, three projects are presented: 1) optimizing synthesis and grafting of diazonium tosylates to develop TPE immunosensors for the detection of c-reactive protein (CRP), 2) using polystyrene (PS) as an aromatic TPE binder and characterizing PS TPE properties related to direct detection of small molecules, and 3) utilizing PS TPE materials for simultaneous direct detection of ascorbic acid (AA), dopamine (DA), and uric acid (UA) biomarkers.

Chapter 2 focuses on optimizing the synthesis and grafting of diazonium tosylates onto TPE surfaces for the development of the first TPE immunosensors. TPE immunosensors are then

used to perform electrochemical immunoassays for CRP, a protein biomarker of cardiovascular disease. Diazonium tosylates were of interest for TPE modification as they are particularly soluble and stable diazonium salts that can graft to carbon electrodes spontaneously achieving monolayer coverage in minutes. These qualities make diazonium tosylates ideal for functionalizing composite electrodes for immunoassay applications, but they had not been used this way previously. With diazonium tosylates, TPEs were amine functionalized either directly through grafting of p-aminophenyl diazonium salt or indirectly through grafting p-nitrophenyl diazonium salt followed by electrochemical reduction to an amine. Amine functionalized TPEs were conjugated to CRP antibodies and applied for detection of CRP. Assays were performed in a sandwich enzyme-linked immunosorbent assays (ELISA) format with square wave voltammetry (SWV) detection. Clinically relevant dynamic ranges and detection limits were achieved and the TPE immunosensors retained sensitivity and selectivity in serum. TPEs used in Chapter 2 were made with 2:1 mass ratio polycaprolactone (PCL): polymethyl methacrylate (PMMA) binder, as PCL-PMMA blend TPEs had better electrode properties than PCL TPEs but were easier to fabricate than PMMA TPEs (Appendix 1). Although TPEs made with PCL and PMMA binders exhibit excellent electrode properties, all TPE binders up to this point only contained aliphatic hydrocarbons. Thus, we decided to investigate how aromatic binder functionalities would impact TPE properties, and whether aromatic binders could improve performance for biomarker detection. Chapter 3 focuses on the use of PS plastics for the development of the first TPE materials with aromatic binders for direct detection applications. PS plastics of different molecular weights expanded polystyrene (EPS) waste plastic, and PS-PCL blends were explored as binders for TPEs, and previously developed PCL TPEs were used for comparison. The conductivity, capacitance, surface morphology, and electrochemistry of different redox probes were measured for the various

TPE compositions. Capacitance and conductivity data showed that even small additions of PS to PCL electrodes substantially lowered capacitance and that PS-PCL binder blends could increase conductivity. Low capacitance is beneficial for electrochemical sensing as capacitance increases background current. Surface morphology examined with scanning electron microscopy (SEM) and optical profilometry (OP). SEM data showed PS TPEs had graphitic edge-plane rich 3D microscale surface structures. PCL and PS-PCL TPE SEM images had fewer edge-plane features and the graphite was more immersed in the polymer matrix. Optical profilometry (OP) showed lower macroscale surface roughness for all PS and PS-PCL blend TPEs than PCL TPEs which explains the lower capacitance. The electrochemistry of these materials was investigated with cyclic voltammetry (CV) using various common and biologically relevant redox probes. CV data showed all PS and waste EPS TPEs exhibit similar electrochemistry, surpass the performance of traditional electrode materials, and show similar behavior to nanomaterial-modified electrodes. PS-PCL TPEs showed similar CV behavior to PCL TPEs. The SEM data suggests that the excellent PS TPE voltammetry stems from the edge-plane rich surface morphology.

Chapter 4 focuses on the use of PS TPEs for simultaneous analysis of AA, DA, and UA, biomarkers that coexist in bodily fluids. AA, DA, and UA are redox active and can be detected directly with electrochemistry, however, their oxidation peaks are poorly resolved at most unmodified electrodes. Surface modifications are therefore often required for simultaneous analysis of these biomarkers which increases costs and complicates fabrication and surface chemistry. In this chapter PS TPEs are used for simultaneous analysis of AA, DA, and UA without the need for surface modification. PS TPEs were optimized for conductivity, capacitance, and electrochemistry using different conductive carbon fillers. CV was used to characterize TPE electrochemistry for the three analytes, and SWV was used for simultaneous analysis. PS TPEs

were also challenged for simultaneous analysis in urine. Separation between peaks, detection limits, and % recoveries in urine were comparable to that of recent literature. Additional work isneeded in the future for low level detection of DA, but with TPEs tunable properties and ease of incorporation into fluidic devices this should be achievable.

In this thesis, TPE materials and sensors were successfully developed for detection of protein and small molecule biomarkers. The first TPE immunosensors were developed for the detection of CRP using diazonium tosylate grafting as a novel functionalization method. In Chapter 3 PS was explored as a new aromatic binder for TPEs; the PS TPEs exhibited unique edge-plane rich morphology and exceptional voltammetry for biologically relevant redox molecules. The excellent electrochemistry of PS TPEs made them promising materials for simultaneous analysis, so PS TPEs were applied to direct detection of AA, UA, and DA in Chapter 4. Unmodified PS TPEs were used successfully for simultaneous direct detection of AA, DA, and UA biomarkers. This thesis expands knowledge of how composition and surface modification can impact carbon composite electrode properties and uses that knowledge for direct and immunoassay detection of biomarkers. The TPE electrode materials and sensors in this work are versatile and can also be adapted for a wide range of applications.

ACKNOWLEDGEMENTS

I would first like to thank my advisor Dr. Chuck Henry. Throughout my five years in graduate school, he has always been inspiring, supportive, and kind. His assistance and optimism throughout my most challenging PhD moments has helped me persevere and become the researcher I am today. I would also like to thank my fellow Henry Group members for their assistance and support. In particular, I would like to thank postdocs Dr. Rob Channon and Dr. Tugba Ozer. Dr. Rob Channon for all his mentorship and help with getting started in the lab, and Dr. Tugba Ozer for struggling through long hours of immunoassay experiments with me. I would like to also thank my undergraduate researcher Bali Summers for her excellent work ethic and contributions to the research in this document.

I would also like to thank all my wonderful friends and family for their support during this journey. In particular I would like to thank my parents, and my fiancé Ian Anderson. My parents for always supporting my endeavors, giving excellent advice, and always letting me know they are proud of me. My fiancé Ian making sure I take good care of myself and always cheering me up after long days of failed experiments. I would also particularly like to thank all my friends from the 2016 chemistry cohort for struggling through this journey with me and making it more fun. Lastly, I would like to thank the National Science Foundation, National Institute of Health, and Department of Defense for funding various projects during my time at CSU.

TABLE OF CONTENTS

ABSTRACT…..…….ii
ACKNOWLEDGEMENTS……..vi
CHAPTER 1. INTRODUCTION.....1
1.1 Electrochemical Detection of Biomarkers……..…….....……1
1.2 Carbon Electrode Materials……..…….....3
1.3 Thermoplastic Electrodes…….....5
1.4 Electrode Pre-treatment……...……8
1.5 Electrochemical Immunoassays……..…….....9
1.6 Direct Detection of Biomarkers……..……..…….....12
1.7 Electroanalytical Techniques……..…….....14
REFERENCES…….....17
CHAPTER 2: SYNTHESIS AND GRAFTING OF DIAZONIUM TOSYLATES FOR THERMOPLASTIC ELECTRODES.....30
2.1 Chapter Overview……..…….....…….....30
2.2 Introduction…….....31
2.3 Experimental…….....33
2.4 Results and Discussion……42
2.5 Conclusion.....,.....50
REFERENCES……..52
CHAPTER 3: REDOX BEHAVIOR AND SURFACE MORPHOLOGY OF POLYSTYRENE THERMOPLASTIC ELECTRODES.....57
3.1 Chapter Overview……..…….....…….....57
3.2 Introduction…….....58
3.3 Experimental…….....60
3.4 Results and Discussion……63
3.5 Conclusion.....,.....74
REFERENCES……..76
CHAPTER 4. SIMULTANEOUS ANALYSIS OF ASCORBIC ACID URIC ACID AND DOPAMINE AT BARE POLYSTYRENE THERMOPLASTIC ELECTRODES.....84
4.1 Chapter Overview……..…….....…….....84
4.2 Introduction…….....85
4.3 Experimental…….....87
4.4 Results and Discussion……90
4.5 Conclusion.....,.....101
REFERENCES……102
CHAPTER 5. CONCLUSIONS AND FUTURE DIRECTIONS.....109
REFERENCES……116
APPENDIX 1: CHARACTERIZATION OF PCL-PMMA TPEs…….....121
APPENDIX 2: SUPPLEMENTARY INFORMATION FOR CHAPTER 2.....124
APPENDIX 3: SUPPLEMENTARY INFORMATION FOR CHAPTER 3.....129
APPENDIX 4: SUPPLEMENTAL INFORMATION FOR CHAPTER 4….....131

CHAPTER 1: INTRODUCTION

1.1 Electrochemical Detection of Biomarkers

A biomarker is "a defined characteristic that is measured as an indicator of normal biological processes, pathogenic processes or responses to an exposure or intervention" and are often molecular species of interest such as proteins or small molecules.[1] Monitoring biomarkers is therefore essential to understanding and monitoring health. Protein and small molecule biomarkers are focused on in this dissertation. A variety of diagnostic tools exist for small molecule and protein biomarkers; however, access to diagnostic and monitoring tools can be limited or unaffordable.[2-3] For many health conditions, early diagnosis along with monitoring disease progression and therapeutic effects can greatly improve individualized treatment and health outcomes.[4-6] Thus the development of simpler, faster, and more affordable techniques for biomarker detection is a growing focus in the analytical community.[2, 6-7]

C-reactive protein (CRP), ascorbic acid (AA), uric acid (UA), and dopamine (DA) are the main biomarkers focused on in this work, although other electroactive biomarkers are touched on in Chapter 3. CRP is used herein as a model analyte for a new immunoassay platform (Chapter 2). CRP is a protein biomarker of systematic inflation related to cardiovascular disease, the leading cause of death worldwide.[8] Rising CRP levels often proceed clinical events and can be helpful to predict cardiovascular risk.[9] Simultaneous analysis of AA, DA, and UA are focused on in Chapter 4. AA is a vitamin and antioxidant that plays important roles in various biological processes such as cell metabolism and mRNA transcription.[10-11] UA is also an antioxidant and the end product of purine metabolism.[12] DA is an important neurotransmitter with a role in controlling the cardiovascular and central nervous systems.[13-14] AA, UA, and DA coexist in biological fluids and

can be biomarkers for a wide range of neurological, cardiovascular, and organ diseases.[11, 13, 15-18] For quantitative analysis of protein biomarkers, immunoassay methods which utilize antibody-antigen binding are often used for specificity, and analyte-antibody complexes are detected with optical, or mass spectrometry methods.[19] For CRP specifically, commercial optical immunoassay kits and clinical analyzers based on turbidity, fluorescence, and nephelometry measurements are used for analysis.[20] For quantitative analysis of small molecule biomarkers like AA, DA, and UA, often enzymes or analytical separation techniques such as high-performance liquid chromatography (HPLC) or electrophoresis are used for specificity.[11, 21-22] Following separations and/or specific enzyme activity, analysis is typically performed using spectrophotometry or mass spectrometry.[11, 21-22] These methods, although quantitative and accurate, typically require expensive instruments, and trained personnel. Analysis methods for protein and small molecule biomarkers that are available at the point of care tend to be qualitative visual tests with limited specificity that are primarily used for screening.[19, 23-24]

Electrochemical methods have many advantages over conventional methods for biomarker detection. Some key advantages for electrochemical detection of biomarkers include fast measurement times, lack of optical interference, and low sample and reagent volumes needed.[2, 7] A common commercial example of electrochemical detection of biomarkers are enzymatic glucose sensors for diabetics. Enzymatic glucose sensors typically work by measuring current generated from a reaction between glucose, a mediator, and an enzyme (usually glucose oxidase GOx) which is immobilized on an electrochemical sensor.[25] With recent technological developments, electrochemical sensors are becoming increasingly feasible for a variety of biomarkers, yet many challenges remain.[2, 26] The development of high-performance inexpensive electrode materials, ease of fabrication for mass production, and improving analytical figures of merit (sensitivity,

selectivity, and detection limits) remain important focuses of research in this field.[2, 7, 26] For electrochemical biomarker detection, key considerations that will be discussed in this chapter include detection motifs, electrode materials, electrode modifications, and electroanalytical techniques.

Common electrochemical detection motifs used for biomarkers include direct detection, ion selective electrodes (ISE) detection, enzymatic detection, and affinity-based detection. Direct detection is the simplest motif, when the analyte in question is redox active its electrochemical response can be measured directly. ISEs convert the activity of an ion in solution to an electrical potential using an ionophore that interacts specifically with the ion of interest.[27] For enzymatic detection, detection is achieved through enzyme activity or inhibition in the presence of the analyte which leads to a change in signal from a mediator or enzymatic product.[26] Affinity-based detection involves a capture molecule such as an antibody, aptamer, or molecularly imprinted polymer that can selectively recognize the analyte, and analyte binding results in a change in electrical/electrochemical signal.[26] Antibody-based affinity assays are referred to as electrochemical immunoassays, and the electrochemical platforms as immunosensors. ISE and enzymatic detection motifs have long had widespread commercial use, with ISEs for pH or metal ions and enzymatic electrodes for glucose detection.[25, 28] Improving electrode materials and analytical methods can make other detection motifs more viable for widespread commercial use in the future.[2, 26, 29] In this work immunoassay detection is used in Chapter 2, and direct detection in Chapters 3 and 4.

1.2 Carbon Electrode Materials

This dissertation focuses on carbon electrode materials. Carbon-based electrodes are often used for bioanalysis, as they exhibit wide potential windows compared to metal electrodes,

superior biocompatibility, and high chemical stability.[30] Conductive carbon exists in many forms in which structure strongly affects electrochemistry. Common carbon allotropes include graphite, diamond, and fullerenes.[30] Most carbon electrode materials are graphitic in nature, as are the carbon electrodes discussed in this work. Graphitic material structures are composed of stacked sheets of graphene (hexagonal polycyclic aromatic sheets).[31] In graphitic materials, the ordered plane parallel with the graphene sheets is referred to as the "basal plane" and irregular sites perpendicular to this are called "edge plane".[30] Edge plane sites are generally considered to have much faster charge transfer kinetics than the basal plane, and typically dominate carbon electrochemistry.[30, 32] However, through Scanning Electrochemical Cell Microscopy (SECCM), it was shown that pristine basal plane is also quite electroactive but this activity decreases quickly with surface fouling.[33]

In this dissertation, graphite is primarily used as the source of conductive carbon. Graphite consists of stacked sheets of sp^2 hybridized polyaromatic hydrocarbons with typical particle sizes of 0.5–150 μm.[30] Graphite is often used for electrochemical applications because it exhibits high conductivity like metals but is more chemically inert.[34] Graphite materials are available in different varieties such as the natural flake, surface enhanced flake (SEFG), and synthetic graphite used in this work. Natural and synthetic graphite both have polycrystalline structures; however, in natural graphite, crystals are mainly oriented in the same direction whereas crystals are more randomly oriented in synthetic graphite.[34] Natural flake graphite for electrochemical applications is typically mined, milled and purified; synthetic graphite is prepared by heating unstructured carbon at high temperatures.[34] Surface enhanced flake graphite is made from natural flake graphite that has been chemically treated through a proprietary process to have roughly double the surface area of typical

flake graphite particles.[35] Natural flake graphite is used throughout this work and compared with synthetic and SEFG in TPEs in Chapter 4.

Other graphitic materials used in this work include acetylene carbon black, graphene nanoplatelets, and glassy carbon. Acetylene carbon black is carbon black manufactured by the thermal decomposition of acetylene gas and has similar structure to graphite but is much smaller in size ~50 nm.[36-37] Graphene nanoplatelets consist of 10-100 layers of graphene and are typically 3-30 nm thick.[31] Glassy carbon is formed through polymer pyrolysis and its structure consists of randomly oriented tangled graphitic ribbons.[38-39] Commercial glassy carbon electrodes are widely available and commonly used for bioanalysis and they are used for comparison to novel materials in this work.

Carbon composite electrodes consist of conductive carbon particles dispersed in a polymer or paraffin matrix. Ralph N. Adams pioneered the field in 1958 with the first report of carbon paste electrodes consisting of conductive carbon in a bromoform matrix.[40] Common examples include screen-printed carbon electrodes (SPCEs), carbon paste electrodes, and epoxy-based composite electrodes.[41-43] Unfortunately, electrode patterning via molding and embossing can be limited or difficult for these materials and the electron transfer kinetics of composite electrodes are often poor.

1.3 Thermoplastic Electrodes

In recent years, our group has investigated thermoplastics as alternative binders in carbon composite electrodes, yielding highly electroactive materials that can be easily molded.[44-47] Thermoplastics are polymers that can be melted and cooled repeatedly without degrading or changing the properties of the plastic.[48] Thermoplastic electrodes (TPEs) were first proposed as a new class of high-performance carbon composite electrode materials by Klunder et. al in 2017.[44]

TPEs are fabricated via a simple method in which thermoplastic binder is first dissolved in organic solvent and conductive carbon filler is mixed in. The thermoplastic-carbon mixture is then dried or partially dried to a gum-like paste and heat pressed into templates under pressure into the desired shape.[44, 47] When used as composite binders, thermoplastics retain their mechanical properties, enabling the fabrication of small and intricate electrode designs, limited only by the size of the conductive carbon particles and resolution of the molding technique.[44, 47] The impressive moldability of these materials has been utilized to incorporate TPEs into a variety of paper and plastic channel fluidic devices.[45, 47, 49-50] TPEs have achieved high carbon filler loadings (up to 10:1 graphite:plastic) and conductivities of up to ~1000 S/m, whereas what is considered "high" conductivity for SPCEs is ~100× lower.[47, 51] High carbon filler loadings and conductivity likely contribute to the excellent electrochemistry of TPEs which is comparable to that of traditional electrode materials such as noble metals and glassy carbon.[44, 47]

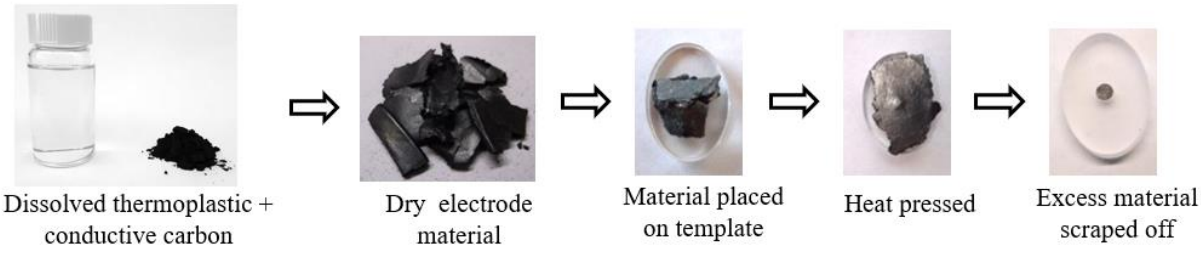

Fig. 1.1 Thermoplastic electrode fabrication process.

A variety of thermoplastic binders have been used thus far in TPE fabrication including polymethyl methacrylate (PMMA),[44, 49] polycaprolactone (PCL),[47, 49-50, 52] and cyclic olefin copolymer (COC).[45-46, 49] The thermoplastics used in this work to fabricate TPEs include PMMA, PCL, and polystyrene (PS). The first reported TPEs used PMMA as a binder.[44] PMMA is an inexpensive (typically 0.2–2 cents/cm^2), easily moldable thermoplastic with a melting point of ~160 °C.[53-54] PMMA TPE material is typically solvent-processed by pressing material into

templates when only partially dried to allow the material to be processed at lower temperatures with a wide variety of templates. However, solvent processing TPE materials can lead to issues when too much or too little organic solvent is still present, such as the formation of gaps or cracks in the material. To eliminate solvent processing issues, PCL was investigated as an alternative low melting point binder to PMMA.[47] PCL, like PMMA is inexpensive (~4 cents/gram) and easily moldable but exhibits a much lower melting point (59–64 ◦C).[55] The lower melting point allows for PCL TPEs to be processed easily when fully dry. Although easier to fabricate, PCL TPE properties were somewhat inferior to PMMA TPE properties. PCL TPEs had lower conductivity, higher capacitance, and slightly lower peak currents for ferri/ferrocyanide than PMMA TPEs, therefore the preferable binder to use is application dependent.[49] However, when the thermoplastics are blended together at a 2:1 PCL:PMMA ratio in TPEs the material properties can be improved while retaining the ability to dry process the TPE material (Appendix 1). PMMA-PCL blend TPEs are utilized in Chapter 2.

In Chapter 3 TPE materials containing PS plastics were investigated as the first TPEs with aromatic binder functionalities. PS is also of interest as a TPE binder for detection of biomarkers as it is one of the most used substrates for bioanalysis.[56] In Chapter 3, the electrochemistry and morphology of these PS TPEs are characterized to investigate the impact aromatic binders on composite electrodes. PS waste is a major environmental problem as PS is abundantly used and rarely recycled, so the use of PS waste plastic in TPEs was also explored.[57] PS TPEs were found to have unique electrochemical properties, and in Chapter 4 unmodified PS TPEs were utilized successfully for simultaneous direct detection of AA, DA, and UA, when electrode modifiers are typically required.[58]

1.4 Electrode Pre-treatment

Carbon electrodes are typically pre-treated prior to electroanalysis or modification. The electrode pre-treatment method can greatly influence electrode performance stability and reproducibility.[44, 59-60] Mechanical abrasion through polishing is quite common, and often performed prior other pre-treatments. Polishing can improve electroactivity by removing surface contamination and/or increasing active surface area.[44, 59, 61] Insulating binders tend to coat conductive particles in composite electrodes which mechanical polishing can remove, exposing more conductive material.[44, 61] Rough polishing can be performed with silicon carbide sandpaper although this can leave behind surface irregularities and scratches.[44, 59] Fine polishing is often performed with micro-fiber pads in the presence of slurries of microscale metal or diamond particles, can leave smoother more uniform surfaces.[30,59] However, for TPEs, fine polishing can deactivate the surfaces by coating the conductive carbon with the softer insulator, thus sandpaper polishing is necessary for optimal performance.[44]

Aside from polishing, electrochemical pre-treatment[62-63] and plasma treatment[30, 44, 64] are common. Plasma consists of partially ionized gas capable of causing physical and mechanical changes to electrode surfaces.[64] Plasma treatment can cause material ablation of composite electrode binder at the surface and generation of reactive free radical species that bind to the electrode which can improve electroactivity and surface area.[30, 44, 64] Electrochemical pre-treatments can be anodic or cathodic and are performed via holding a set potential with amperometry[60, 63] or through potential cycling.[62] These processes are pH and time dependent.[60, 63] Anodic pre-treatment leads to a more oxidized and hydrophilic surface where organic contaminants can be more easily displaced with water; anodic pre-treatment can also increase surface roughness.[65-66] Cathodic pre-treatment can reduce surface oxides caused by ambient air

oxidation or other aging processes that dampen electrochemical signal.[62] Both electrochemical pre-treatment methods can lead to faster redox kinetics and higher active surface area like plasma treatment, but unlike plasma treatment do not require special equipment beyond a potentiostat.

1.5 Electrochemical Immunoassays

Electrochemical immunoassays are affinity-based assays that utilize antibodies for analyte capture and electrochemical detection methods. The field was pioneered by Heineman in the 1980s who detected NADH and IgG antibodies using glassy carbon, carbon paste and gold electrodes.[67-70] Improving and simplifying electrode materials, modifications, and electroanalytical methods remain important challenges to overcome in this field.[2] Assay format, electrode material, and electrode modifications are key considerations for the development of electrochemical immunosensors.

The most used format for electrochemical immunoassays is enzyme-linked immunosorbent assay (ELISA) where the antibody-antigen interaction is quantified by an enzymatic label on the antibody generating an electroactive product.[71] Other assay types such as nanozyme-labeled, and label-free immunoassays have also been gaining popularity in recent years. Nanomaterial catalysts, often referred to as "nanozymes" have started being used as enzyme alternatives to lower costs and improve stability.[72-74] Immunosensors are also increasingly being developed without labels for greater assay simplicity.[75-77] Label-free immunosensors instead quantify analyte-antibody binding through changes in surface chemistry caused by the binding event which increase resistance to charge transfer (Rct).[78] For this work, an ELISA format was used to test the first TPE immunoassay platform, however, this platform is easy to adapt to other assay formats. In a recent work, aspects of this platform have been adapted for label-free E. coli detection.[52]

ELISA assays are performed in a "sandwich" format in this work where the analyte is captured with a primary antibody then sandwiched between an additional enzyme-labeled antibody. For electrochemical ELISA, the sandwich complex is introduced to a substrate with an enzymatic product that can be detected electrochemically. The sandwich assay is a popular ELISA format due to the selectivity provided from the analyte needing to bind two antibodies for detection. Alkaline phosphatase was chosen as the enzymatic label for its low cost, stability, and wide selection of substrates.[79] ALP is used in this work along with the enzymatic substrate p-aminophenyl phosphate (pAPP). This enzyme-substrate pair is excellent for electrochemical immunoassays because its enzymatic product p-aminophenol (pAP) has a low oxidation potential, and fast charge transfer kinetics relative to other common products.[70, 80]

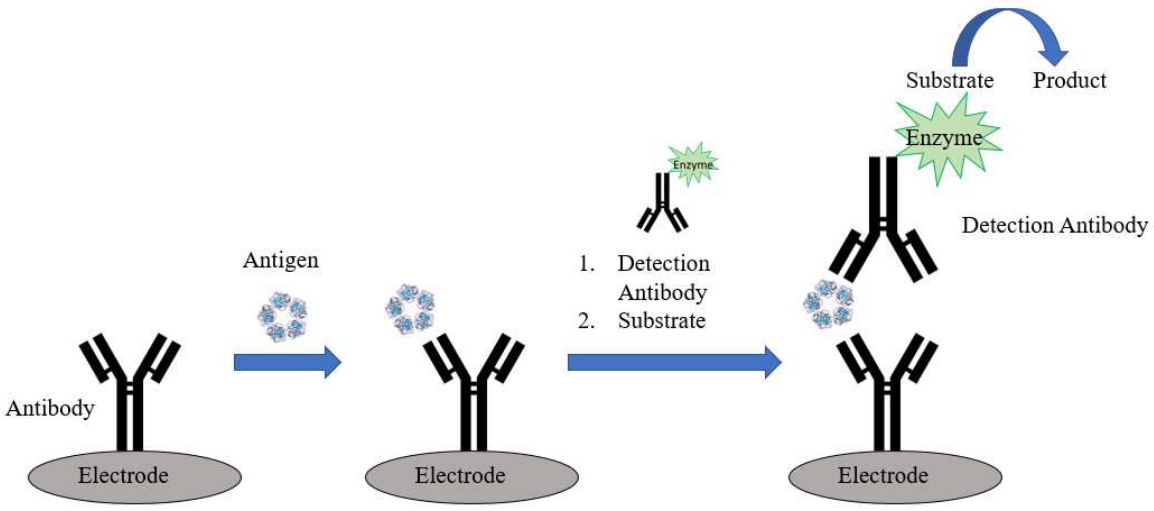

Fig. 1.2 Electrochemical sandwich ELISA.

Another important component of electrochemical immunosensors, is antibody attachment to the electrode surface. Antibody attachment is typically achieved through direct adsorption, or chemical binding. Antibody attachment through adsorption can lack stability and reproducibility so superior analytical performance is often achieved through binding.[81-83] To bind antibodies to

electrode surfaces, electrodes are typically functionalized with groups that have established coupling chemistries with antibodies.[71, 81] Popular functional groups include carboxylic acids, amines and alkynes, TPEs are amine functionalized in this work.[71, 81]

Electrode functionalization is achieved through covalent or non-covalent affinity-based methods. Common affinity-based attachment strategies are gold-thiol and π-π stacking attachment. On carbon electrodes, for gold-thiol attachment, the electrodes are first modified with gold nanoparticles to create affinity sites.[84-85] For π-π stacking, strong affinity with the graphitic π-bonds is the source of attachment.[86] This is typically achieved through π-bond rich small molecules such as pyrene derivatives[75, 87] or carbon nanomaterials like reduced graphene oxide.[88-89] Affinity attachment methods are relatively simple and effective but can require long incubation times and organic solvents that are non-compatible with carbon composite electrodes.[86, 90] Also both thiol and π-π stacking attachment methods have issues with modification stability.[86, 90]

Covalent modification of electrodes with functional groups have also been explored for antibody attachment and can lead to more stable functionalized surfaces. In the past, diazonium salts have been explored as a promising method for electrode functionalization.[91-93] Diazonium salt functionalization is simple, fast, and versatile.[82, 92] Unfortunately, diazonium salts can be extremely unstable and potentially explosive which limits their potential for widespread use.[83, 94] In situ synthesis and modification at low temperatures (~0°C)[83, 95] or the use of stabilized tetrafluoroborate salts can mitigate these risks.[96-97] The in situ reaction conditions or organic solvents required to dissolve tetrafluoroborate salts are not ideal for TPE functionalization. For this reason, diazonium tosylates were explored as a new immunosensor functionalization strategy in Chapter 4.

Diazonium tosylates are a particularly stable and soluble type of diazonium salt that can be synthesized solvent-free under ambient conditions.[98-99] Diazonium tosylates have excellent qualities for biosensor applications but have not been widely used or studied like tetrafluoroborate salts. In Chapter 4, synthesis and grafting of diazonium tosylates was optimized to amine functionalize TPEs both directly through grafting of p-aminophenyl diazonium salt or indirectly through grafting p-nitrophenyl diazonium salt followed by electrochemical reduction to convert grafted nitro groups to amines.

Carbodiimide chemistry can be used to crosslink amine terminated TPEs to the carboxylic acid groups on antibodies. The crosslinking chemicals used in this work were 1-ethyl-3-(3(dimethylamino)propyl)carbodiimide hydrochloride (EDC) and N-hydroxysuccinimide (NHS); this crosslinker chemistry is commonly referred to as EDC/NHS coupling. EDC/NHS coupling is simple and versatile zero-length crosslinker procedure that forms an amide bond between former primary amine and carboxylic acid groups.[100] Following crosslinker attachment of antibodies the analyte can be introduced, and subsequent assay steps can be performed.

1.6 Direct Detection of Biomarkers

Direct detection is often a proposed electroanalysis motif for biomarkers that are redox active due to its simplicity. There has long been an interest in direct electrochemical detection of neurotransmitters and other small molecules, and for earlier work direct detection was frequently performed on glassy carbon or carbon fiber electrodes.[101-104] However, now the field is shifting towards developing inexpensive materials for direct detection, that can be easily incorporated into fluidic and array device formats.[26, 105] Thus TPEs are a promising class of materials for direct detection.

Typical bare electrode materials have insufficient sensitivity and selectivity for direct detection of biomarkers. Often modifiers are used which can enhance direct detection by increasing the active surface area and surface conductivity which can increase mass transport and improve electrode kinetics and sensitivity, respectively.[106] Modifiers can also coat the electrode surface with materials or functional groups that reduce biofouling or increase signal.[58] Common modifiers include metallic or carbon nanomaterials, ionic liquids, conductive polymers, and surfactants.[106 26, 58]

In biological, pharmaceutical, and food samples, redox active molecules often coexist within the same matrix and can elucidate different relevant information about the systems in question. Therefore, the ability to resolve multiple voltametric peaks is also of interest to direct detection. Simultaneous analysis strategies rely on achieving sharper peaks with less overlap through improved mass transport and separating the peak potentials through enhancing the kinetics of certain species over others.[22, 58, 107] Electrostatic interactions between the species and the electrode surface are useful for separation, for example positively charged DA and negatively charged UA are better separated using electronegative surfaces.[107] Nanomaterial modified or porous surfaces experience better mass transport and sharper peaks.[22, 58] Some species like DA rely on adsorption for oxidation while for outer sphere AA electron transfer can occur without bonding to the surface therefore changing surface morphology can aid separation.[30]

Although many of the electrode modifications discussed in this section improve detection, they are often time consuming and complex which limits use. The PS TPE materials discussed in Chapter 3–4 require no complex treatments or modifications for sensitive direct detection. The PS TPE fabrication and sandpaper polishing process generates surface morphology and electrochemistry reminiscent of carbon nanomaterial modified electrodes.

1.7 Electroanalytical Techniques

For both immunoassay and direct detection, many electroanalytical techniques are employed for surface characterization and detection. Often to characterize a new material or modification cyclic voltammetry (CV) is employed.[44, 62, 98] For CV, a triangular waveform is applied, and the potential is scanned in either the positive or negative direction before switching to the opposite direction. CV peaks shown for the forward and reverse scans correspond to oxidation and reduction processes of species in solution and on the electrode surface. For reversible or quasi-reversible redox processes separation between oxidation and reduction reactions is referred to as ΔE; higher ΔE corresponds to slower redox kinetics.[108] Theoretically, ΔE for a kinetically fast, diffusion limited, single electron transfer redox reaction should be 59 mV but experimental values are typically higher.[108] Irreversible processes show a peak in only one direction. Peak potentials correspond to the energy required for the redox reaction and peak currents correspond to kinetics and surface area.[108]

For direct or immunoassay detection of biomarkers, more sensitive techniques such as amperometry, pulsed voltammetry, and impedance spectroscopy are used. Amperometry is advantageous due to its simplicity and the selectivity of the set potential; the electrode is held at a set potential and the current response is used to detect the analyte of interest. Pulsed voltammetry techniques are advantageous due to the suppression of current from background processes through subtraction between on and off pulses. Impedance spectroscopy measures frequency dependent resistance to charge transfer. Impedance spectroscopy is highly sensitive to changes in surface chemistry and provides insight into electrochemical processes occurring at the surface that would take multiple experiments using other techniques.[78]

In this dissertation, pulsed voltammetry, specifically square wave voltammetry (SWV) is the method of biomarker detection. SWV is becoming increasingly popular as a detection method for bioanalysis because it is good at suppressing interference from background processes and is faster than other techniques with similar analytical performances.[71, 108-110] In SWV a pulsed potential waveform is superimposed on a stepped waveform. Current readings are taken at the end of forward and reverse pulses allowing the capacitive current time to decay and the difference in current is plotted versus the stepped potential.[108] In Chapters 2 and 4 SWV is used for immunoassay and direct detection of biomarkers.

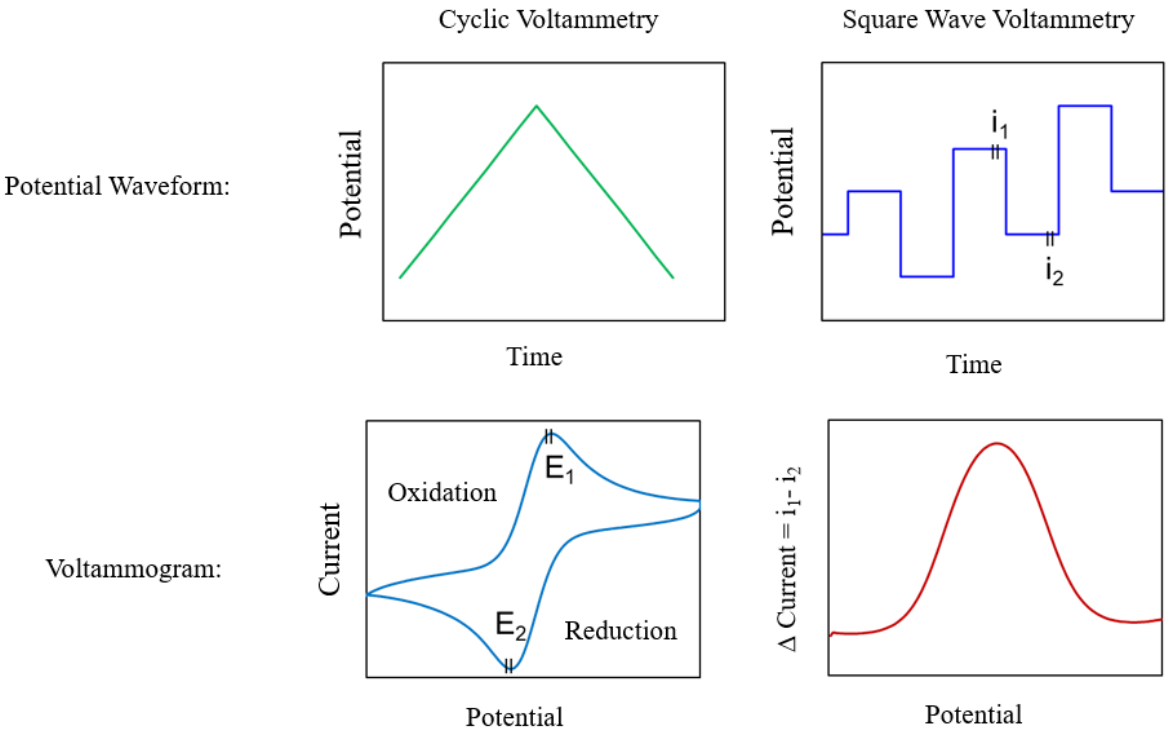

Fig. 1.3 Potential waveforms and voltammograms for cyclic voltammetry and square wave voltammetry, respectively.

In summary, this dissertation focuses on the development and characterization of new TPE materials and modifications for detection of biomarkers. Chapter 2 focuses on the first TPE immunosensors developed for detection of CRP and a novel immunosensor functionalization method is presented using grafting of diazonium tosylates. Chapter 3 explores the use of PS plastics

as the first TPE binders containing aromatic functionalities. PS TPEs were found to exhibit unique morphology and exceptional voltammetry, so their use was further explored for simultaneous analysis of AA, DA, and UA in Chapter 4. Unmodified PS TPEs were able to resolve AA, DA, and UA oxidation peaks remarkably for simultaneous analysis when modifiers are required for resolution at most bare electrode materials. This work expands knowledge of carbon composite electrodes, and of how composition and surface modification can impact direct and immunoassay detection of biomarkers. The TPE immunosensors, and electrode materials developed in this thesis can also be easily adapted for a wider range of applications.

REFERENCES

1. Califf, R. M., Biomarker definitions and their applications. *Experimental Biology and Medicine* **2018,** *243* (3), 213-221.

2. Campuzano, S.; Pedrero, M.; Yáñez-Sedeño, P.; Pingarrón, J. M., New challenges in Point of Care electrochemical detection of clinical biomarkers. *Sensors and Actuators B: Chemical* **2021**, 130349.

3. Bernabé-Ortiz, A.; Zafra-Tanaka, J. H.; Moscoso-Porras, M.; Sampath, R.; Vetter, B.; Miranda, J. J.; Beran, D., Diagnostics and monitoring tools for noncommunicable diseases: a missing component in the global response. *Globalization and Health* **2021,** *17* (1), 1-5.

4. Bahadir, E. B.; Sezginturk, M. K., Applications of electrochemical immunosensors for early clinical diagnostics. *Talanta* **2015,** *132*, 162-174.

5. Rusling, J. F.; Kumar, C. V.; Gutkind, J. S.; Patel, V., Measurement of biomarker proteins for point-of-care early detection and monitoring of cancer. *Analyst* **2010,** *135* (10), 2496-2511.

6. Bai, Y.; Xu, T.; Zhang, X., Graphene-based biosensors for detection of biomarkers. *Micromachines* **2020,** *11* (1), 60.

7. Morais, A. L.; Rijo, P.; Batanero Hernan, M. B.; Nicolai, M., Biomolecules and Electrochemical Tools in Chronic Non-Communicable Disease Surveillance: A Systematic Review. *Biosensors* **2020,** *10* (9), 121.

8. Huang, Y.; Gulshan, K.; Nguyen, T.; Wu, Y. P., Biomarkers of Cardiovascular Disease. *Dis. Markers* **2017**, 2.

9. Brandt, E. J., C-Reactive Protein and Other Inflammatory Markers in Cardiovascular Disease: Inflammatory Disorders and Atherosclerosis. In *Therapeutic Lipidology*, Springer: 2021; pp 565-583.

10. Tallaksen, C.; Bøhmer, T.; Bell, H., Concentrations of the water-soluble vitamins thiamin, ascorbic acid, and folic acid in serum and cerebrospinal fluid of healthy individuals. *The American journal of clinical nutrition* **1992,** *56* (3), 559-564.

11. Dhara, K.; Debiprosad, R. M., Review on nanomaterials-enabled electrochemical sensors for ascorbic acid detection. *Analytical biochemistry* **2019,** *586*, 113415.

12. Maiuolo, J.; Oppedisano, F.; Gratteri, S.; Muscoli, C.; Mollace, V., Regulation of uric acid metabolism and excretion. *International journal of cardiology* **2016,** *213*, 8-14.

13. Liu, X.; Liu, J., Biosensors and sensors for dopamine detection. *View* **2021,** *2* (1), 20200102.

14. Iversen, S. D.; Iversen, L. L., Dopamine: 50 years in perspective. *Trends in neurosciences* **2007,** *30* (5), 188-193.

15. Arrigoni, O.; De Tullio, M. C., Ascorbic acid: much more than just an antioxidant. *Biochimica et Biophysica Acta (BBA)-General Subjects* **2002,** *1569* (1-3), 1-9.

16. Black, C. N.; Bot, M.; Scheffer, P. G.; Snieder, H.; Penninx, B. W., Uric acid in major depressive and anxiety disorders. *Journal of affective disorders* **2018,** *225*, 684-690.

17. Liu, J.; Xu, C.; Ying, L.; Zang, S.; Zhuang, Z.; Lv, H.; Yang, W.; Luo, Y.; Ma, X.; Wang, L., Relationship of serum uric acid level with non-alcoholic fatty liver disease and its inflammation progression in non-obese adults. *Hepatology Research* **2017,** *47* (3), E104-E112.

18. Perez-Ruiz, F.; Dalbeth, N.; Bardin, T., A review of uric acid, crystal deposition disease, and gout. *Advances in therapy* **2015,** *32* (1), 31-41.

19. Abraham, R. S.; Barnidge, D. R., Protein Analysis in the Clinical Immunology Laboratory. *Manual of Molecular and Clinical Laboratory Immunology* **2016**, 26-45.

20. Vashist, S. K.; Venkatesh, A.; Schneider, E. M.; Beaudoin, C.; Luppa, P. B.; Luong, J. H., Bioanalytical advances in assays for C-reactive protein. *Biotechnology advances* **2016,** *34* (3), 272-290.

21. Lakshmi, D.; Whitcombe, M. J.; Davis, F.; Sharma, P. S.; Prasad, B. B., Electrochemical detection of uric acid in mixed and clinical samples: a review. *Electroanalysis* **2011,** *23* (2), 305-320.

22. Zhang, L.; Liu, C.; Wang, Q.; Wang, X.; Wang, S., Electrochemical sensor based on an electrode modified with porous graphitic carbon nitride nanosheets (C 3 N 4) embedded in graphene oxide for simultaneous determination of ascorbic acid, dopamine and uric acid. *Microchim. Acta* **2020,** *187* (2), 1-10.

23. Unic, A.; Nikolac Gabaj, N.; Miler, M.; Culej, J.; Lisac, A.; Horvat, A.; Vrkic, N., Ascorbic acid—A black hole of urine chemistry screening. *Journal of clinical laboratory analysis* **2018,** *32* (5), e22390.

24. Park, H.-D., Current Status of Clinical Application of Point-of-Care Testing. *Archives of Pathology & Laboratory Medicine* **2021,** *145* (2), 168-175.

25. Teymourian, H.; Barfidokht, A.; Wang, J., Electrochemical glucose sensors in diabetes management: an updated review (2010–2020). *Chem. Soc. Rev.* **2020**.

26. Noviana, E.; McCord, C. P.; Clark, K. M.; Jang, I.; Henry, C. S., Correction: Electrochemical paper-based devices: sensing approaches and progress toward practical applications. *Lab Chip* **2020,** *20* (1), 185-185.

27. Bakker, E.; Buhlmann, P.; Pretsch, E., Carrier-based ion-selective electrodes and bulk optodes. 1. General characteristics. *Chem. Rev.* **1997,** *97* (8), 3083-3132.

28. Frant, M. S., Historical perspective. History of the early commercialization of ion-selective electrodes. *Analyst* **1994,** *119* (11), 2293-2301.

29. Hersey, M.; Berger, S. N.; Holmes, J.; West, A.; Hashemi, P., Recent Developments in Carbon Sensors for At-Source Electroanalysis. *Analytical chemistry* **2018,** *91* (1), 27-43.

30. McCreery, R. L., Advanced carbon electrode materials for molecular electrochemistry. *Chem. Rev.* **2008,** *108* (7), 2646-2687.

31. Pumera, M., Graphene-based nanomaterials and their electrochemistry. *Chem. Soc. Rev.* **2010,** *39* (11), 4146-4157.

32. Banks, C. E.; Compton, R. G., New electrodes for old: from carbon nanotubes to edge plane pyrolytic graphite. *Analyst* **2006,** *131* (1), 15-21.

33. Lai, S. C.; Patel, A. N.; McKelvey, K.; Unwin, P. R., Definitive evidence for fast electron transfer at pristine basal plane graphite from high-resolution electrochemical imaging. *Angewandte Chemie* **2012,** *124* (22), 5501-5504.

34. Wissler, M., Graphite and carbon powders for electrochemical applications. *J. Power Sources* **2006,** *156* (2), 142-150.

35. Tamashausky, A. V. In *Surface enhanced flake graphite and its utility as a functional extender for molybdenum disulfide*, NLGI Spokesman-Including NLGI Annual Meeting-National Lubricating Grease Institute, [Kansas City, Mo.] National Lubricating Grease Institute.: 2006; pp 8-16.

36. Pierson, H. O., *Handbook of Carbon, Graphite, Diamonds and Fullerenes*. Noyes Publications: Park Ridge, New Jersey, 1993.

37. Bigg, D. M., An Investigation of the Effect of Carbon Black Structure, Polymer Morphology, and Processing History on the Electrical Conductivity of Carbon-Black-Filled Thermoplastics. *J. Rheol.* **1984,** *28* (5), 501-516.

38. Jenkins, G.; Kawamura, K., Structure of glassy carbon. *Nature* **1971,** *231* (5299), 175-176.

39. Dekanski, A.; Stevanović, J.; Stevanović, R.; Nikolić, B. Ž.; Jovanović, V. M., Glassy carbon electrodes: I. Characterization and electrochemical activation. *Carbon* **2001,** *39* (8), 1195-1205.

40. Adams, R. N., Carbon paste electrodes. *Analytical chemistry* **1958,** *30* (9), 1576-1576.

41. Taleat, Z.; Khoshroo, A.; Mazloum-Ardakani, M., Screen-printed electrodes for biosensing: a review (2008-2013). *Microchim. Acta* **2014,** *181* (9-10), 865-891.

42. Antiochia, R.; Lavagnini, I.; Magno, F.; Valentini, T.; Palleschi, G., Single-wall carbon nanotube paste electrodes: a comparison with carbon paste, platinum and glassy carbon electrodes via cyclic voltammetric data. *Electroanalysis* **2004,** *16* (17), 1451-1458.

43. Manea, F.; Radovan, C.; Pop, A.; Corb, I.; Burtica, G.; Malchev, P.; Picken, S.; Schoonman, J., Carbon Composite Electrodes Applied for Electrochemical Sensors. In *Sensors for Environment, Health and Security: Advanced Materials and Technologies*, Baraton, M. I., Ed. Springer: Dordrecht, 2009; pp 179-189.

44. Klunder, K. J.; Nilsson, Z.; Sambur, J. B.; Henry, C. S., Patternable Solvent-Processed Thermoplastic Graphite Electrodes. *J. Am. Chem. Soc.* **2017,** *139* (36), 12623-12631.

45. Noviana, E.; Klunder, K. J.; Channon, R. B.; Henry, C. S., Thermoplastic Electrode Arrays in Electrochemical Paper-Based Analytical Devices. *Analytical Chemistry* **2019,** *91* (3), 2431-2438.

46. Berg, K. E.; Leroux, Y. R.; Hapiot, P.; Henry, C. S., Increasing Applications of Graphite Thermoplastic Electrodes with Aryl Diazonium Grafting. *ChemElectroChem* **2019,** *6* (18), 4811-4816.

47. Klunder, K. J.; Clark, K. M.; McCord, C.; Berg, K. E.; Minteer, S. D.; Henry, C. S., Polycaprolactone-enabled sealing and carbon composite electrode integration into electrochemical microfluidics. *Lab Chip* **2019,** *19* (15), 2589-2597.

48. Introduction to Thermoplastic Materials. http://www.stephen-webster.co.uk/wp-content/uploads/2017/10/Thermoplastics-Materials-general-introduction-Athlone.pdf (accessed 3/8/18).

49. Pradela-Filho, L. A.; Noviana, E.; Araujo, D.; Takeuchi, R.; Santos, A.; Henry, C. S., Rapid Analysis in Continuous Flow Electrochemical Paper-Based Analytical Devices. *ACS Sens.* **2020**.

50. Berg, K. E.; Clark, K. M.; Li, X.; Carter, E. M.; Volckens, J.; Henry, C. S., High-throughput, semi-automated dithiothreitol (DTT) assays for oxidative potential of fine particulate matter. *Atmospheric Environment* **2020,** *222*, 117132.

51. Randviir, E. P.; Brownson, D. A. C.; Metters, J. P.; Kadara, R. O.; Banks, C. E., The fabrication, characterisation and electrochemical investigation of screen-printed graphene electrodes. *Physical Chemistry Chemical Physics* **2014,** *16* (10), 4598-4611.

52. Ozer, T.; McCord, C.; Geiss, B. J.; Dandy, D.; Henry, C. S., Thermoplastic Electrodes for Detection of Escherichia coli. *Journal of The Electrochemical Society* **2021,** *168* (4), 047509.

53. Becker, H.; Locascio, L. E., Polymer microfluidic devices. *Talanta* **2002,** *56* (2), 267-287.

54. A comparison of electron beam lithography resists PMMA and ZEP520A. http://nanolithography.gatech.edu/etching/PMMA_ZEP520_resist_comparison_summary.pdf (accessed 3/8/18).

55. Woodruff, M. A.; Hutmacher, D. W., The return of a forgotten polymer-Polycaprolactone in the 21st century. *Prog. Polym. Sci.* **2010,** *35* (10), 1217-1256.

56. Salminen, K.; Grönroos, P.; Eskola, J.; Nieminen, E.; Härmä, H.; Kulmala, S., Immunoassay of C-reactive protein by hot electron-induced electrochemiluminescence at polystyrene-carbon black composite electrodes. *Electrochimica Acta* **2018,** *282*, 147-154.

57. Gil-Jasso, N. D.; Segura-González, M. A.; Soriano-Giles, G.; Neri-Hipolito, J.; López, N.; Mas-Hernández, E.; Barrera-Díaz, C. E.; Varela-Guerrero, V.; Ballesteros-Rivas, M. F., Dissolution and recovery of waste expanded polystyrene using alternative essential oils. *Fuel* **2019,** *239*, 611-616.

58. Baig, N.; Rana, A.; Kawde, A. N., Modified electrodes for selective voltammetric detection of biomolecules. *Electroanalysis* **2018,** *30* (11), 2551-2574.

59. Kamau, G., Surface preparation of glassy carbon electrodes. *Anal. Chim. Acta* **1988,** *207*, 1-16.

60. Beilby, A. L.; Sasaki, T. A.; Stern, H. M., Electrochemical pretreatment of carbon electrodes as a function of potential, pH, and time. *Analytical Chemistry* **1995,** *67* (5), 976-980.

61. Cumba, L. R.; Foster, C. W.; Brownson, D. A.; Smith, J. P.; Iniesta, J.; Thakur, B.; Do Carmo, D. R.; Banks, C. E., Can the mechanical activation (polishing) of screen-printed electrodes enhance their electroanalytical response? *Analyst* **2016,** *141* (9), 2791-2799.

62. Gyan, I. O.; Wojcik, P. M.; Aston, D. E.; McIlroy, D. N.; Cheng, I. F., A study of the electrochemical properties of a new graphitic material: GUITAR. *ChemElectroChem* **2015,** *2* (5), 700-706.

63. Cui, G.; Yoo, J. H.; Lee, J. S.; Yoo, J.; Uhm, J. H.; Cha, G. S.; Nam, H., Effect of pre-treatment on the surface and electrochemical properties of screen-printed carbon paste electrodes. *Analyst* **2001,** *126* (8), 1399-1403.

64. Wang, S. C.; Chang, K. S.; Yuan, C. J., Enhancement of electrochemical properties of screen-printed carbon electrodes by oxygen plasma treatment. *Electrochimica Acta* **2009,** *54* (21), 4937-4943.

65. Musameh, M.; Lawrence, N. S.; Wang, J., Electrochemical activation of carbon nanotubes. *Electrochemistry Communications* **2005,** *7* (1), 14-18.

66. Rice, M. E.; Galus, Z.; Adams, R. N., Graphite paste electrodes: Effects of paste composition and surface states on electron-transfer rates. *Journal of Electroanalytical Chemistry* **1983,** *143* (1-2), 89-102.

67. Eggers, H. M.; Halsall, H.; Heineman, W., Enzyme immunoassay with flow-amperometric detection of NADH. *Clin. Chem.* **1982,** *28* (9), 1848-1851.

68. Heineman, W. R.; Halsall, H. B., Strategies for electrochemical immunoassay. *Analytical chemistry* **1985,** *57* (12), 1321A-1331A.

69. Wehmeyer, K. R.; Halsall, H.; Heineman, W., Heterogeneous enzyme immunoassay with electrochemical detection: competitive and" sandwich"-type immunoassays. *Clin. Chem.* **1985,** *31* (9), 1546-1549.

70. Tang, H. T.; Lunte, C. E.; Halsall, H. B.; Heineman, W. R., P-AMINOPHENYL PHOSPHATE - AN IMPROVED SUBSTRATE FOR ELECTROCHEMICAL ENZYME-IMMUNOASSAY. *Anal. Chim. Acta* **1988,** *214* (1-2), 187-195.

71. Ricci, F.; Adornetto, G.; Palleschi, G., A review of experimental aspects of electrochemical immunosensors. *Electrochimica Acta* **2012,** *84*, 74-83.

72. Niu, X.; Cheng, N.; Ruan, X.; Du, D.; Lin, Y., Nanozyme-based immunosensors and immunoassays: recent developments and future trends. *Journal of The Electrochemical Society* **2019,** *167* (3), 037508.

73. Zhang, X.; Wu, D.; Wu, Y.; Li, G., Bioinspired nanozyme for portable immunoassay of allergenic proteins based on A smartphone. *Biosensors and Bioelectronics* **2021,** *172*, 112776.

74. Choi, H.; Son, S. E.; Hur, W.; Tran, V.-K.; Lee, H. B.; Park, Y.; Seong, G. H., electrochemical immunoassay for Determination of Glycated Albumin using nanozymes. *Scientific reports* **2020,** *10* (1), 1-12.

75. Sethi, J.; Van Bulck, M.; Suhail, A.; Safarzadeh, M.; Perez-Castillo, A.; Pan, G., A label-free biosensor based on graphene and reduced graphene oxide dual-layer for electrochemical determination of beta-amyloid biomarkers. *Microchim. Acta* **2020,** *187*, 1-10.

76. Foubert, A.; Beloglazova, N. V.; Hedstrom, M.; De Saeger, S., Antibody immobilization strategy for the development of a capacitive immunosensor detecting zearalenone. *Talanta* **2019,** *191*, 202-208.

77. Channon, R. B.; Yang, Y. Y.; Feibelman, K. M.; Geiss, B. J.; Dandy, D. S.; Henry, C. S., Development of an Electrochemical Paper-Based Analytical Device for Trace Detection of Virus Particles. *Analytical Chemistry* **2018,** *90* (12), 7777-7783.

78. Daniels, J. S.; Pourmand, N., Label-free impedance biosensors: Opportunities and challenges. *Electroanalysis* **2007,** *19* (12), 1239-1257.

79. Nsabimana, A.; Lan, Y.; Du, F.; Wang, C.; Zhang, W.; Xu, G., Alkaline phosphatase-based electrochemical sensors for health applications. *Analytical methods* **2019,** *11* (15), 1996-2006.

80. Niwa, O.; Xu, Y.; Halsall, H. B.; Heineman, W. R., SMALL-VOLUME VOLTAMMETRIC DETECTION OF 4-AMINOPHENOL WITH INTERDIGITATED ARRAY

ELECTRODES AND ITS APPLICATION TO ELECTROCHEMICAL ENZYME-IMMUNOASSAY. *Analytical Chemistry* **1993,** *65* (11), 1559-1563.

81. Welch, N. G.; Scoble, J. A.; Muir, B. W.; Pigram, P. J., Orientation and characterization of immobilized antibodies for improved immunoassays. *Biointerphases* **2017,** *12* (2).

82. Yanez-Sedeno, P.; Campuzano, S.; Pingarron, J. M., Integrated Affinity Biosensing Platforms on Screen-Printed Electrodes Electrografted with Diazonium Salts. *Sensors* **2018,** *18* (2).

83. Svalova, T.; Malysheva, N.; Bubekova, A.; Saigushkina, A.; Medvedeva, M.; Kozitsina, A., Effect of the Method for Immobilizing Receptor Layer on the Analytical Characteristics of a Label-Free Electrochemical Immunosensor for the Determination of Measles Antibodies. *Journal of Analytical Chemistry* **2020,** *75* (2), 254-261.

84. Pereira, S. V.; Bertolino, F. A.; Fernandez-Baldo, M. A.; Messina, G. A.; Salinas, E.; Sanz, M. I.; Raba, J., A microfluidic device based on a screen-printed carbon electrode with electrodeposited gold nanoparticles for the detection of IgG anti-Trypanosoma cruzi antibodies. *Analyst* **2011,** *136* (22), 4745-4751.

85. Zeng, S. W.; Yong, K. T.; Roy, I.; Dinh, X. Q.; Yu, X.; Luan, F., A Review on Functionalized Gold Nanoparticles for Biosensing Applications. *Plasmonics* **2011,** *6* (3), 491-506.

86. Cao, M.; Fu, A.; Wang, Z.; Liu, J.; Kong, N.; Zong, X.; Liu, H.; Gooding, J. J., Electrochemical and theoretical study of π–π stacking interactions between graphitic surfaces and pyrene derivatives. *The Journal of Physical Chemistry C* **2014,** *118* (5), 2650-2659.

87. Chekin, F.; Singh, S. K.; Vasilescu, A.; Dhavale, V. M.; Kurungot, S.; Boukherroub, R.; Szunerits, S., Reduced graphene oxide modified electrodes for sensitive sensing of gliadin in food samples. *ACS Sens.* **2016,** *1* (12), 1462-1470.

88. Thunkhamrak, C.; Chuntib, P.; Ounnunkad, K.; Banet, P.; Aubert, P. H.; Saianand, G.; Gopalan, A. I.; Jakmunee, J., Highly sensitive voltammetric immunosensor for the detection of prostate specific antigen based on silver nanoprobe assisted graphene oxide modified screen printed carbon electrode. *Talanta* **2020,** *208*.

89. Assari, P.; Rafati, A. A.; Feizollahi, A.; Joghani, R. A., An electrochemical immunosensor for the prostate specific antigen based on the use of reduced graphene oxide decorated with gold nanoparticles. *Microchim. Acta* **2019,** *186* (7).

90. Srisombat, L.; Jamison, A. C.; Lee, T. R., Stability: A key issue for self-assembled monolayers on gold as thin-film coatings and nanoparticle protectants. *Colloids and Surfaces A: Physicochemical and Engineering Aspects* **2011,** *390* (1-3), 1-19.

91. Baranton, S.; Belanger, D., Electrochemical derivatization of carbon surface by reduction of in situ generated diazonium cations. *Journal of Physical Chemistry B* **2005,** *109* (51), 24401-24410.

92. Mahouche-Chergui, S.; Gam-Derouich, S.; Mangeney, C.; Chehimi, M. M., Aryl diazonium salts: a new class of coupling agents for bonding polymers, biomacromolecules and nanoparticles to surfaces. *Chem. Soc. Rev.* **2011,** *40* (7), 4143-4166.

93. Hetemi, D.; Noël, V.; Pinson, J., Grafting of Diazonium Salts on Surfaces: Application to Biosensors. *Biosensors* **2020,** *10* (1), 4.

94. Sheng, M.; Frurip, D.; Gorman, D., Reactive chemical hazards of diazonium salts. *Journal of Loss Prevention in the Process Industries* **2015,** *38*, 114-118.

95. Sun, X. B.; Ma, Z. F., Highly stable electrochemical immunosensor for carcinoembryonic antigen. *Biosensors & Bioelectronics* **2012,** *35* (1), 470-474.

96. Liu, G.; Gooding, J. J., Towards the fabrication of label-free amperometric immunosensors using SWNTs. *Electrochemistry communications* **2009,** *11* (10), 1982-1985.

97. Abdulsattar, J. O.; Greenway, G. M.; Wadhawan, J. D., Electrochemical immunoassay for the detection of stress biomarkers. *Heliyon* **2020,** *6* (3), e03558.

98. Via, G. G.; Shugart, C. L.; Melnyk, S. L.; Hupman, S. R.; Cline, K. K., One-step Solvent-free Synthesis and Grafting of Diazonium Ions at Glassy Carbon Electrodes. *Electroanalysis* **2018,** *30* (10), 2421-2426.

99. Filimonov, V. D.; Trusova, M.; Postnikov, P.; Krasnokutskaya, E. A.; Lee, Y. M.; Hwang, H. Y.; Kim, H.; Chi, K.-W., Unusually stable, versatile, and pure arenediazonium tosylates: their preparation, structures, and synthetic applicability. *Organic letters* **2008,** *10* (18), 3961-3964.

100. Booth, M. A.; Kannappan, K.; Hosseini, A.; Partridge, A., In-depth electrochemical investigation of surface attachment chemistry via carbodiimide coupling. *Langmuir* **2015,** *31* (29), 8033-8041.

101. Wang, J.; Li, M.; Shi, Z.; Li, N.; Gu, Z., Electrocatalytic oxidation of norepinephrine at a glassy carbon electrode modified with single wall carbon nanotubes. *Electroanalysis* **2002,** *14* (3), 225-230.

102. Lau, O.-W.; Luk, S.-F.; Cheung, Y.-M., Simultaneous determination of ascorbic acid, caffeine and paracetamol in drug formulations by differential-pulse voltammetry using a glassy carbon electrode. *Analyst* **1989,** *114* (9), 1047-1051.

103. Gonon, F.; Buda, M.; Cespuglio, R.; Jouvet, M., Voltammetry in the striatum of chronic freely moving rats: detection of catechols and ascorbic acid. *Brain research* **1981,** *223* (1), 69-80.

104. Rozgaité, J.; Pocius, A.; Kulys, J., Electrocatalytic oxidation of NADH and ascorbic acid on electrochemically pretreated glassy carbon electrodes. *Journal of Electroanalytical Chemistry and Interfacial Electrochemistry* **1983,** *154* (1-2), 121-128.

105. Nontawong, N.; Amatatongchai, M.; Wuepchaiyaphum, W.; Chairam, S.; Pimmongkol, S.; Panich, S.; Tamuang, S.; Jarujamrus, P., Fabrication of a three-dimensional electrochemical paper-based device (3D-ePAD) for individual and simultaneous detection of ascorbic acid, dopamine and uric acid. *Int. J. Electrochem. Sci.* **2018,** *13* (7), 6940-6957.

106. Sajid, M.; Nazal, M. K.; Mansha, M.; Alsharaa, A.; Jillani, S. M. S.; Basheer, C., Chemically modified electrodes for electrochemical detection of dopamine in the presence of uric acid and ascorbic acid: a review. *TrAC Trends in Analytical Chemistry* **2016,** *76*, 15-29.

107. Wang, L.; Yang, R.; Qu, L.; Harrington, P. d. B., Electrostatic repulsion strategy for high-sensitive and selective determination of dopamine in the presence of uric acid and ascorbic acid. *Talanta* **2020,** *210*, 120626.

108. Bard, A. J. F., L. R. , *Electrochemical Methods: Fundamentals and Applications*. 2 ed.; John Wiley & Sons Inc.: 2001.

109. Pandey, B.; Demchenko, A. V.; Stine, K. J., Nanoporous gold as a solid support for protein immobilization and development of an electrochemical immunoassay for prostate specific antigen and carcinoembryonic antigen. *Microchim. Acta* **2012,** *179* (1-2), 71-81.

110. Kaya, S. I.; Kurbanoglu, S.; Ozkan, S. A., Nanomaterials-based nanosensors for the simultaneous electrochemical determination of biologically important compounds: ascorbic acid, uric acid, and dopamine. *Crit. Rev. Anal. Chem.* **2019,** *49* (2), 101-125.

CHAPTER 2: SYNTHESIS AND GRAFTING OF DIAZONIUM TOSYLATES FOR THERMOPLASTIC ELECTRODE IMMUNOSENSORS

2.1 Chapter Overview

Most of the content of this chapter is taken from a manuscript in preparation titled "Synthesis and Grafting of Diazonium Tosylates for Thermoplastic Electrode Immunosensors" with authors Cynthia P. McCord, Tugba Ozer, and Charles S. Henry*. For electrochemical immunosensors, inexpensive electrodes with fast redox kinetics, and simple stable methods of electrode functionalization are vital. However, many inexpensive and easy to fabricate electrodes suffer from poor redox kinetics, and functionalization can often be difficult and/or unstable. Diazonium tosylates are particularly stable soluble salts that can be useful for electrode functionalization. Recently developed thermoplastic electrodes (TPEs) are inexpensive, moldable, and highly electroactive carbon composite materials. Herein, synthesis and grafting of diazonium tosylate salts were optimized for modification of TPEs and used to develop the first TPE immunosensors. With diazonium tosylates, TPEs were amine functionalized either directly through grafting of p-aminophenyl diazonium salt or indirectly through grafting p-nitrophenyl diazonium salt followed by electrochemical reduction to an amine. Diazonium tosylates were synthesized in situ as a paste in 6 min. Once the reaction paste was spread over the electrodes, near monolayer coverage (1.0 ± 0.2 nmol/cm^2) was achieved for p-nitrophenyl diazonium salt within 5 min. Amine functionalized electrodes were conjugated to C-reactive protein (CRP) antibodies. Antibody-modified TPEs were applied for the sensitive detection of CRP, a biomarker of cardiovascular disease using electrochemical enzyme-linked immunosorbent assays (ELISA). LODs were determined to be 2 ng/mL in buffer, with high selectivity against interfering species

for both functionalization methods. The direct p-aminophenyl modification method had the highest sensitivity to CRP and was further tested in spiked serum with an LOD of 10 ng/mL. This low-cost and robust TPE immunosensor platform can be easily adapted for other analytes and multiplexed detection.

2.2 Introduction

Electrochemical immunoassays are attractive for bioanalysis due to their fast measurement times (s to min), as well as their excellent sensitivity and selectivity.[1-3] Carbon-based electrodes are often used for immunosensors, as they exhibit wide potential windows compared to metal electrodes, superior biocompatibility, and high chemical stability.[4-5] Composite carbon electrodes are inexpensive and easy to fabricate and therefore often used in biosensors. Recently, our group reported thermoplastic electrodes (TPEs) as an alternative to traditional carbon composite electrodes. TPEs can be easily fabricated and molded into complex geometries for various sensor and flow device designs.[5-9] The electrochemical behavior of these materials is similar to traditional commercial electrode materials such as platinum and glassy carbon but far more moldable and inexpensive, making them excellent materials for electrochemical immunosensors.[5-6]

Often, the first key step in making an electrochemical immunosensor is modifying the electrode surface. For electrochemical immunoassays, sufficient antibody coverage on the electrode surface is crucial for sensitive detection of analyte of interest.[10-11] To achieve this, antibodies are adsorbed or coupled to the electrode surface. Adsorption is a simple process; however, coverage can lack the reproducibility, stability, sensitivity, and specificity of coupled antibodies.[10, 12-13] To couple antibodies to electrodes, electrodes are modified with functional groups including amines, alkynes, and carboxylic acids.[10-11] Non-

covalent affinity-based methods such as pyrene π-π stacking[14-16] and gold-thiol affinity attachment[17-19] are often used, but these methods have their own stability issues, can require lengthy incubations, and often organic solvents are used for modifier dissolution.[20-21] Many organic solvents are incompatible with common composite binders. Another common functionalization technique is the covalent grafting of diazonium salts.[8] This type of modification can be simple, rapid, versatile, and robust.[12, 22-23] However, diazonium salts are extremely reactive, thermally unstable, and potentially explosive[24-25] so synthesis is generally performed around 0°C followed by in situ modification[13, 26-29] or modification is performed in organic solvent with the more stable tetrafluoroborate salts.[8, 30-32]

Diazonium tosylate salts have advantages over other diazonium salts but have not been as widely used or studied. The solubility of tosylate salts is higher than that of the more commonly used tetrafluoroborates or hexafluorophosphates.[33] Synthesis and modification can be performed solvent-free in a water reaction paste.[33-36] Tosylate salts have also proven to be extremely stable, they can be kept dry or in a paste form at room temperature and retain reactivity for months.[33] The source of this stability is hypothesized to be electrostatic interactions causing particularly close contact between the diazonium cation and three tosylate anions as seen with X-ray crystallography.[33] The first paper using diazonium tosylates to modify carbon electrodes was published by Via et al. in 2018. In this report, they used a commercial glassy carbon electrode to grind a water paste consisting of aryl amines, p-toluenesulfonic acid, and sodium nitrite for one-step solvent-free synthesis and spontaneous modification.[36] In this work, we have modified their procedure to be generalizable to a wider range of electrode geometries and optimized the modification for TPEs.

To demonstrate applicability of diazonium tosylate modification for TPE immunoassays, the modification was used for the detection of C-reactive protein (CRP). This biomarker can be monitored in blood serum or saliva and is useful for diagnosis of cardiovascular disease and systemic inflammation.[37-38] Unlike electrochemical assays, common commercial CRP assays, such as immuno-turbidimetric or immuno-nephelometric methods, can be lengthy and require heavy laboratory equipment.[37] Herein, TPEs were first amine functionalized through two different methods: synthesis of p-nitrophenyl diazonium salt followed by the electrochemical reduction of grafted nitro groups to amines, and direct synthesis of p-aminophenyl diazonium salt. These two diazonium salt modifications were compared in terms of electrode coverage to increase anti-CRP attachment on TPEs for further development of the biosensors. Here, detection of CRP was performed in a sandwich ELISA format and CRP was quantified through alkaline phosphatase enzymatic turnover of p-aminophenyl phosphate to p-aminophenol. To the best our knowledge, this is the first report directly synthesizing p-aminophenyl diazonium as a tosylate salt and using TPEs as immunosensor platforms.

2.3 Experimental

Reagents

Bup^{HTM} Phosphate Buffered Saline Packs (PBS), SuperBlock™ (PBS) Blocking Buffer, sulfo-NHS-biotin, sodium nitrite (99.55%), sulfuric acid (H_2SO_4), isopropanol (IPA, HPLC grade), methylene chloride (DCM, Fisher Scientific), and magnesium chloride ($MgCl_2$) were sourced from Thermo Fisher Scientific. p-Toluenesulfonic acid (≥98%), N-(3-Dimethylaminopropyl)-N'-ethylcarbodiimide hydrochloride (EDC), potassium ferrocyanide (≥98.5%), potassium ferricyanide (99%), sodium chloride (NaCl, ≥99.5%),

and myoglobin from horse heart were sourced from Sigma-Aldrich. P-nitroaniline (99.9%) was sourced from CHEM-IMPEX INT'L INC., and p-phenylenediamine (99%) from Frontier Scientific. Sodium hydroxide (NaOH, 1N), and TRIS-HCl were sourced from J.T. Baker. Bovine serum albumin (BSA, Microbiological grade) was sourced from MP Biomedicals, streptavidin-ALP from MABTECH, and p-aminophenol phosphate (p-APP) from BIOSYNTH. N-hydroxysuccinimide (NHS, ≥98.5%) was sourced from Fluka, and 2-ethanesulfonic acid (MES, 99+%) from Acros Organics. Anti-CRP Goat Polyclonal Antibody and Anti-CRP Mouse Monoclonal Antibody C7 (Biotin) were sourced from Abnova. Human CRP protein (>95% pure) was sourced from Fitzgerald. The fetal bovine serum (FBS, 100%) was sourced from Atlas biological. The buffer concentrations used were 0.1 M sodium phosphate 0.15 M NaCl (pH 7.4) for PBS, 0.1 M MES (pH 6), and 0.1 M tris-HCl 0.1 M NaCl 5 mM $MgCl_2$ (pH 9) for tris-HCl.

Electrochemical Measurements

Electrochemical measurements and pre-treatments were performed with a CHI 660b potentiostat. For 2.5 mm disk electrode experiments, a saturated calomel (SCE) reference electrode was used. The SCE and potentiostat were both sourced from CH Instruments Inc. Cyclic voltammetry (CV) measurements of the modified TPEs were conducted between -0.8 and 0.8 V vs. SCE with a scan rate of 100 mV/s. Nitrophenyl coverage calculations were performed as previously described in the literature.[36] A homemade Ag/AgCl electrode was used for SWV measurements. Square wave voltammetry measurements were taken from -0.2 V to 0.3 V vs. Ag/AgCl with a 4 mV increment voltage, 25 mV amplitude, and 15 Hz frequency for blocking optimization experiments. Further SWV measurements, following SWV parameter optimization, were taken from -0.15 to 0.25 V vs. Ag/AgCl with

a 2 mV increment voltage, 50 mV amplitude, and 10 Hz frequency. Replicate electrode measurements are shown herein as averaged values with error bars representing the standard deviations.

Electrode Fabrication

For the working (WE) and counter electrodes (CE), Thermomorph™ was used as an inexpensive source of polycaprolactone (PCL). Optix poly(methyl methacrylate) (PMMA) was sourced from Plaskolite and used in the binder and for the electrode template material. PMMA templates were cut with an Epilog CO_2 laser cutter (settings: speed=30% power=100% and frequency=5000 Hz) and designed with the graphic design program CorelDRAW. High Purity Micronized Graphite (~15 μm, 99.5–99.99%, Great Lakes Graphite) was used as the conductive carbon source. TPEs were fabricated by dissolving 1.5 g of plastic (2:1 PCL:PMMA) in ~15 mL of DCM. Three grams of graphite were added to the dissolved plastic, and the material was mixed while drying on a silicon wafer plate. The dried material was removed from the plate with a razor blade and milled in a coffee bean grinder before use. Electrodes were heat pressed into templates at 80–90 °C using a hydraulic heated press (Carver, Inc.) at a pressure of 300–500 psi. Excess electrode material was sanded off and connections were made with silver paint, copper wires, and epoxy purchased from a local store. Initial modification studies were performed on 2.5 mm diameter disk electrodes with 4 mm diameter CE due to the simplicity of fabricating larger electrodes. Later assays were performed on electrode arrays consisting of six 1 mm WE and 1.5 mm diameter CE pairs with laser cutter etched circles to keep solution droplets separate.

Electrode Pre-Treatment

Prior to modification, electrodes were sanded with 150 grit sandpaper for bulk removal of surface material and any prior modification, then the surfaces were smoothed out via polishing

with 600 grit sandpaper. After each polish, the electrodes were sonicated for one min in Milli-Q water to remove loosely packed material. Cathodic pre-treatments were performed at -1.5 V vs. SCE for 30 seconds in 0.1 M sulfuric acid. Anodic pre-treatments were performed at +1.5 V vs. SCE for 30 seconds in 0.1 M sodium hydroxide. Electrodes were stored in Milli-Q water when not in use and allowed to air dry prior to modification.

Safety

No violent reactions were observed for these syntheses; however, diazonium salts are highly reactive. Working in small quantities and performing synthesis on smooth surfaces is recommended.[25, 36] P-toluene sulfonic acid acts as a stabilizing agent for the diazonium salts so it is vital to mix in excess prior to adding the sodium nitrite reactant.[36] Toxic substances and nitrogen oxides are produced in this reaction, so PPE such as a lab coat and goggles, as well as working in a chemical hood are necessary.[36]

Diazonium salt synthesis and modification

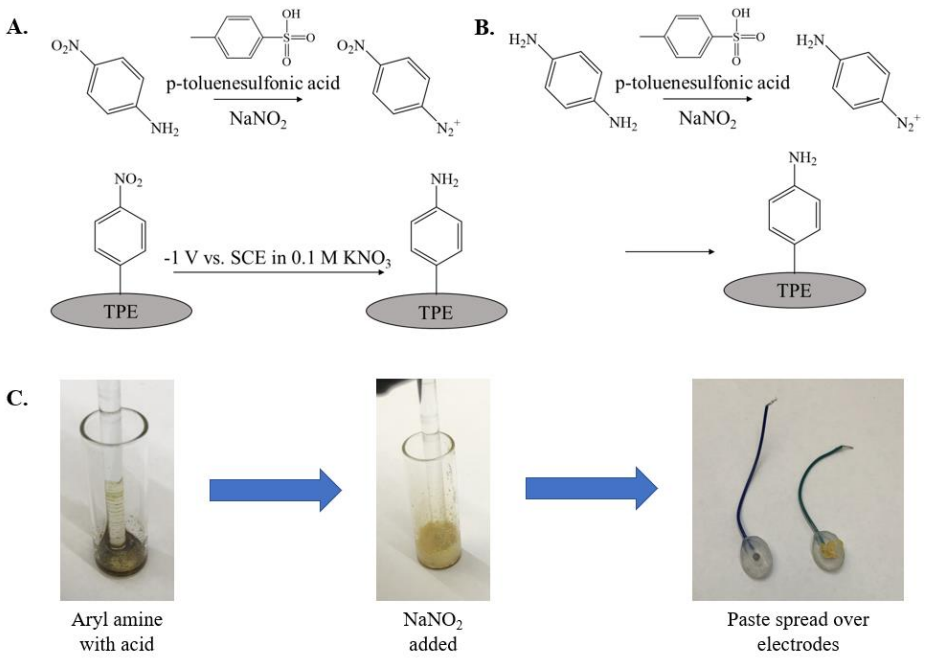

Fig. 2.1 Diazonium salt synthesis and modification schematics. A) p-nitrophenyl diazonium salt modification and subsequent reduction of nitro groups to amines, B) p-aminophenyl diazonium salt modification, and C) reaction and modification images with p-nitrophenyl diazonium salt shown.

The diazonium synthesis reactions and modification are shown in Fig. 2.1 Reaction pastes were synthesized by grinding the aryl amine and p-toluene sulfonic acid in an open glass vial using a glass stir rod. After 1 min passed and a homogenous paste was observed, sodium nitrite was added, and the paste was mixed vigorously for another 5 min. For early optimization of the synthesis and modification, p-nitrophenyl diazonium salt was synthesized using 0.2 mmol p-nitroaniline, 0.6 mmol p-toluenesulfonic acid, 75 µL water, and 0.5 mmol sodium nitrite. For p-aminophenyl diazonium salt synthesis, p-phenylene diamine can be added in excess of sodium nitrite to produce primarily monodiazonium salts.[39] p-Aminophenyl diazonium salt was synthesized using 0.3 mmol p-phenylene diamine, 0.6 mmol p-toluenesulfonic acid, 200 µL water, and 0.2 mmol sodium nitrite. The batch quantities were tripled for TPE array modifications, thus, up to three TPE arrays could be modified using a single batch of diazonium paste. The amounts of

water to add for each paste type were optimized by adding water in 25 µL aliquots until an easily spreadable paste was achieved.

Following synthesis, the diazonium salt reaction pastes were spread over the TPE surfaces and left in petri dishes containing wet paper towels to prevent the paste from drying out. After 5 min, the paste was rinsed off with 0.1 M sulfuric acid, then the electrodes were washed thoroughly with Milli-Q water. To remove unreacted paste components with poor water-solubility, the electrodes were sonicated in isopropanol, then rinsed thoroughly with Milli-Q water again.

Electrode pre-treatment, sonication time, and paste incubation time were optimized using the p-nitrophenyl diazonium salt modification and nitrophenyl coverage was determined with CV. Coverage stability was also tested by looking at nitrophenyl coverage with CV. For the CRP ELISA experiments, aryl amines were pre-ground with a mortar and pestle to achieve a more uniform paste and more consistent voltammetry (S2.1).

Blocking Optimization

Different blockers of nonspecific adsorption were incubated on the diazonium modified TPE surfaces. Blocking optimization was performed on reduced p-nitrophenyl and p-aminophenyl diazonium salt modified electrodes. Nitrophenyl surface groups were electrochemically reduced at -1V vs. SCE for 30s in 0.1 M KNO_3. Diazonium modified electrodes were incubated with 1% (w/v) BSA in PBS, SuperBlock™, and 1% (w/v) BSA diluted in SuperBlock™ for one hour. 1:100 dilutions of streptavidin-ALP solutions were prepared in Tris-HCl and incubated on the electrode surfaces for 30 min. Electrodes were incubated in 4 mM p-APP substrate in tris-HCL for 20 min. Nonspecific enzymatic turnover of p-AP was measured following the 20 min incubation period with SWV. Three Tris-HCl washes were performed between each step. 20 µL aliquots were used

for all modification and wash steps. All modification steps for this experiment and further assays were performed in humidified petri dishes to prevent evaporation.

Streptavidin-ALP biotin assay as proof of concept

To provide a proof-of-concept for the use of diazonium tosylate modified TPEs for immunosensors, biotin was conjugated to TPEs and used to capture streptavidin-ALP as a model system, shown in Fig. 2.2a Biotin-streptavidin-ALP assays were performed on reduced p-nitrophenyl, p-aminophenyl and reduced p-aminophenyl diazonium salt modified electrodes. Nitrophenyl and aminophenyl modified electrodes were electrochemically reduced at -1V vs. SCE for 30s in 0.1 M KNO_3. Electrodes were incubated with 1 mM sulfo-NHS-biotin in PBS for one hour. 1:100 dilutions of streptavidin-ALP solutions were prepared in Tris-HCl and incubated on the electrode surfaces for 30 min. 1% (w/v) BSA in Superblock was incubated on the electrodes for 1 h to block nonspecific binding. Background signal was tested with SWV in Tris-HCl prior to 20 min incubation in 4 mM p-APP substrate in tris-HCL. Enzymatic turnover of p-AP was measured following the 20-min incubation period with SWV. Three tris-HCl washes were performed between each step. 20 µL aliquots were used for all modification and wash steps. Relative streptavidin-biotin binding was quantified by background subtracting the Tris-HCl blank measurements from the measurements taken after 20 min in p-APP and integrating the resulting p-AP peaks to determine peak area.

CRP ELISA

For CRP ELISA experiments, aminophenyl, and reduced p-aminophenyl diazonium salt modified electrodes were further modified as shown in Fig. 2.2b Nitrophenyl and aminophenyl modified electrodes were electrochemically reduced at -1V vs. SCE for 30s in 0.1 M KNO_3.

Modified TPEs were incubated with 4 mM NHS in PBS for one hour. Anti-CRP/EDC (25 µg/mL; 4 mM) solutions were prepared in MES buffer and incubated on the electrode surfaces for one hour. 1% (w/v) BSA in SuperBlock™ was incubated on the electrodes for one hour to block nonspecific binding. CRP samples (0.1, 1, 10, 100, 1000, 10000 ng/mL in PBS) and myoglobin controls (1000 ng/mL in PBS) were incubated for 30 min. Biotinylated anti-CRP (5 µg/mL in PBS) was incubated for 30 min. A 1:1000 dilution of streptavidin-alkaline phosphatase was made in Tris-HCl and incubated on the electrode surfaces for 30 min. Background signal was tested with SWV in Tris-HCl prior to 20 min incubation in 4 mM p-APP substrate in Tris-HCl. Enzymatic turnover of p-AP was measured following the 20 min incubation period with SWV. Three washes were performed between each step. For the early steps, washes were performed in PBS. Following biotinylated anti-CRP modification, washes were performed in Tris-HCl. 20 µL aliquots were used for all modification and wash steps.

Assay response was quantified by subtracting background signal of the Tris-HCl as a blank solution from the SWV signal obtained after 20 min in p-APP. The final p-AP peaks were used to determine peak area and generate CRP calibration curves for the the reduced nitrophenyl and reduced aminophenyl modified electrodes shown in Fig. 2.6. The calibration curves in Fig. 2.6 were fitted with four-parameter logistic (4PL) regressions using MATLAB (S2.5).

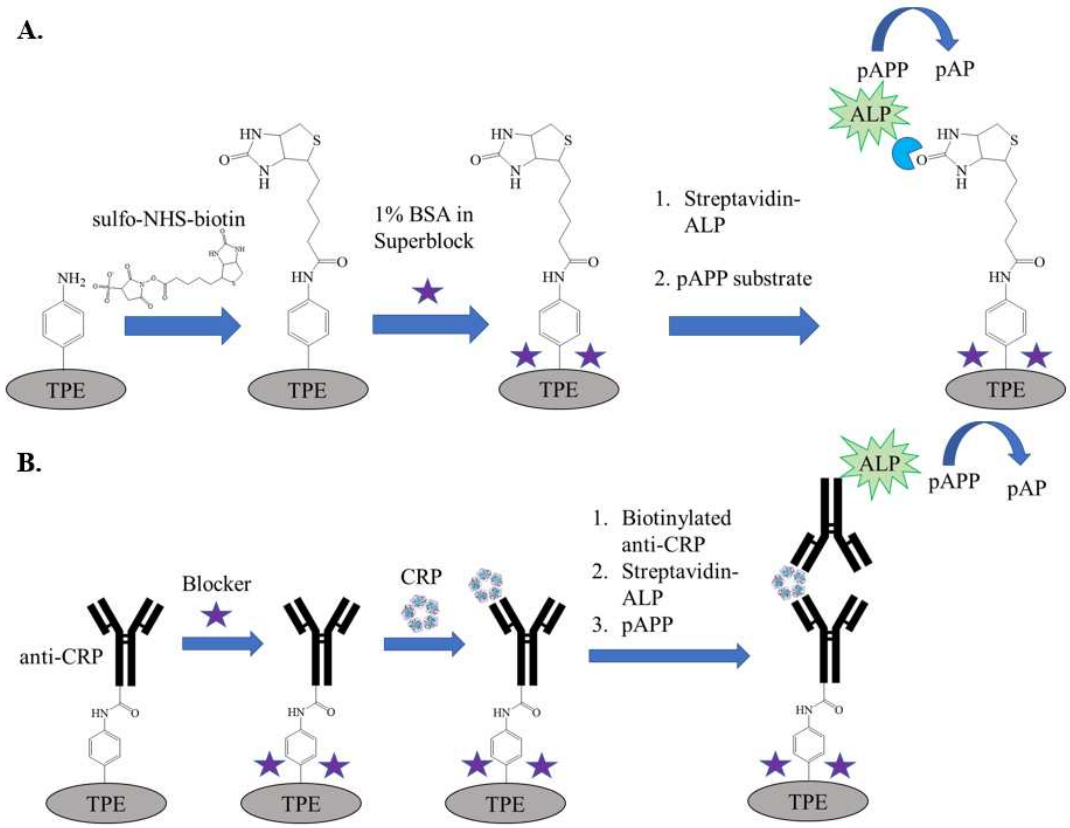

Fig. 2.2 Assay modification schematics. A) Streptavidin-ALP biotin proof of concept assay. B) CRP ELISA assay.

Serum Samples

Electrodes were modified with anti-CRP and blocker as described in the previous section. FBS serum was used as a surrogate for human serum. The serum sample was diluted and spiked with CRP to final concentrations of 0, 1, 10, 100, and 1000 ng/mL CRP in 100-fold diluted serum. Diluted serum samples were incubated for 30 min on the modified electrode surfaces and further washes and modification steps were performed as described in the previous section.

2.4 Results and Discussion

Electrode Pre-Treatment Optimization

Electrode pre-treatment optimization included: (i) sanding alone, (ii) sanding and anodic treatment, and (iii) sanding and cathodic treatment. Following pre-treatment electrodes were modified and nitrophenyl coverage was calculated for each pre-treatment (Fig. 2.3a). Pre-treatment voltammetry is shown in Fig. S2.2 and quantitative coverage data is presented in Fig. 2.3a. It was observed that anodic treatment of the electrodes resulted in inconsistent nitrophenyl coverage, high background current, and poorly resolved peaks. Sanded and cathodically treated electrodes had more consistent nitrophenyl coverage compared to oxidized electrodes. Since cathodic treatment of the electrodes exhibited higher coverage and sharper peaks than sanding pre-treatment, cathodic pre-treatment was used for further experiments.

Sonication Optimization

To investigate the effect of the duration of sonication on nitrophenyl coverage, the electrodes were sonicated in IPA for durations of zero to 20 min. The nitrophenyl coverage of the electrodes was calculated and presented in Fig. 2.3b. It was observed that nitrophenyl coverage was much higher without the sonication step compared to coverage after sonication in IPA. For the modified electrode CVs without sonication, there was a double peak for nitro reduction, indicating a large amount of adsorbed p-nitroaniline and nitrophenyl diazonium salt. After 5 min sonication in IPA, there was a large decrease in coverage to an expected level for a nitrophenyl monolayer (0.5–0.8 nmol/cm^2).[36] This suggests the removal of loosely adsorbed paste material.[36] After 10 min the nitrophenyl coverage stabilized and coverage variability between electrodes was at its lowest, so 10 min sonication in IPA was used for further experiments.

Modification Time

The impact of incubation time and humidity were evaluated, and the data is presented in Fig. 2.3c. To increase the humidity, electrodes were placed in petri dish containing wet paper towels. Increasing the reaction time or humidity did not have a statistically significant impact on the nitrophenyl coverage. However, performing the reaction in a humidified petri dish kept the paste from drying out making it easier to remove the reaction paste through rinsing following modification. Whereas the nitrophenyl coverage for 5 min incubation of reaction paste was 0.5 ± 0.2 nmol/cm^2, it was 0.6 ± 0.1 nmol/cm^2 for 15 min under humidified conditions. Since most to all the modification occurs within the first 5 min of incubation of reaction paste on the electrode surface, a 5 min modification in a humidified petri dish was used for all further experiments.

Coverage Stability

Stability tests were performed with the electrodes modified with the optimized diazonium procedure and kept in Milli-Q water in a covered beaker for up to a week. The nitrophenyl coverage was determined using CV. The obtained data for this experiment is shown in Fig. 2.3d. As can be seen in Fig. 2.3d, coverage did not decrease with time; the replicates tested the day of modification had 0.3 ± 0.1 nmol/cm^2 coverage and the replicates tested a week later had 0.4 ± 0.1 nmol/cm^2 coverage. This shows that this nitrophenyl modification on TPEs is stable for at least one week.

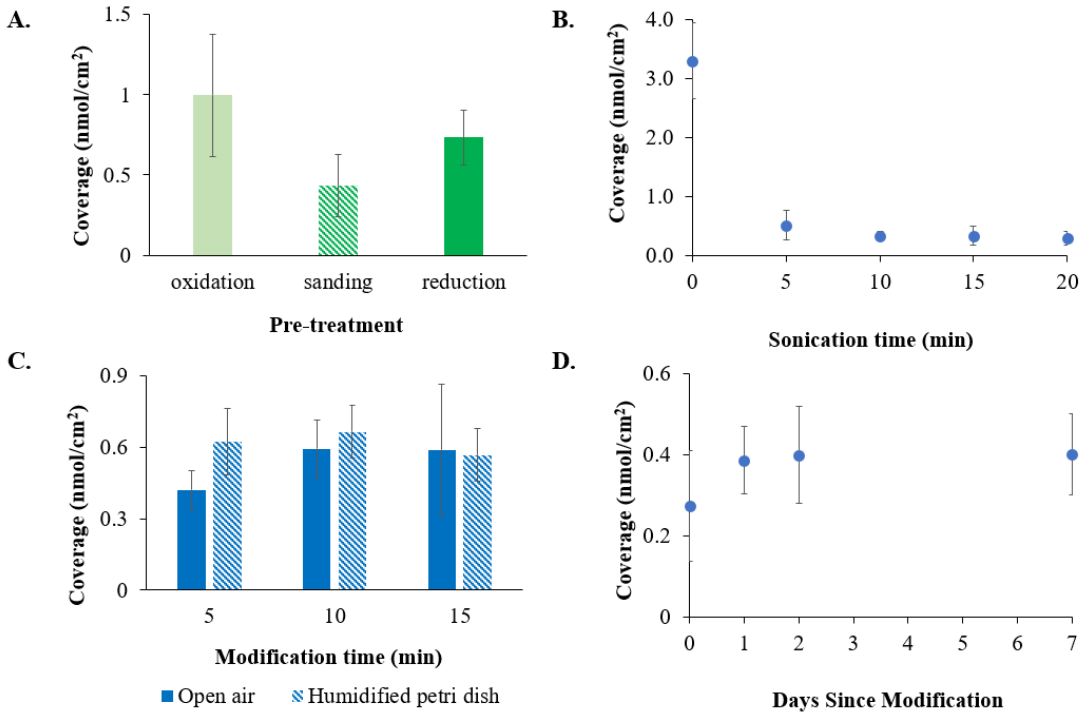

Fig. 2.3. P-nitroaniline modification optimization and stability testing. A) Pretreatment optimization (n=4), B) sonication time in IPA following modification (n=4), C) modification time and conditions: open air (5 and 10 min n=5; 15 min n=7) and humidified petri dish (5 min n=9; 10 and 15 min n=5), and D) Coverage stability.

Geometry and Nitrite Impact on Nitrophenyl Coverage

The effect of sodium nitrite on nitrophenyl coverage of the electrodes was investigated by employing CV using 1 mm diameter electrode arrays modified with the optimized procedure in the presence and absence of sodium nitrite. As can be seen in Fig. 2.4a from the substantial increase in nitrophenyl reduction peak area when sodium nitrite is used, the reaction with sodium nitrite is responsible for the majority of the nitrophenyl coverage on the electrode surface. The average nitrophenyl coverage calculated for the 2.5 mm diameter disk electrodes in Fig. 2.3c was compared to the average coverage calculated from the 1 mm diameter array electrodes to investigate the impact of electrode geometry on coverage. The average coverage/geometric area on 1 mm electrode arrays (1.0 ± 0.2 nmol/cm^2) was two-fold higher than 2.5 mm disks (0.5 ± 0.2 nmol/cm^2). Further investigation into the coverage and capacitance of arrays vs. disks (S2.3) shows that the

capacitance/geometric area for the 1 mm arrays is 2.6 times higher than that of the 2.5 mm disks: 490 ± 50 μF/cm^2 for arrays, and 190 ± 70 μF/cm^2 for single recipe disks. Higher capacitance suggests higher real surface area/geometric surface area. Therefore, we hypothesize this coverage disparity is due to higher surface roughness on the array electrodes introduced during the electrode fabrication and modification steps.

Direct Modification with p-Aminophenyl Diazonium Salt

Aminophenyl monodiazonium salts can be synthesized directly by limiting the amount of sodium nitrite to prevent didiazonium salt formation.[39] Lyskawa, et al. demonstrated that when 1 molar equivalence of sodium nitrite to p-phenylenediamine is used 90% of the product is the monodiazonium and 10% of the product is the didiazonium salt.[39] When 1 molar equivalence was used for the diazonium tosylate reaction paste, the thickness and color of the paste varied significantly between batches. As small amounts were used, this inconsistency was likely due to variability in whether the nitrite or aryl amine was the limiting reactant. High background current was also seen for a wide potential range from several unanticipated peaks in the CVs shown in Fig. S2.4 To reduce paste variability, 0.75 molar equivalence was tried instead, and the paste color became more consistent and there were fewer background peaks in the CVs, shown in Fig. S2.4 The CVs of the optimized aminophenyl modification (Fig. 2.4b) with and without sodium nitrite also show that the reaction with sodium nitrite is responsible for the majority of the electroactive surface groups.

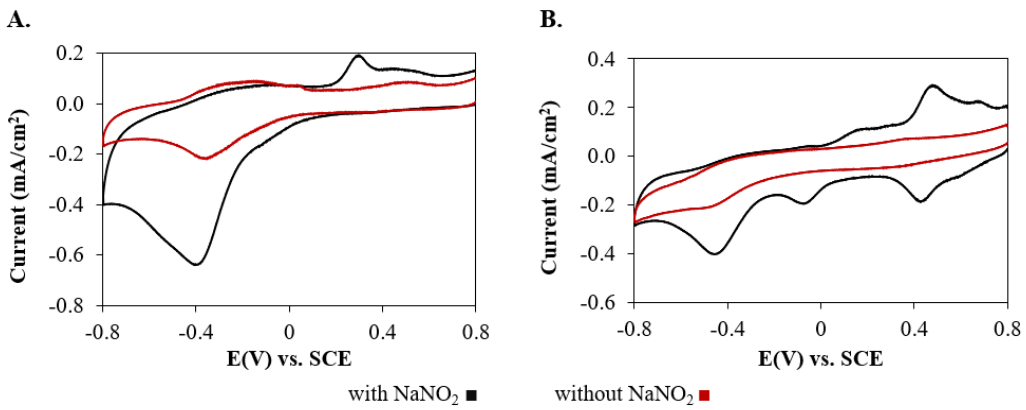

Fig. 2.4 Averaged cyclic voltammetry of modified 1 mm diameter TPEs in N_2 degassed 0.1 M H_2SO_4 v=100 mV/s, modified with and without $NaNO_2$. A) p-nitrophenyl diazonium salt modification (with $NaNO_2$ n=16; without $NaNO_2$ n=6), B) p-aminophenyl diazonium salt modification (with $NaNO_2$ n=6; without $NaNO_2$ n=6).

Blocking Optimization

To prevent signal from nonspecific adsorption, different blockers were evaluated. Peak currents for p-AP were used to quantify relative nonspecific adsorption and quantitative data is shown in Fig. 2.5a When SuperBlock™ alone was used, the highest amounts of nonspecific adsorption were seen for both diazo modification strategies, 0.23 ± 0.03 µA and 0.24 ± 0.02 µA p-AP peak current for PN and PPD, respectively. BSA showed less nonspecific adsorption on average but higher variability in blocking on reduced p-nitrophenyl electrodes, but much higher blocking for p-aminophenyl modification than SuperBlock™, 0.15 ± 0.08 µA and 0.02 ± 0.01 µA for PN and PPD, respectively. BSA diluted in SuperBlock™ was the best blocker for aminophenyl modification and was not statistically different from BSA for reduced p-nitrophenyl modification 0.039 ± 0.004 µA and 0.04 ± 0.03 µA for PN and PPD, respectively. Therefore, BSA in Superblock™ was used for all subsequent experiments.

Streptavidin-ALP Biotin Assay

All amine functionalization strategies showed promising signal response on biotinylated electrodes and low response on unbiotinylated controls. Data for this experiment is shown in Fig. 2.5b–d. Reduced p-nitrophenyl-modified electrodes had the lowest signal, but the sharpest and best resolved peaks. Aminophenyl-modified electrodes, without further reduction, show similar response to reduced nitrophenyl modified electrodes. However, aminophenyl-modified electrodes have broader response peaks and lower reproducibility. When aminophenyl-modified electrodes are reduced electrochemically prior to further modification, the signal is significantly higher and much more reproducible, although the peaks are still broader than reduced nitrophenyl-modified electrodes. These results, along with the results of blocking optimization, suggest denser surface coverage is achieved from direct aminophenyl-modification. Improvement of the signal following reduction agrees with our hypothesis that oxidized amine forms exist on the surface following direct aminophenyl modification.

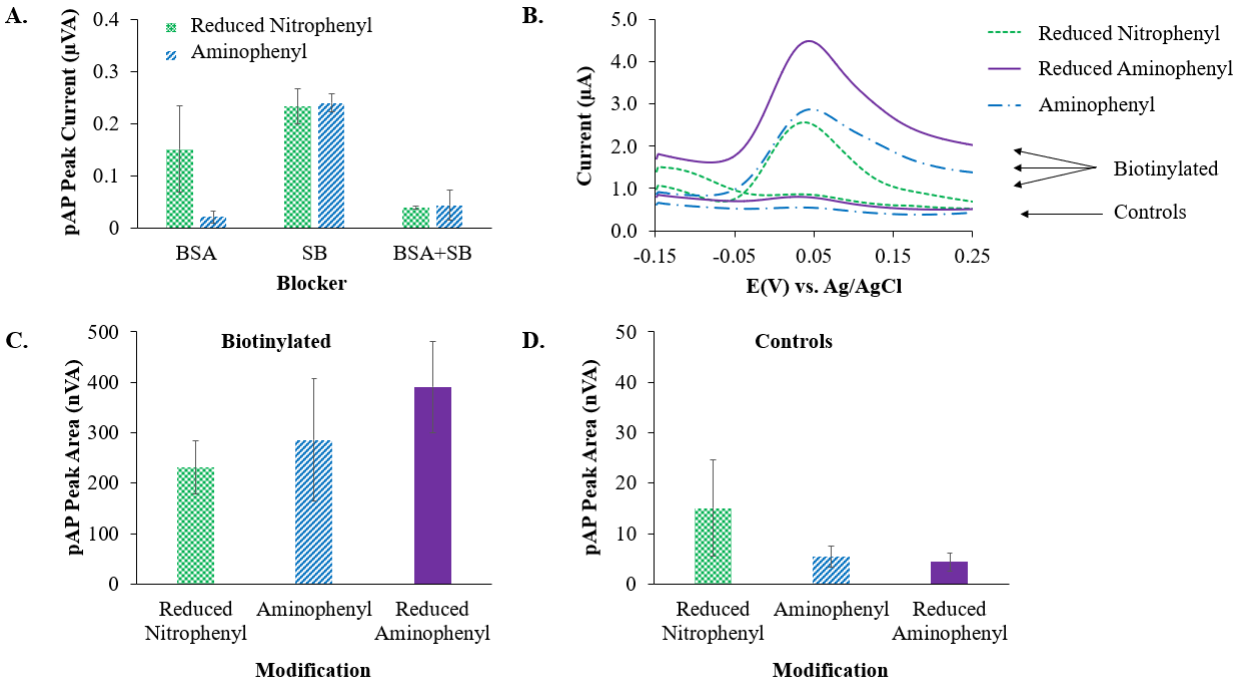

Fig. 2.5. Streptavidin-ALP assay data for reduced nitrophenyl, direct aminophenyl, and reduced aminophenyl modified electrodes from ALP generated p-AP SWV. A) Quantitative blocking optimization peak current data (BSA n=6; SB and BSA+SB n=3), B) averaged voltammograms for biotinylated TPEs and unbiotinylated controls (biotinylated n=6; controls n=3), C) quantitative peak area data for biotinylated electrodes, and D) quantitative peak area data for unbiotinylated controls.

CRP ELISA Calibration in Buffer

These sensors were used to generate a calibration curve for CRP, calibration data is shown in Fig. 2.6. For the CRP ELISA assays in buffer, both methods showed similar dynamic ranges from 1–1000 ng/mL. The ELISA results indicate that the assay is useful for monitoring CRP in serum at 100-fold dilutions. Healthy CRP levels in blood are <1 µg/mL, but levels can rise 10^3-fold in patients with cardiovascular risk.[40] The LODs for both methods were 2 ng/mL CRP and were calculated from the myoglobin blanks (blank+3SD_{blank}), as the presence of other protein is more representative of a real system than buffer blanks. The myoglobin blank pAP peak areas for each modification strategy (19 ± 2 nVA for nitrophenyl; 44 ± 1 nVA for aminophenyl modification) were not statistically different from pAP peak areas from buffer blanks (20 ± 2 nVA

for nitrophenyl; 44 ± 4 nVA for aminophenyl modification) showing that the assay is specific to CRP. Although the LODs were the same: 2 ng/mL, the reduced aminophenyl modification strategy showed more sensitive response to increasing CRP concentration in the dynamic range and was therefore used for the assay in serum.

CRP ELISA in Spiked Serum Samples

Calibration data for spiked serum samples is also shown in Fig. 2.6. The LOD in serum was five times higher than the LOD in myoglobin at 10 ng/mL due to an increase in nonspecific signal and variability in the 0 ng/mL serum blank. This may be attributed to some degree of cross-reactivity of the CRP antibodies and bovine CRP present in FBS. The pAP peak area data for spiked 100-fold diluted serum showed no loss in sensitivity relative to that of buffer. The 4-PL fit coefficients determined in serum fell within the 95% confidence interval of the fit coefficients in buffer (S.5). The serum results were not significantly different from the buffer results for the concentrations tested, apart from 1 ng/mL concentration which is below the assay LOD.

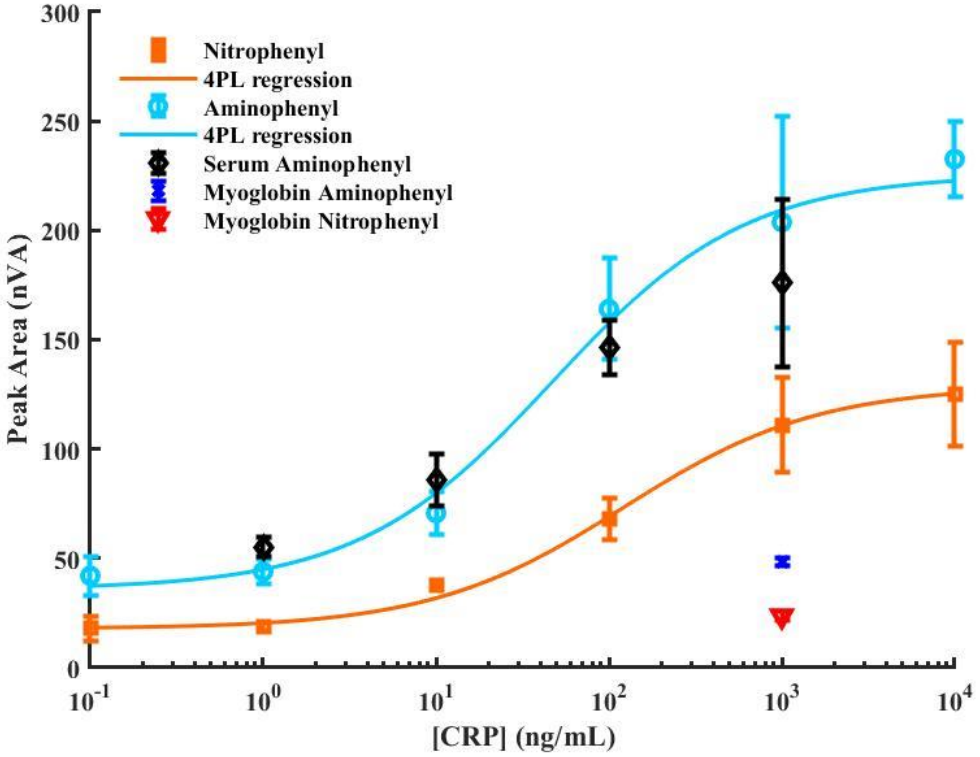

Fig. 2.6. CRP ELISA assay p-AP peak area data for reduced nitrophenyl (Nitrophenyl) modified electrodes and reduced aminophenyl (Aminophenyl) modified electrodes for various concentration of CRP in PBS buffer pH=7.4 (0.1-10^4 ng/mL; n=4 for all but PPD 10^3 ng/mL [n=3]), CRP spiked 100x diluted serum (1-10^3 ng/mL; n=3), and 10^3 ng/mL myoglobin (n=3).

2.5 Conclusion

In this study, nitrophenyl and aminophenyl diazonium tosylates were in situ synthesized in water reaction pastes from aryl amines under ambient conditions and were used to successfully modify TPEs with amine functional groups. Functionalized TPEs were conjugated to antibodies and used to perform selective CRP ELISAs in PBS buffer, with clinically relevant detection limits. These TPE biosensors also demonstrated no loss in sensitivity when the assay was performed in serum. Further optimization would be required for determination in saliva where healthy CRP levels average around 289 pg/mL and cardiovascular disease patients average just below the LOD at 1680 pg/mL.[37] However, with further assay optimization and volume reduction, determination in saliva could likely be achieved. In addition, this sensing platform can be easily adapted for

simultaneous detection of various biomarkers with the use of modified TPE-microarray for POC diagnostics at reduced costs.

REFERENCES

1. Bahadir, E. B.; Sezginturk, M. K., Applications of electrochemical immunosensors for early clinical diagnostics. *Talanta* **2015,** *132*, 162-174.

2. Heineman, W. R.; Halsall, H. B., Strategies for electrochemical immunoassay. *Analytical chemistry* **1985,** *57* (12), 1321A-1331A.

3. Wehmeyer, K. R.; Halsall, H.; Heineman, W., Heterogeneous enzyme immunoassay with electrochemical detection: competitive and" sandwich"-type immunoassays. *Clin. Chem.* **1985,** *31* (9), 1546-1549.

4. McCreery, R. L., Advanced carbon electrode materials for molecular electrochemistry. *Chem. Rev.* **2008,** *108* (7), 2646-2687.

5. Klunder, K. J.; Nilsson, Z.; Sambur, J. B.; Henry, C. S., Patternable Solvent-Processed Thermoplastic Graphite Electrodes. *J. Am. Chem. Soc.* **2017,** *139* (36), 12623-12631.

6. Klunder, K. J.; Clark, K. M.; McCord, C.; Berg, K. E.; Minteer, S. D.; Henry, C. S., Polycaprolactone-enabled sealing and carbon composite electrode integration into electrochemical microfluidics. *Lab Chip* **2019,** *19* (15), 2589-2597.

7. Noviana, E.; Klunder, K. J.; Channon, R. B.; Henry, C. S., Thermoplastic Electrode Arrays in Electrochemical Paper-Based Analytical Devices. *Analytical Chemistry* **2019,** *91* (3), 2431-2438.

8. Berg, K. E.; Leroux, Y. R.; Hapiot, P.; Henry, C. S., Increasing Applications of Graphite Thermoplastic Electrodes with Aryl Diazonium Grafting. *ChemElectroChem* **2019,** *6* (18), 4811-4816.

9. Pradela-Filho, L. A.; Noviana, E.; Araujo, D.; Takeuchi, R.; Santos, A.; Henry, C. S., Rapid Analysis in Continuous Flow Electrochemical Paper-Based Analytical Devices. *ACS Sens.* **2020**.

10. Welch, N. G.; Scoble, J. A.; Muir, B. W.; Pigram, P. J., Orientation and characterization of immobilized antibodies for improved immunoassays. *Biointerphases* **2017,** *12* (2).

11. Ricci, F.; Adornetto, G.; Palleschi, G., A review of experimental aspects of electrochemical immunosensors. *Electrochimica Acta* **2012,** *84*, 74-83.

12. Yanez-Sedeno, P.; Campuzano, S.; Pingarron, J. M., Integrated Affinity Biosensing Platforms on Screen-Printed Electrodes Electrografted with Diazonium Salts. *Sensors* **2018,** *18* (2).

13. Svalova, T.; Malysheva, N.; Bubekova, A.; Saigushkina, A.; Medvedeva, M.; Kozitsina, A., Effect of the Method for Immobilizing Receptor Layer on the Analytical Characteristics of a Label-Free Electrochemical Immunosensor for the Determination of Measles Antibodies. *Journal of Analytical Chemistry* **2020,** *75* (2), 254-261.

14. Sethi, J.; Van Bulck, M.; Suhail, A.; Safarzadeh, M.; Perez-Castillo, A.; Pan, G., A label-free biosensor based on graphene and reduced graphene oxide dual-layer for electrochemical determination of beta-amyloid biomarkers. *Microchim. Acta* **2020,** *187*, 1-10.

15. Chekin, F.; Singh, S. K.; Vasilescu, A.; Dhavale, V. M.; Kurungot, S.; Boukherroub, R.; Szunerits, S., Reduced graphene oxide modified electrodes for sensitive sensing of gliadin in food samples. *ACS Sens.* **2016,** *1* (12), 1462-1470.

16. Singh, V.; Krishnan, S., Voltammetric immunosensor assembled on carbon-pyrenyl nanostructures for clinical diagnosis of type of diabetes. *Analytical chemistry* **2015,** *87* (5), 2648-2654.

17. Channon, R. B.; Yang, Y. Y.; Feibelman, K. M.; Geiss, B. J.; Dandy, D. S.; Henry, C. S., Development of an Electrochemical Paper-Based Analytical Device for Trace Detection of Virus Particles. *Analytical Chemistry* **2018,** *90* (12), 7777-7783.

18. Pereira, S. V.; Bertolino, F. A.; Fernandez-Baldo, M. A.; Messina, G. A.; Salinas, E.; Sanz, M. I.; Raba, J., A microfluidic device based on a screen-printed carbon electrode with electrodeposited gold nanoparticles for the detection of IgG anti-Trypanosoma cruzi antibodies. *Analyst* **2011,** *136* (22), 4745-4751.

19. Sharafeldin, M.; McCaffrey, K.; Rusling, J. F., Influence of antibody immobilization strategy on carbon electrode immunoarrays. *Analyst* **2019,** *144* (17), 5108-5116.

20. Cao, M.; Fu, A.; Wang, Z.; Liu, J.; Kong, N.; Zong, X.; Liu, H.; Gooding, J. J., Electrochemical and theoretical study of π–π stacking interactions between graphitic surfaces and pyrene derivatives. *The Journal of Physical Chemistry C* **2014,** *118* (5), 2650-2659.

21. Srisombat, L.; Jamison, A. C.; Lee, T. R., Stability: A key issue for self-assembled monolayers on gold as thin-film coatings and nanoparticle protectants. *Colloids and Surfaces A: Physicochemical and Engineering Aspects* **2011,** *390* (1-3), 1-19.

22. Mahouche-Chergui, S.; Gam-Derouich, S.; Mangeney, C.; Chehimi, M. M., Aryl diazonium salts: a new class of coupling agents for bonding polymers, biomacromolecules and nanoparticles to surfaces. *Chem. Soc. Rev.* **2011,** *40* (7), 4143-4166.

23. Gooding, J. J., Advances in interfacial design sensors: Aryl diazonium salts for electrochemical biosensors and for modifying carbon and metal electrodes. *Electroanalysis* **2008,** *20* (6), 573-582.

24. Hetemi, D.; Noël, V.; Pinson, J., Grafting of Diazonium Salts on Surfaces: Application to Biosensors. *Biosensors* **2020,** *10* (1), 4.

25. Sheng, M.; Frurip, D.; Gorman, D., Reactive chemical hazards of diazonium salts. *Journal of Loss Prevention in the Process Industries* **2015,** *38*, 114-118.

26. Siuzdak, K.; Niedziałkowski, P.; Sobaszek, M.; Łęga, T.; Sawczak, M.; Czaczyk, E.; Dziąbowska, K.; Ossowski, T.; Nidzworski, D.; Bogdanowicz, R., Biomolecular influenza virus detection based on the electrochemical impedance spectroscopy using the nanocrystalline boron-doped diamond electrodes with covalently bound antibodies. *Sensors and Actuators B: Chemical* **2019,** *280*, 263-271.

27. Sun, X. B.; Ma, Z. F., Highly stable electrochemical immunosensor for carcinoembryonic antigen. *Biosensors & Bioelectronics* **2012,** *35* (1), 470-474.

28. Sánchez-Tirado, E.; González-Cortés, A.; Yáñez-Sedeño, P.; Pingarrón, J., Electrochemical immunosensor for the determination of the cytokine interferon gamma (IFN-γ) in saliva. *Talanta* **2020,** *211*, 120761.

29. Martinez-Garcia, G.; Agui, L.; Yanez-Sedeno, P.; Pingarron, J. M., Multiplexed electrochemical immunosensing of obesity-related hormones at grafted graphene-modified electrodes. *Electrochimica Acta* **2016,** *202*, 209-215.

30. Liu, G.; Gooding, J. J., Towards the fabrication of label-free amperometric immunosensors using SWNTs. *Electrochemistry communications* **2009,** *11* (10), 1982-1985.

31. Harper, J. C.; Polsky, R.; Wheeler, D. R.; Brozik, S. M., Maleimide-activated aryl diazonium salts for electrode surface functionalization with biological and redox-active molecules. *Langmuir* **2008,** *24* (5), 2206-2211.

32. Abdulsattar, J. O.; Greenway, G. M.; Wadhawan, J. D., Electrochemical immunoassay for the detection of stress biomarkers. *Heliyon* **2020,** *6* (3), e03558.

33. Filimonov, V. D.; Trusova, M.; Postnikov, P.; Krasnokutskaya, E. A.; Lee, Y. M.; Hwang, H. Y.; Kim, H.; Chi, K.-W., Unusually stable, versatile, and pure arenediazonium tosylates: their preparation, structures, and synthetic applicability. *Organic letters* **2008,** *10* (18), 3961-3964.

34. Moon, M. E.; Choi, Y.; Lee, Y. M.; Vajpayee, V.; Trusova, M.; Filimonov, V. D.; Chi, K. W., An expeditious and environmentally benign preparation of aryl halides from aryl amines by solvent-free grinding. *Tetrahedron Lett.* **2010,** *51* (51), 6769-6771.

35. Gorlushko, D. A.; Filimonov, V. D.; Krasnokutskaya, E. A.; Semenischeva, N. I.; Go, B. S.; Hwang, H. Y.; Cha, E. H.; Chi, K. W., Iodination of aryl amines in a water-paste form via stable aryl diazonium tosylates. *Tetrahedron Lett.* **2008,** *49* (6), 1080-1082.

36. Via, G. G.; Shugart, C. L.; Melnyk, S. L.; Hupman, S. R.; Cline, K. K., One-step Solvent-free Synthesis and Grafting of Diazonium Ions at Glassy Carbon Electrodes. *Electroanalysis* **2018,** *30* (10), 2421-2426.

37. Punyadeera, C.; Dimeski, G.; Kostner, K.; Beyerlein, P.; Cooper-White, J., One-step homogeneous C-reactive protein assay for saliva. *Journal of Immunological Methods* **2011,** *373* (1-2), 19-25.

38. Zhang, X.; Wan, Y. X.; Chata, R.; Brazzale, A.; Atherton, J. J.; Kostner, K.; Dimeski, G.; Punyadeera, C., A pilot study to demonstrate diagnostic potential of galectin-3 levels in saliva. *Journal of Clinical Pathology* **2016,** *69* (12), 1100-1104.

39. Lyskawa, J.; Belanger, D., Direct modification of a gold electrode with aminophenyl groups by electrochemical reduction of in situ generated aminophenyl monodiazonium cations. *Chem. Mat.* **2006,** *18* (20), 4755-4763.

40. Pedrero, M.; Campuzano, S.; Pingarron, J. M., Electrochemical Biosensors for the Determination of Cardiovascular Markers: a Review. *Electroanalysis* **2014,** *26* (6), 1132-1153.

CHAPTER 3: REDOX BEHAVIOR AND SURFACE MORPHOLOGY OF POLYSTYRENE THERMOPLASTIC ELECTRODES

3.1 Chapter Overview

Most of the content of this chapter is taken from a 2021 manuscript published in *Electrochimica Acta* titled "Redox Behavior and Morphology of Polystyrene Thermoplastic Electrodes" with authors Cynthia P. McCord, Bali Summers, and Charles S. Henry*. Carbon composite electrodes consisting of graphite and a non-conductive binder are widely used due to their low cost and ease of fabrication but often suffer from slow electrode kinetics and high capacitance relative to traditional electrode materials such as gold and glassy carbon. Modifiers including metallic nanoparticles and carbon nanotubes are used to enhance electrode performance, but this complicates electrode preparation, increases cost, and limits reusability. Our group recently reported a new type of carbon composite electrodes called thermoplastic electrodes (TPEs) that use common thermoplastics mixed with graphite in a solvent processing system that give enhanced electrochemical performance. The polymers reported to date include polymethylmethacrylate, cyclic olefine copolymer, polycaprolactone (PCL), and blends of these materials. Polystyrene (PS) is an inexpensive and commonly used thermoplastic substrate, however, there are only several reports incorporating PS as a binder in carbon composite electrodes. Here, we report the first PS TPEs and show their unique electrochemical behavior relative to electrodes made with other binders. These unmodified composite materials surpass the performance of traditional electrode materials and show similar behavior to nanomaterial-modified electrodes. The capacitance and conductivity were measured for PS and PS-PCL blends using PCL TPEs as a reference. Even small additions of PS to PCL TPEs substantially lowered capacitance

and increased conductivity. The electrochemistry of PS and PS-PCL TPEs was investigated using cyclic voltammetry with various common and biologically relevant redox probes. The effect of differing molecular weight and the use of waste expanded polystyrene (EPS) were explored as well, and all PS binder TPEs were found to exhibit similar redox behavior. Optical profilometry (OP) and scanning electron microscopy (SEM) were used to examine morphological characteristics. OP showed lower surface roughness for PS electrodes than for PCL ones, explaining the lower capacitance. SEM data suggests the source of this enhanced redox behavior stems from the edge-plane rich PS TPE surfaces.

3.2. Introduction

Carbon composite electrodes are useful for many applications ranging from energy storage[1-3] to bioanalysis.[4-7] Carbon electrodes exhibit advantages over metallic electrodes such as biocompatibility, wide potential windows, and low cost.[6, 8] Compared to other common carbon electrode materials such as HOPG, glassy carbon, and BDD, composite carbon electrodes are inexpensive, easy to fabricate, and more mechanically robust.[5, 7-8] However, carbon composite electrodes often suffer from poor moldability, low conductivity, and poor electron transfer kinetics.[9-10] To mitigate these disadvantages, nanomaterials such as graphene and metallic nanomaterials are frequently added. However, these modifications can complicate electrode preparation and reproducibility, limit reusability, and increase cost.

In recent years, our group has reported on the development and characterization of thermoplastic electrodes (TPEs) as easily moldable carbon composites with excellent conductivity and electron transfer kinetics.[10-14] TPEs are made by a simple fabrication process wherein the thermoplastic binder is dissolved in a volatile solvent, mixed with graphite or carbon black, dried, and heat pressed into a template. Thermoplastic binders polymethyl methacrylate (PMMA),[10, 14]

polycaprolactone (PCL),[11, 14-16] and cyclic olefin copolymer (COC)[12-14] were previously used in TPEs. While these thermoplastics were all effective at generating electrodes with good performance, none of them contained aromatic functionalities that could interact with the graphite surfaces through π-π interactions.

Polystyrene (PS) is an inexpensive aromatic thermoplastic and one of the most commonly used substrates in bioanalysis.[17] PS is also a major source of plastic waste, often in the form of expanded polystyrene (EPS), which is rarely recycled.[18] In the literature, PS has been used as a binder in electrodes previously for biosensors,[17, 19-20 21-22] metals,[23-24] chemical oxygen demand, [22, 25] and small organic molecule detection[26-32] applications. However, none of these reports investigate the unique impacts PS as a binder can have on electrode morphology and electrochemistry. PS electrodes fabricated as TPEs also achieve enhanced electrode kinetics not seen with previous PS electrodes.

Here we examine the impact PS as a binder has on conductivity, capacitance, surface morphology, and the voltammetry of various redox probes. PS TPEs, in general have much lower capacitance and faster electrode kinetics than PCL TPEs. When PS is blended with PCL as a binder, the resulting TPEs are more conductive than TPEs made with either polymer on its own. These improved electrode properties likely result from the PS TPE morphology; PS TPE surfaces have lower roughness but more graphitic edge-plane rich features than PCL TPEs. In this study it is demonstrated that the composite binder can make a tremendous difference in the morphology and redox behavior of carbon composite electrodes.

3.3. Experimental

Chemicals

BupH™ Phosphate Buffered Saline Packs (PBS), isopropanol (IPA, HPLC grade), and methylene chloride (DCM) were sourced from Thermo Fisher Scientific. Potassium ferrocyanide (≥98.5%), potassium ferricyanide (99%), ascorbic acid (99%), uric acid (99+%), paracetamol (99.0%), and (±) norepinephrine (+) bitartrate salt were sourced from Sigma-Aldrich. Serotonin hydrochloride (99%), and dopamine hydrochloride (99%) were sourced from Alfa Aesar. Sodium hydroxide (NaOH, 1N) was sourced from J.T. Baker. P-Aminophenol was sourced from EMD Millipore. Ferrocene–trimethylamine (FcTMA+) was synthesized based on a previously reported method.[33] PBS buffer was prepared using the buffer packs to be 0.1 M sodium phosphate and 0.15 M NaCl; the pH was adjusted with NaOH to 7.4. High purity micronized graphite (15 μm, 99.5-99.99%, Great Lakes Graphite) was used as the graphite source. Polystyrene binders were sourced from Sigma-Aldrich with average molecular weights of 45,000 (45K PS), 192,000 (192K PS), and 350,000 (350K PS). Expanded polystyrene (EPS) was sourced from chemical packaging waste. Thermomorph™ was used as the source of polycaprolactone (PCL).

Electrode Fabrication

TPE materials were made by dissolving ~1 g of thermoplastic in ~15 mL of DCM and mixing in graphite at a 2:1 graphite:plastic mass ratio. The electrode templates were made from Optix poly(methyl methacrylate) (PMMA) sourced from Plaskolite. Templates were designed with the graphic design program CorelDRAW, and 3.175 mm thickness PMMA sheets were cut with an Epilog CO_2 laser cutter. All TPEs were heat pressed with a manually operated hydraulic heated press (Carver, Inc.) set to 88 °C and the pressures applied to the TPEs were kept between 300 and 500 psi. For electrodes made with PCL and 45K PS, the composite materials were fully dried

before heat pressing into templates. For higher PS molecular weights (192K, 350K, and EPS), the material was not able to be heat pressed dry using the same technique due to higher glass transition temperatures. The higher molecular weight PS materials were partially dried into a gum-like paste and allowed to dry fully on the heated press under pressure, for 2 h. Excess electrode material was sanded off and connections were made with silver paint, copper wires, and epoxy. All the TPE working electrodes used were 2.5 mm diameter disk electrodes.

Electrochemical Measurements

Electrochemical measurements were performed on a CHI 660b potentiostat. TPE working electrodes were polished with 600 grit sandpaper prior to use. TPE materials were compared to 4 mm diameter screen-printed carbon electrodes (SPCEs) sourced from DropSens and used as received, and a polished 3 mm diameter glassy carbon electrode (GCE). The GCE was freshly polished between each replicate with 1, 0.3, and 0.05 µm alumina powder with 1 min sonication in Milli-Q water between each polish. The counter electrode used was a 4 mm diameter disk electrode made from PCL TPE material (2:1 graphite:PCL) and sanded with 150 grit sandpaper for a higher surface area. The reference electrode used was a saturated calomel electrode (SCE) sourced from CH Instruments Inc. All electrical potential values given in this work are versus the SCE reference electrode.

Conductivity and Capacitance Testing

Capacitance and conductivity tests were performed as described in previous TPE work.[10-11] Tests were performed on 2.5 mm disks ~3 mm in thickness. For conductivity tests, TPEs were made at a 2:1 graphite:plastic ratio. PCL, 45K PS, 192K PS, 350K PS, and EPS were tested as the binder materials, as well as 3:1, 2:1, 1:1, 1:2, and 1:3 45K PS:PCL blends. At lower mass loadings binder-filler interactions affect conductivity more dramatically,[34] so to better elucidate

conductivity trends, binders were tested at 1:2 graphite:plastic ratios as well. Conductivity tests were performed on 2.5 mm disks prior to making the wire connections with a Fluke 187 multimeter, accuracy of 0.01 Ω. Capacitance tests were performed as reported previously in 0.1 M KNO_3, and the current was measured at 0.2 V vs. SCE.[10]

Cyclic Voltammetry of Redox Molecules

Cyclic voltammograms were performed at 100 mV/s scan rates. Ferri/ferrocyanide was tested at a 5 mM concentration (2.5 mM of each oxidation state), and all other redox probes were tested at 1 mM concentrations. The background electrolyte used for voltammetry experiments was 0.1 M PBS pH 7.4. CVs were scanned in the positive direction first for all species except benzoquinone, which was scanned in the negative direction first. For ferri/ferrocyanide, ascorbic acid, and dopamine CVs were taken from -0.2 to 0.6 V vs. SCE. For FcTMA+ and uric acid, the CVs were taken from 0.0 to 0.7 V vs. SCE. For serotonin and norepinephrine, CVs were taken from -0.4 to 0.7 vs. SCE. For p-aminophenol, benzoquinone, and paracetamol the CVs were taken from -0.4 to 0.3, 0.5 to -0.3, and -0.2 to 0.7 vs. SCE, respectively. SPCE, GCE, the different PS TPE types, and PCL TPEs were tested with ferri/ferrocyanide, uric acid, and ascorbic acid. The 45K PS, 1:1 PS:PCL, and PCL binder electrodes were tested with all redox probes.

Surface Imaging Measurements

For SEM sample preparation, the TPE materials were heat pressed into flat ~ 2 mm thick sheets and a 6 mm biopsy punch was used to cut out sample disks for analysis. Prior to analysis, disks were sanded with 600 grit sandpaper. SEM was performed with a JSM6500F field emission scanning electron microscope (JEOL, Tokyo, Japan) at 15 kV acceleration voltage. Profilometry measurements were performed with a ZeScope optical profilometer (Zemetrics, Arizona, U.S.A.) and the 2.5 mm diameter disk electrodes in PMMA templates were used. Rectangular profiles were

taken at ×12.581 magnification. Optical profilometry data was analyzed with Scanning Probe Image Processor (SPIP^{TM} 5.1.11) software to determine root mean squared (RMS) surface roughness of each profile.

3.4. Results and Discussion

Conductivity and Capacitance

Electrode conductivity (through-plane) and capacitance were analyzed, and the data are shown in Fig. 3.1. For the 2:1 graphite:polymer mass loadings, pure 45K PS and pure PCL electrodes had similar conductivities, 500 ± 200 (n=8), and 700 ± 200 S/m (n=9), respectively. When the polymers were blended the conductivity increased, with 1:1 45K PS:PCL electrodes having the highest conductivity of the blends at 1300 ± 400 S/m (n=9). Average conductivity was found to increase with PS molecular weight, with 1200 ± 100 S/m (n=6) conductivity for 350K PS. At the lower graphite loadings (1:2), as shown in Table 3.1, the trends in conductivity are even more pronounced. 1:1 45K PS:PCL TPEs were roughly five orders of magnitude more conductive (16 ± 6 S/m) than 45K PS TPEs (0.0002 ± 0.0004 S/m), and three orders of magnitude more conductive than PCL TPEs (0.2 ± 0.2 S/m). Improved conductivity for blends is expected because higher conductivity and lower percolation thresholds can be achieved in carbon composite materials if the conductive filler has a higher affinity for one binder in a blend.[34] An increased average conductivity as a function of PS molecular weight was also more pronounced at 1:2 graphite loadings. 350K PS TPEs (0.22 ± 0.08 S/m) were three orders of magnitude more conductive than 45K PS ones (0.0002 ± 0.0004 S/m), showing that molecular weight can greatly impact graphite distribution throughout the binder. Longer polymer chains may be distributing the graphite more evenly throughout the electrodes and shorter chains may lead to more random distribution and graphite aggregation.

Table 1. Conductivity data for TPEs at a 1:2 graphite: plastic ratio (n=6).

Binder	**PCL**	**1:1 PS:PCL**	**45K PS**	**192K PS**	**350K PS**	**EPS**
Conductivity (S/m)	0.2 ± 0.2	16 ± 6	0.0002 ± 0.0004	0.1 ± 0.1	0.22 ± 0.08	0.01 ± 0.2

Capacitance was the lowest for 45K PS TPEs at 81 ± 8 μF/cm^2 (n=6), less than a third of the capacitance of PCL TPEs, 290 ± 40 μF/cm^2 (n=6). The capacitance for PS TPEs was comparable to other carbon electrode materials such as edge plane HOPG (60 μF/cm^2) and lower capacitance glassy carbon electrodes which range from 24-318.0 μF/cm^2.[6, 35] PS-PCL blends also had significantly lower capacitance than PCL; this effect was pronounced even at 1:3 PS:PCL ratios. Capacitance data shows the addition of PS dominates the capacitive behavior. Capacitance increased slightly with increasing PS molecular weight, with 150 ± 20 μF/cm^2 (n=6) for 350K PS, but still had significantly lower capacitance than PCL. At 2:1 graphite:plastic ratios, both conductivity (910 ± 90 S/m, n=6) and capacitance (130 ± 10 μF/cm^2, n=5) of EPS TPEs showed similar results to that of 192K PS TPEs (900 ± 100 S/m, n=6; 135 ± 8 μF/cm^2, n=6). EPS and 192K results are encouraging, as typical EPS molecular weights are 160,000 to 260,000,[36] and this shows that using waste EPS has little impact on conductivity and capacitance and could lead to recycling the waste into valuable electrodes. Overall, the lower capacitance allows lower background current and lower LODs,[7] which is an improvement over the higher capacitance of previously reported TPEs.[10-11]

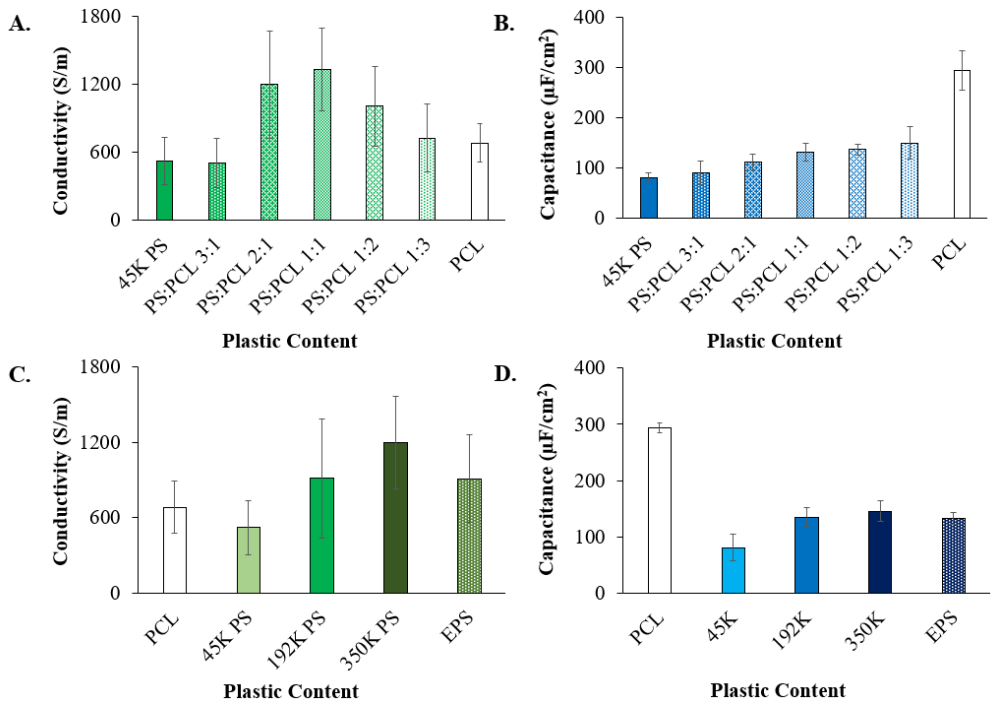

Fig. 3.1. Conductivity and capacitance of measurements of TPEs. A) Conductivity (n=9; n=8 for 45K PS) and B) capacitance (n=6) of 45K PS, PCL, and 45K PS-PCL blend TPEs. C) Conductivity (n=6; n=8 for 45K PS; n=9 for PCL), and D) capacitance (n=6; n=5 for EPS) of 45K to 350K PS, EPS, and PCL TPEs.

Redox Comparison of Carbon Electrode Materials

PS TPEs, PCL TPEs, GCE, and SPCE were evaluated using common redox molecules by CV with results shown in Fig. 3.2. PS TPEs showed the highest peak current densities for all the redox molecules tested (n=1 SPCE; n=3 all other types). For the reversible redox couple ferri/ferrocyanide, both TPEs had similar peak current densities, 1.05 ± 0.07 and 0.95 ± 0.06 mA/cm^2 oxidation peaks on PS and PCL, respectively. PS TPEs had ferri/ferrocyanide oxidation peak current densities 24% and 65% higher than GCE and SPCE, respectively. As ferri/ferrocyanide has little surface sensitivity, much of the current density differences can be attributed to TPEs having higher surface roughness than the other materials.[6, 10] ΔE values were lowest for PS TPEs, showing the fastest redox kinetics at 70 ± 2 mV, the other three materials had ΔE of 93 ± 8, 90 ± 10, and 241 mV for PCL TPEs, GCE, and SPCE, respectively. Remarkably,

uric acid was quasi-reversible for PS electrodes and irreversible for all other electrode materials. Uric acid typically exhibits irreversible voltammetry at most unmodified carbon electrodes.[37-39] The uric acid peak current density was also higher for PS TPEs, 160%, 40%, and 200% higher for PCL TPEs, GCE, and SPCE, respectively. The quasi-reversibility and high peak current of uric acid on PS TPEs suggests morphology of high surface area with 3D electroactive features.[40] For the highly surface sensitive and irreversible ascorbic acid, PS TPEs showed a greatly reduced overpotential relative to all other carbon electrode materials tested. The oxidative peak potential of ascorbic acid on PS TPEs was lowered by 180 ± 30, 140 ± 10, and 340 ± 7 mV relative to PCL TPEs, GCE, and SPCE, respectively. The sharp oxidation peak shape, and quasi-reversibility of uric acid, as well as the low peak potential of ascorbic acid seen with PS TPEs resemble voltammetry seen in the literature from carbon materials modified with 3D structured graphene nanomaterials.[38, 41-42]

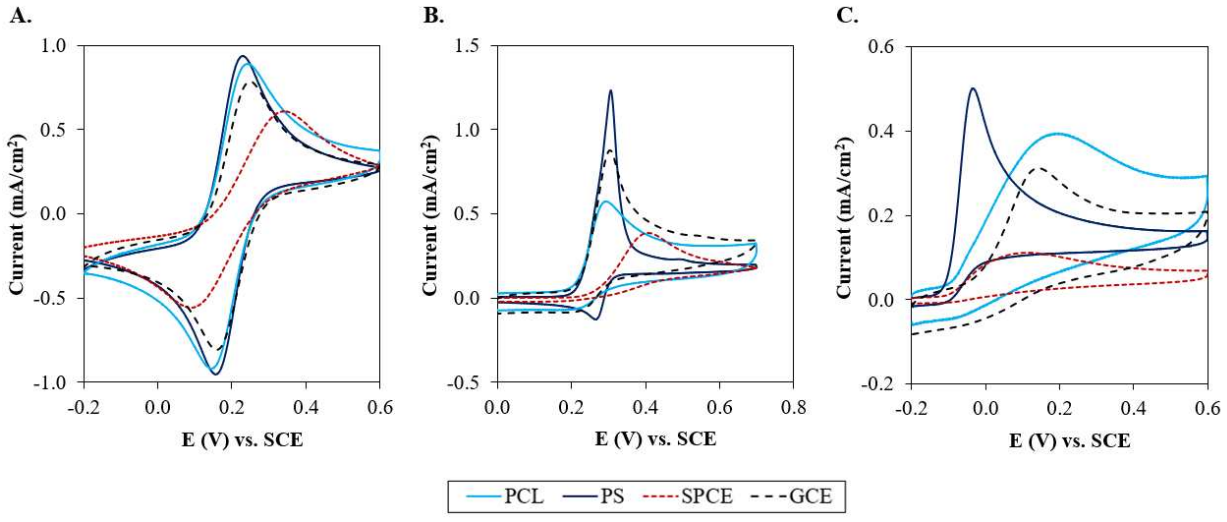

Fig. 3.2. Averaged (n=3), v=100 mV/s CVs of PS and PCL TPEs, compared with averaged (n=3) GCE and (n=1) SPCE data. CVs were compared for A) 5 mM ferri/ferrocyanide, B) 1 mM uric acid, and C) ascorbic acid in PBS.

Different PS sources for TPEs were compared with ferri/ferrocyanide, uric acid, and ascorbic acid to assess the impact of using higher PS molecular weights and EPS waste in TPEs.

As shown in Fig 3.3, there were some small variations in peak current and ΔE between the PS TPE types, however, the overall redox behavior was similar for all PS TPEs. The lack of clear trends between molecular weight and redox behavior suggest that these differences may have more to do with small variations in fabrication than the molecular weight itself. The high peak currents, low ΔE, and low overpotential of EPS TPEs is promising for future applications of incorporating waste plastics into functional composite electrodes.

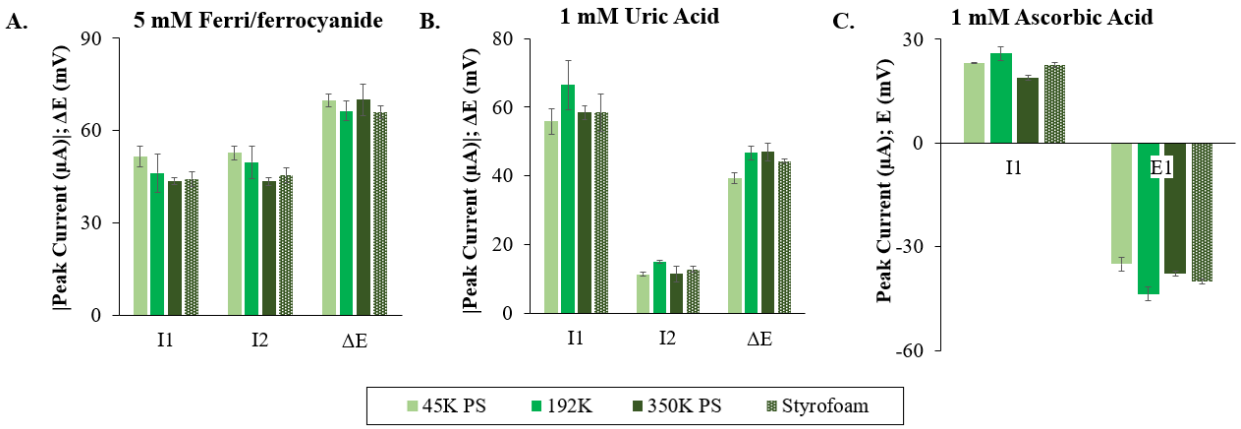

Fig. 3.3. Averaged (n=3), v=100 mV/s quantitative CV data of 45K PS, 192K PS, 350K PS, and EPS TPEs for A) 5 mM ferri/ferrocyanide, B) 1 mM uric acid, and C) ascorbic acid in PBS.

Surface Characterization of TPEs

Surface morphology plays a significant role on the electrochemical performance of electrodes, and SEM and OP were used to characterize surface morphology. The SEM and OP data gave insight into the differences in electrode behavior for the TPEs with different binders. Overall, TPEs with PS as a binder component had lower surface roughness on a macroscale but had microscale features consisting of graphene-like sheets creating edge-plane rich 3D surface structures. From the OP data shown in Table 3.2, PCL TPEs showed ~2.5× RMS roughness of 45K PS TPEs. PS-PCL TPEs had ~1.5× RMS roughness of 45K PS TPEs. Other PS binder types also showed similarly low RMS surface roughness to 45K PS, (578.501, 450.718, 580.247, and 553.69 nm for 45K, 192K, 350K, and EPS, respectively) the OP data for other PS sources is shown

in Table S3.1. The OP data suggests much of the differences in capacitance between the TPE types can be attributed to surface roughness, higher surface roughness leads to higher capacitance.

Table 3.2. Quantitative OP roughness data for TPEs.

Binder	***RMS Roughness (nm)***	***Roughness Ratio (Binder/45K PS)***
45K PS	578.501	1
PS-PCL	848.45	1.4666
PCL	1464.35	2.53128

Sandpaper polished PS TPEs surfaces reveal graphite sheets thin enough to be translucent in SEM images, as seen in Fig. 3.4d, suggesting graphene or few layer graphene-rich surfaces. Some of these sheets are bent or folded to create 3D structures with abundant nanoscale edge-plane features. These sheets are likely generated via graphite fracture and exfoliation during the sanding process. This morphology could be enabled by the brittle nature of PS and the graphite dispersion and orientation in the binder matrix. On the PCL and PS-PCL TPEs, the graphite is more immersed in the binder matrix and 3D graphene nanomaterial-like structures are not apparent. During material abrasion, softer materials undergo more micro-ploughing as opposed to micro-cracking and fracture.[43] The softer PCL binder material is predicted to undergo plastic deformation around the graphite, making it more difficult for the graphite to fracture. In the PCL TPEs, raised clumps of composite material are also present on the surface, as shown in Fig. 3.4c, possibly contributing to the overall surface roughness. These raised clumps also contained white charging regions indicative of inhomogeneous graphite distribution. Other PS binder sources showed similar morphology to 45K PS, the data for this is shown in Fig. S3.2.

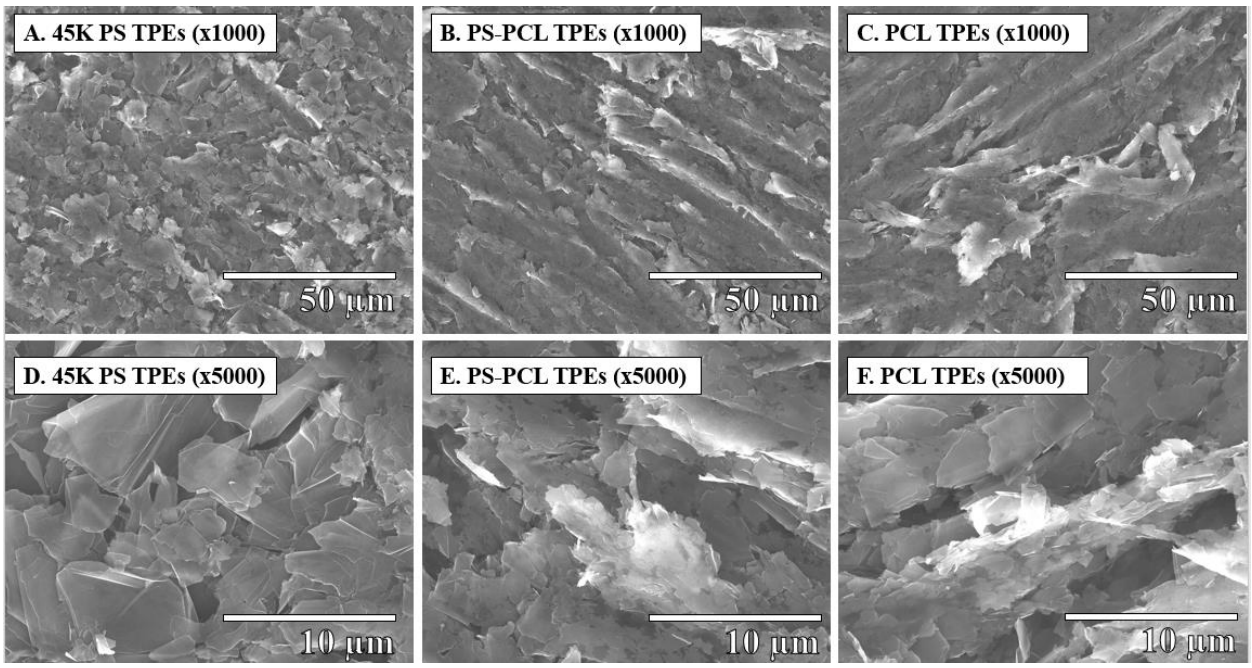

Fig. 3.4. 15.0 kV SEM images of 2:1 graphite: plastic TPEs at ×1000 for A) 45K PS, B) PS-PCL, and C) PCL binders; ×5000 for D) 45K PS, E) PS-PCL, and F) PCL TPEs.

Cyclic Voltammetry of Redox Molecules on PS, PCL, and PS-PCL Blend TPEs

Benzoquinone, ferri/ferrocyanide, and ferrocene derivatives such as ferrocene–trimethylamine (FcTMA+) are well-behaved redox molecules often used to characterize new electrode materials and were used herein for this reason.[6, 11, 33, 44-45] Voltammetry data for these common redox probes is shown in Fig. 3.5. Firstly, the TPEs were tested with $FcTMA^+$, an outer sphere redox probe whose peak current response should be directly related to the electroactive surface area.[11, 33] The peak separations were close to the theoretical ΔE for a reversible redox reaction 59 mV/e^{-}[46] at 59 ± 2, 60 ± 4, 56 ± 0 mV for PS, PS-PCL, and PCL TPEs, respectively. The ΔE values below the theoretical value could be indicative of some degree of electrode porosity and have been seen for $FcTMA^+$ previously with TPEs.[11] The $FcTMA^+$ oxidation peak current on PS TPEs was on average 22% higher than PS-PCL TPEs and 10% higher than PCL TPEs, indicating that PS TPEs have the highest and PS-PCL TPEs have the lowest electroactive surface area. The $FcTMA^+$ reduction peaks currents were on average 27%, 9.4%, and 21% smaller than

the oxidation peaks for PS, PS-PCL, and PCL, respectively. PS TPEs had the largest difference between reduction and oxidation peak current which could be due to enhanced π-π interactions with the PS increasing adsorption, since adsorption is known to cause smaller reverse currents for $FcTMA^+$ on HOPG.[47] Peak current and ΔE was improved on PS relative to PCL TPEs for ferri/ferrocyanide and benzoquinone. For ferri/ferrocyanide, this was a smaller improvement, likely due to the more edge-plane rich morphology, and no improvement was seen for PS-PCL TPEs. Oxidative peak currents for PS were on average 15% higher than PS-PCL TPEs and 11% higher than PCL ones. Ferri/ferrocyanide values for ΔE were 70 ± 2, 101 ± 5, 93 ± 8 mV for PS, PS-PCL, and PCL TPEs, respectively. For benzoquinone, ΔE improvement was more dramatic and occurred with PS-PCL TPEs as well. Benzoquinone values for ΔE were 35 ± 5, 76 ± 2, 95 ± 4 mV for PS, PS-PCL, and PCL TPEs, respectively. The dramatic improvement in benzoquinone kinetics on PS and PS-PCL TPEs, even with their differing morphologies, suggests the π-π interactions between the PS binder and certain aromatic redox probes can additionally enhance charge transfer. Benzoquinone reduction peak currents for PS were on average 42% higher than PS-PCL TPE current and 36% higher than PCL ones.

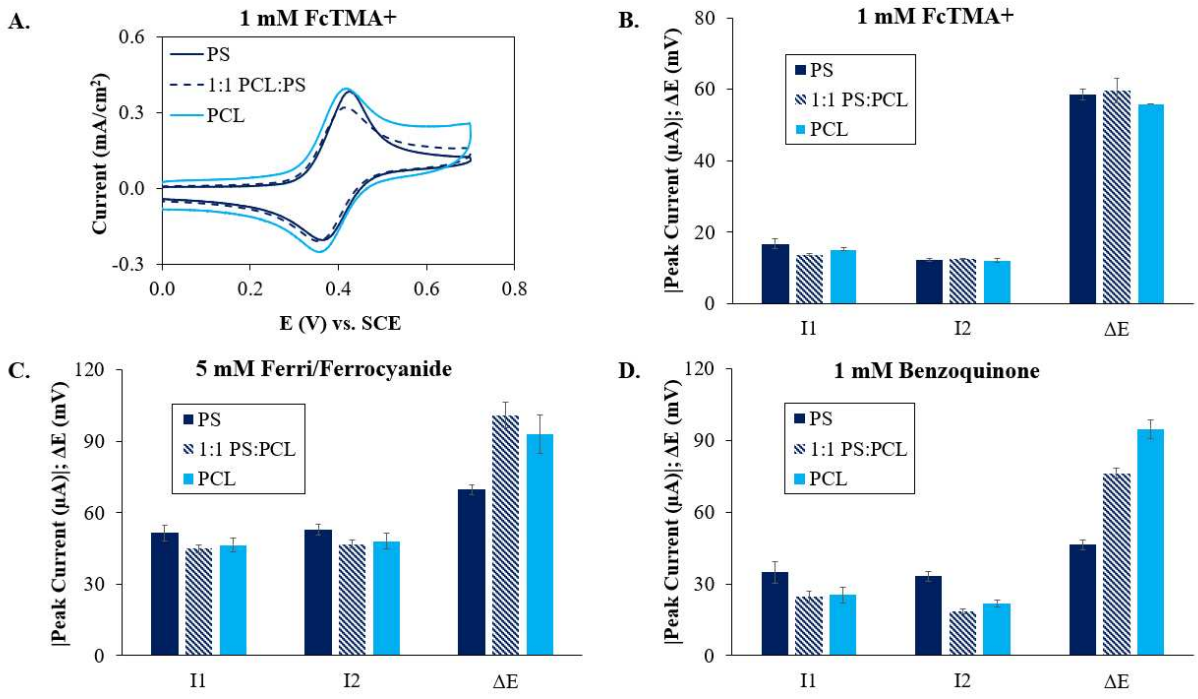

Fig. 3.5. CV data of common redox probes in PBS v=100 mV/s with 45K PS, 1:1 PS:PCL, and PCL TPEs. A) Averaged CVs of 1 mM FCTMA+ and quantitative data for anodic (I1), cathodic (I2), and peak separation (DE) for B) 1 mM FCTMA+, C) 5 mM ferri/ferrocyanide, and D) benzoquinone.

Detecting ascorbic acid, paracetamol, and p-aminophenol is of interest for food and drug analysis,[48-51] and voltammetry for these molecules is shown in Fig. 3.6. PS TPEs redox behavior for paracetamol was far more reversible than other TPE compositions. The ΔE for paracetamol were 65 ± 4, 270 ± 10, and 200 ± 30 mV for PS, PS-PCL, and PCL TPEs, respectively. Paracetamol oxidation peak currents for PS TPEs were 88% and 92% higher than peak currents on PS-PCL and PCL TPEs, showing that this could be an excellent material for paracetamol detection. p-Aminophenol ΔE and peak currents were improved on PS electrodes relative to other types as well, although to a lesser extent. The p-aminophenol ΔE were 40.3 ± 0.6, 55 ± 2, and 54 ± 5 mV for PS, PS-PCL, and PCL TPEs, respectively. Average oxidation peak currents were the same for PS and PCL TPEs (31 µA), however, reduction peak currents were 43% higher for PS TPEs than for PCL TPEs. The higher reduction current for the benzoquinone imine oxidation product shows that this

type of aromatic structure, like benzoquinone, has very favorable reduction kinetics on aromatic PS TPEs. Electrodes were also tested in p-aminophenol at pH 5.0 and 9.0; the results of this pH study are shown in S.3. PS-PCL electrodes show no ΔE advantage over PCL ones at pH 7.4, however, at pH 5.0 PS-PCL TPEs exhibited the smallest ΔE of the three electrode types. At pH 5.0, ΔE values were 190 ± 20, 150 ± 10, and 193 ± 6 mV for PS, PS-PCL, and PCL TPEs, respectively. We hypothesize this is due to the beneficial electrostatics between p-aminophenol and PCL at this pH, as well as enhanced π-π stacking from the PS matrix. Therefore, for certain applications there may be a benefit to using PS-PCL over PS TPEs. For ascorbic acid PS-PCL TPEs exhibited similar oxidation behavior but lower variability between replicates relative to PCL TPEs, and both had far higher overpotentials and lower peak currents to that of PS TPEs.

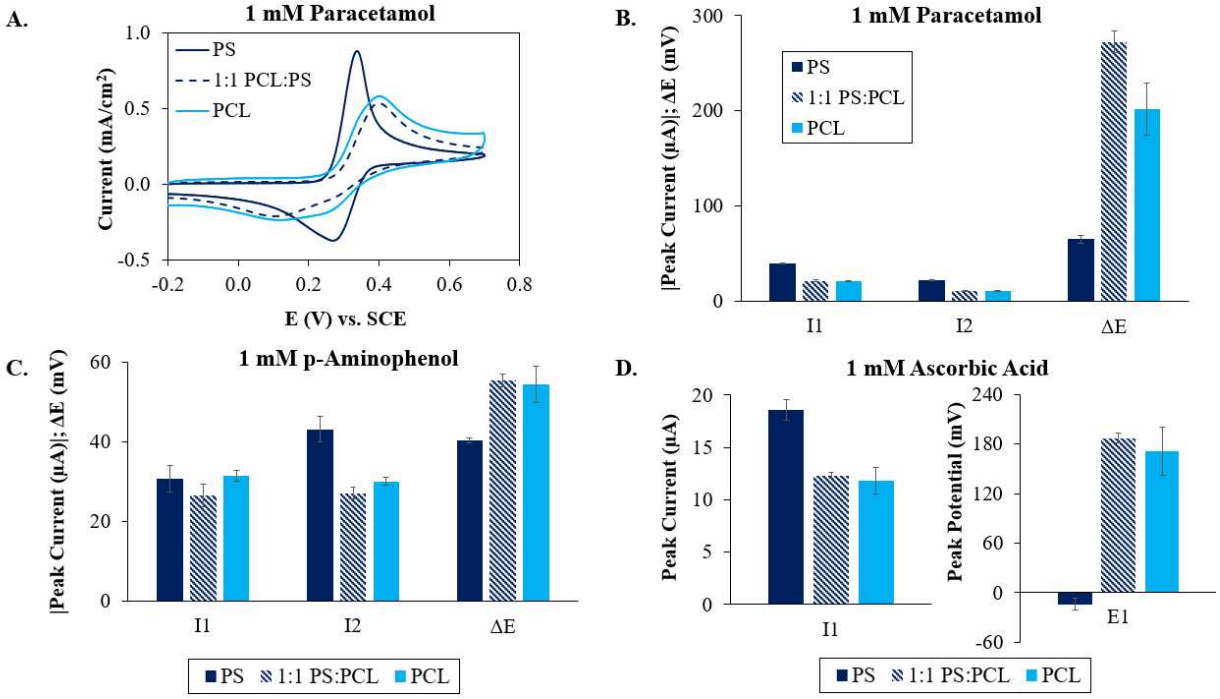

Fig. 3.6. CV data of redox probes related to food and drug analysis in PBS v=100 mV/s with 45K PS, 1:1 PS:PCL, and PCL TPEs. A) Averaged CVs of 1 mM paracetamol and quantitative data for anodic (I1), cathodic (I2), and peak separation (ΔE) or anodic peak potential (E1) for B) 1 mM paracetamol, C) 1 mM p-aminophenol, and D) 1 mM ascorbic acid.

Dopamine, uric acid, serotonin, and norepinephrine are important biomolecules that can be biomarkers of various neurological, cardiovascular, and kidney diseases. [39, 52-53] Voltammetry for these biomolecules is shown in Fig. 3.7. For dopamine, the ΔE was not significantly different between PCL and PS-PCL electrodes, ~60 mV. Peak separation for PS electrodes, 37 ± 2 mV, was far lower than for other binders and close to the theoretical value of 29.5 mV for a two-electron transfer. Dopamine requires adsorption for electrocatalysis and π-π stacking from graphene-like materials can help facilitate interaction with the surface.[54] For uric acid, PS-PCL electrodes exhibited irreversible redox behavior like PCL ones, however the average oxidation current was higher and the peaks were similar in shape to that of PS TPEs (Fig. S3.4). Norepinephrine exhibited quasi-reversible behavior on all TPE types with similar ΔE values. However, for PS TPEs the average overpotential was shifted ~25 mV lower relative to PS-PCL and PCL TPEs. For norepinephrine, PS TPEs had average oxidative peak current 58% and 42% higher than PS-PCL and PCL TPEs, respectively. For serotonin, PS TPEs did not have higher peak currents than PCL TPEs, however they did have reduced overpotentials by ~45 mV relative to PS-PCL and PCL TPEs. Overall, these results demonstrate that PS TPEs are excellent materials for direct detection of biomolecules. The higher peak currents and lowered overpotentials seen in the voltammetry of these molecules could also be beneficial for discriminating between different biomolecules in solutions where they coexist.

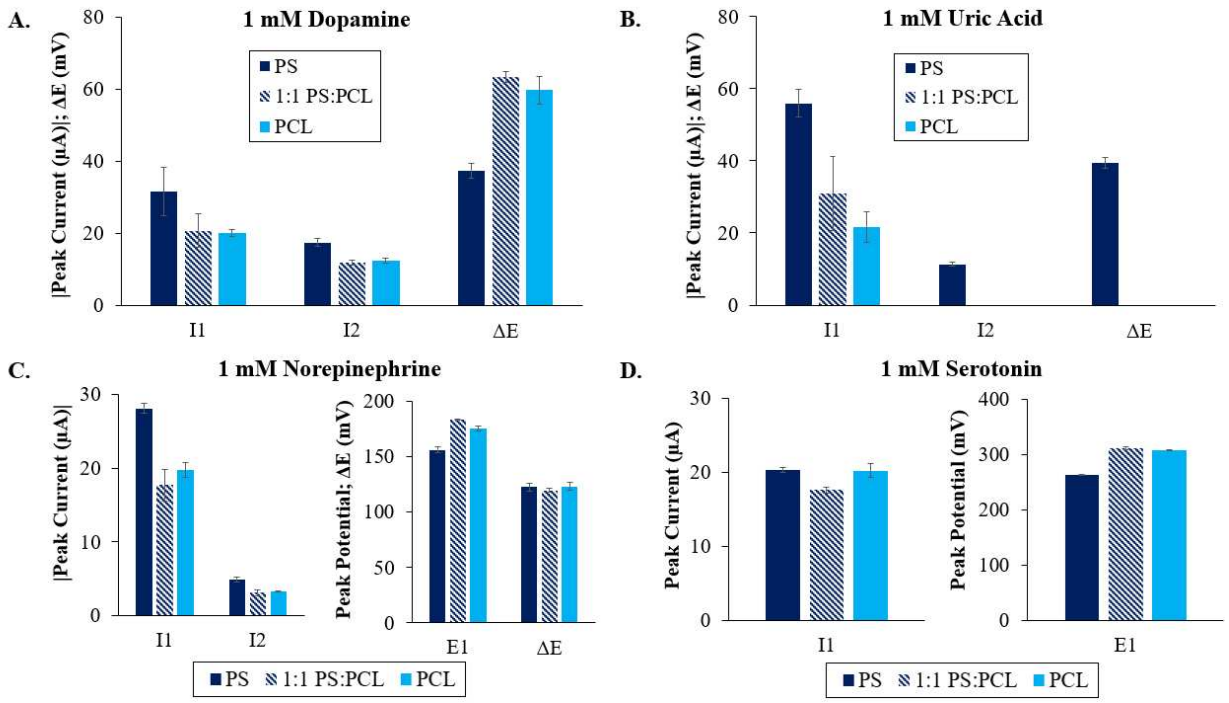

Fig. 3.7. CV data of biologically relevant redox probes in PBS v=100 mV/s with 45K PS, 1:1 PS:PCL, and PCL TPEs. Quantitative data for anodic (I1), cathodic (I2), and peak separation (DE) or anodic peak potential (E1) for A) 1 mM dopamine, B) 1 mM uric acid, C) 1 mM norepinephrine, and D) 1 mM serotonin.

3.5. Conclusion

In conclusion, through the simple TPE fabrication process, using PS as a binder, carbon composite electrodes can be fabricated with reduced capacitance and electrocatalytic behavior similar to composites modified with nanomaterial electrocatalysts. The enhanced redox behavior and morphology is seen when both low and high molecular weight PS binders are used, as well as for waste EPS. Much of these beneficial properties are likely attributed to the edge-plane rich morphology with three-dimensional graphene structures. However, enhanced behavior was seen for certain molecules when PS-PCL blends without that morphology were used. The data from the PS-PCL blends suggests that enhanced π-π stacking interactions from the aromatic PS binder may also play a role in the electrocatalysis. Sharper peaks and lower overpotentials demonstrate these electrodes could be used in the future to better discriminate between electroactive molecules in

complex matrices. The successful use of EPS as a PS binder shows the potential for high performance electrode materials from recycled waste plastics.

REFERENCES

1. Li, S.; Jin, B.; Zhai, X.; Li, H.; Jiang, Q., Review of Carbon Materials for Lithium-Sulfur Batteries. *ChemistrySelect* **2018,** *3* (8), 2245-2260.

2. Kwon, Y. H.; Huie, M. M.; Choi, D.; Chang, M.; Marschilok, A. C.; Takeuchi, K. J.; Takeuchi, E. S.; Reichmanis, E., Toward uniformly dispersed battery electrode composite materials: characteristics and performance. *ACS Appl. Mater. Interfaces* **2016,** *8* (5), 3452-3463.

3. Lee, H.; Yoo, J. K.; Park, J. H.; Kim, J. H.; Kang, K.; Jung, Y. S., A stretchable polymer–carbon nanotube composite electrode for flexible lithium-ion batteries: porosity engineering by controlled phase separation. *Advanced Energy Materials* **2012,** *2* (8), 976-982.

4. Adams, R. N., Carbon paste electrodes. *Analytical chemistry* **1958,** *30* (9), 1576-1576.

5. Aguilar, R.; Davila, M.; Elizalde, M.; Mattusch, J.; Wennrich, R., Capability of a carbon–polyvinylchloride composite electrode for the detection of dopamine, ascorbic acid and uric acid. *Electrochimica acta* **2004,** *49* (6), 851-859.

6. McCreery, R. L., Advanced carbon electrode materials for molecular electrochemistry. *Chem. Rev.* **2008,** *108* (7), 2646-2687.

7. Tallman, D. E.; Petersen, S. L., COMPOSITE ELECTRODES FOR ELECTROANALYSIS - PRINCIPLES AND APPLICATIONS. *Electroanalysis* **1990,** *2* (7), 499-510.

8. O'Hare, D.; Macpherson, J. V.; Willows, A., On the microelectrode behaviour of graphite-epoxy composite electrodes. *Electrochemistry Communications* **2002,** *4* (3), 245-250.

9. Wang, S. C.; Chang, K. S.; Yuan, C. J., Enhancement of electrochemical properties of screen-printed carbon electrodes by oxygen plasma treatment. *Electrochimica Acta* **2009,** *54* (21), 4937-4943.

10. Klunder, K. J.; Nilsson, Z.; Sambur, J. B.; Henry, C. S., Patternable Solvent-Processed Thermoplastic Graphite Electrodes. *J. Am. Chem. Soc.* **2017,** *139* (36), 12623-12631.

11. Klunder, K. J.; Clark, K. M.; McCord, C.; Berg, K. E.; Minteer, S. D.; Henry, C. S., Polycaprolactone-enabled sealing and carbon composite electrode integration into electrochemical microfluidics. *Lab Chip* **2019,** *19* (15), 2589-2597.

12. Noviana, E.; Klunder, K. J.; Channon, R. B.; Henry, C. S., Thermoplastic Electrode Arrays in Electrochemical Paper-Based Analytical Devices. *Analytical Chemistry* **2019,** *91* (3), 2431-2438.

13. Berg, K. E.; Leroux, Y. R.; Hapiot, P.; Henry, C. S., Increasing Applications of Graphite Thermoplastic Electrodes with Aryl Diazonium Grafting. *ChemElectroChem* **2019,** *6* (18), 4811-4816.

14. Pradela-Filho, L. A.; Noviana, E.; Araujo, D.; Takeuchi, R.; Santos, A.; Henry, C. S., Rapid Analysis in Continuous Flow Electrochemical Paper-Based Analytical Devices. *ACS Sens.* **2020**.

15. Berg, K. E.; Clark, K. M.; Li, X.; Carter, E. M.; Volckens, J.; Henry, C. S., High-throughput, semi-automated dithiothreitol (DTT) assays for oxidative potential of fine particulate matter. *Atmospheric Environment* **2020,** *222*, 117132.

16. Ozer, T.; McCord, C.; Geiss, B. J.; Dandy, D.; Henry, C. S., Thermoplastic Electrodes for Detection of Escherichia coli. *Journal of The Electrochemical Society* **2021,** *168* (4), 047509.

17. Salminen, K.; Grönroos, P.; Eskola, J.; Nieminen, E.; Härmä, H.; Kulmala, S., Immunoassay of C-reactive protein by hot electron-induced electrochemiluminescence at polystyrene-carbon black composite electrodes. *Electrochimica Acta* **2018,** *282*, 147-154.

18. Gil-Jasso, N. D.; Segura-González, M. A.; Soriano-Giles, G.; Neri-Hipolito, J.; López, N.; Mas-Hernández, E.; Barrera-Díaz, C. E.; Varela-Guerrero, V.; Ballesteros-Rivas, M. F., Dissolution and recovery of waste expanded polystyrene using alternative essential oils. *Fuel* **2019,** *239*, 611-616.

19. Salminen, K.; Grönroos, P.; Tuomi, S.; Kulmala, S., Cathodic electrogenerated chemiluminescence of aromatic Tb (III) chelates at polystyrene-graphite composite electrodes. *Anal. Chim. Acta* **2017,** *985*, 54-60.

20. Fernandez-Sanchez, C.; Pellicer, E.; Orozco, J.; Jimenez-Jorquera, C.; Lechuga, L. M.; Mendoza, E., Plasma-activated multi-walled carbon nanotube-polystyrene composite substrates for biosensing. *Nanotechnology* **2009,** *20* (33).

21. Quan, H.; Park, S.-U.; Park, J., Electrochemical oxidation of glucose on silver nanoparticle-modified composite electrodes. *Electrochimica Acta* **2010,** *55* (7), 2232-2237.

22. Orozco, J.; Fernandez-Sanchez, C.; Mendoza, E.; Baeza, M.; Cespedes, F.; Jimenez-Jorquera, C., Composite planar electrode for sensing electrochemical oxygen demand. *Anal. Chim. Acta* **2008,** *607* (2), 176-182.

23. Rymansaib, Z.; Iravani, P.; Emslie, E.; Medvidović-Kosanović, M.; Sak-Bosnar, M.; Verdejo, R.; Marken, F., All-Polystyrene 3D-Printed Electrochemical Device with Embedded Carbon Nanofiber-Graphite-Polystyrene Composite Conductor. *Electroanalysis* **2016,** *28* (7), 1517-1523.

24. Promphet, N.; Rattanarat, P.; Rangkupan, R.; Chailapakul, O.; Rodthongkum, N., An electrochemical sensor based on graphene/polyaniline/polystyrene nanoporous fibers modified electrode for simultaneous determination of lead and cadmium. *Sens. Actuator B-Chem.* **2015,** *207*, 526-534.

25. Gutiérrez-Capitán, M.; Baldi, A.; Gómez, R.; García, V.; Jiménez-Jorquera, C.; Fernández-Sánchez, C. s., Electrochemical nanocomposite-derived sensor for the analysis of chemical oxygen demand in urban wastewaters. *Analytical chemistry* **2015,** *87* (4), 2152-2160.

26. Saghatforoush, L.; Hasanzadeh, M.; Shadjou, N., Polystyrene-graphene oxide modified glassy carbon electrode as a new class of polymeric nanosensors for electrochemical determination of histamine. *Chinese Chemical Letters* **2014,** *25* (4), 655-658.

27. Liu, W.; Xiao, J.; Wang, C.; Yin, H.; Xie, H.; Cheng, R., Synthesis of polystyrene-grafted-graphene hybrid and its application in electrochemical sensor of dopamine. *Materials Letters* **2013,** *100*, 70-73.

28. Khaskheli, A. R.; Fischer, J.; Barek, J.; Vyskocil, V.; Sirajuddin; Bhanger, M. I., Differential pulse voltammetric determination of paracetamol in tablet and urine samples at a micro-crystalline natural graphite-polystyrene composite film modified electrode. *Electrochimica Acta* **2013,** *101*, 238-242.

29. Lu, Y.; Wang, X.; Chen, D. F.; Chen, G., Polystyrene/graphene composite electrode fabricated by in situ polymerization for capillary electrophoretic determination of bioactive constituents in Herba Houttuyniae. *Electrophoresis* **2011,** *32* (14), 1906-1912.

30. Pop, A.; Manea, F.; Radovan, C.; Corb, I.; Burtica, G.; Malchev, P.; Picken, S.; Schoonman, J., DETERMINATION OF 4-CHLOROPHENOL USING TWO TYPES OF

GRAPHITE-BASED COMPOSITE ELECTRODES. *Revue Roumaine De Chimie* **2008,** *53* (8), 623-+.

31. Xu, J.; Zhang, H.; Chen, G., Carbon nanotube/polystyrene composite electrode for microchip electrophoretic determination of rutin and quercetin in Flos Sophorae Immaturus. *Talanta* **2007,** *73* (5), 932-937.

32. Manea, F.; Radovan, C.; Corb, I.; Pop, A.; Burtica, G.; Malchev, P.; Picken, S.; Schoonman, J., Electrochemical oxidation and determination of oxalic acid at an exfoliated graphite-polystyrene composite electrode. *Sensors* **2007,** *7* (4), 615-627.

33. Lemay, S. G.; van den Broek, D. M.; Storm, A. J.; Krapf, D.; Smeets, R. M.; Heering, H. A.; Dekker, C., Lithographically fabricated nanopore-based electrodes for electrochemistry. *Analytical chemistry* **2005,** *77* (6), 1911-1915.

34. Boyaci San, F. G.; Tekin, G., A review of thermoplastic composites for bipolar plate applications. *Int. J. Energy Res.* **2013,** *37* (4), 283-309.

35. Antiochia, R.; Lavagnini, I.; Magno, F.; Valentini, T.; Palleschi, G., Single-wall carbon nanotube paste electrodes: a comparison with carbon paste, platinum and glassy carbon electrodes via cyclic voltammetric data. *Electroanalysis* **2004,** *16* (17), 1451-1458.

36. Shin, C.; Chase, G. G., Nanofibers from recycle waste expanded polystyrene using natural solvent. *Polymer Bulletin* **2005,** *55* (3), 209-215.

37. Kumar, S. S.; Mathiyarasu, J.; Phani, K. L.; Jain, Y. K.; Yegnaraman, V., Determination of Uric Acid in the Presence of Ascorbic Acid Using Poly (3, 4-ethylenedioxythiophene)-Modified Electrodes. *Electroanalysis: An International Journal Devoted to Fundamental and Practical Aspects of Electroanalysis* **2005,** *17* (24), 2281-2286.

38. Yang, B.; Wang, H.; Du, J.; Fu, Y.; Yang, P.; Du, Y., Direct electrodeposition of reduced graphene oxide on carbon fiber electrode for simultaneous determination of ascorbic acid, dopamine and uric acid. *Colloids and Surfaces A: Physicochemical and Engineering Aspects* **2014,** *456*, 146-152.

39. Ganesh, P.; Swamy, B. K., Simultaneous electroanalysis of norepinephrine, ascorbic acid and uric acid using poly (glutamic acid) modified carbon paste electrode. *Journal of Electroanalytical Chemistry* **2015,** *752*, 17-24.

40. Premkumar, J.; Khoo, S. B., Electrocatalytic oxidations of biological molecules (ascorbic acid and uric acids) at highly oxidized electrodes. *Journal of Electroanalytical Chemistry* **2005,** *576* (1), 105-112.

41. Feng, S.; Yu, L.; Yan, M.; Ye, J.; Huang, J.; Yang, X., Holey nitrogen-doped graphene aerogel for simultaneously electrochemical determination of ascorbic acid, dopamine and uric acid. *Talanta* **2021,** *224*, 121851.

42. Zhang, K.; Zhang, N.; Zhang, L.; Wang, H.; Shi, H.; Liu, Q., Simultaneous voltammetric detection of dopamine, ascorbic acid and uric acid using a poly (2-(N-morpholine) ethane sulfonic acid)/RGO modified electrode. *RSC advances* **2018,** *8* (10), 5280-5285.

43. Cenna, A.; Doyle, J.; Page, N.; Beehag, A.; Dastoor, P., Wear mechanisms in polymer matrix composites abraded by bulk solids. *Wear* **2000,** *240* (1-2), 207-214.

44. Channon, R. B.; Yang, Y. Y.; Feibelman, K. M.; Geiss, B. J.; Dandy, D. S.; Henry, C. S., Development of an Electrochemical Paper-Based Analytical Device for Trace Detection of Virus Particles. *Analytical Chemistry* **2018,** *90* (12), 7777-7783.

45. Mažeikien, R.; Malinauskas, A., Electrocatalysis of the hydroquinone/benzoquinone redox couple at electrodes covered by a film of polyaniline-like copolymers. *Reactive and Functional Polymers* **2000,** *45* (1), 45-54.

46. Bard, A. J. F., L. R. , *Electrochemical Methods: Fundamentals and Applications*. 2 ed.; John Wiley & Sons Inc.: 2001.

47. Kurapati, N.; Pathirathna, P.; Chen, R.; Amemiya, S., Voltammetric Measurement of Adsorption Isotherm for Ferrocene Derivatives on Highly Oriented Pyrolytic Graphite. *Analytical chemistry* **2018,** *90* (22), 13632-13639.

48. Phong, N. H.; Toan, T. T. T.; Tinh, M. X.; Tuyen, T. N.; Mau, T. X.; Khieu, D. Q., Simultaneous voltammetric determination of ascorbic acid, paracetamol, and caffeine using electrochemically reduced graphene-oxide-modified electrode. *Journal of Nanomaterials* **2018,** *2018*.

49. Sartori, E. R.; Fatibello-Filho, O., Simultaneous voltammetric determination of ascorbic acid and sulfite in beverages employing a glassy carbon electrode modified with carbon nanotubes within a poly (allylamine hydrochloride) film. *Electroanalysis* **2012,** *24* (3), 627-634.

50. Sharifian, S.; Nezamzadeh-Ejhieh, A., Modification of carbon paste electrode with Fe (III)-clinoptilolite nano-particles for simultaneous voltammetric determination of acetaminophen and ascorbic acid. *Materials Science and Engineering: C* **2016,** *58*, 510-520.

51. Wang, J.; Zhang, H.; Zhao, J.; Zhang, R.; Zhao, N.; Ren, H.; Li, Y., Simultaneous determination of paracetamol and p-aminophenol using glassy carbon electrode modified with nitrogen-and sulfur-co-doped carbon dots. *Microchim. Acta* **2019,** *186* (11), 1-9.

52. Álvarez-Martos, I.; Ferapontova, E. E., Electrocatalytic discrimination between dopamine and norepinephrine at graphite and basal plane HOPG electrodes. *Electroanalysis* **2018,** *30* (6), 1082-1090.

53. Wu, K.; Fei, J.; Hu, S., Simultaneous determination of dopamine and serotonin on a glassy carbon electrode coated with a film of carbon nanotubes. *Analytical Biochemistry* **2003,** *318* (1), 100-106.

54. Wu, L.; Feng, L.; Ren, J.; Qu, X., Electrochemical detection of dopamine using porphyrin-functionalized graphene. *Biosensors and Bioelectronics* **2012,** *34* (1), 57-62.

CHAPTER 4: SIMULTANEOUS ANALYSIS OF ASCORBIC ACID URIC ACID AND DOPAMINE AT BARE POLYSTYRENE THERMOPLASTIC ELECTRODES

4.1 Chapter Overview

Most of the content of this chapter is taken from a manuscript in preparation titled "Simultaneous Analysis of Ascorbic Acid, Uric Acid and Dopamine at Bare Polystyrene Thermoplastic Electrodes" with authors Cynthia P. McCord, Bali Summers, and Charles S. Henry*. Ascorbic acid (AA), uric acid (UA), and dopamine (DA) are redox active molecules that often coexist in biological fluids and are vital to human metabolism. Electrochemical detection of these molecules is desirable; however, their oxidation peaks are poorly resolved at most unmodified electrode materials. Often surface modifications are deemed necessary for simultaneous analysis, increasing cost and complicating fabrication and surface chemistry. Recently reported thermoplastic electrodes (TPEs) are inexpensive, easily moldable, and highly electroactive carbon composite materials. Herein, polystyrene thermoplastic electrodes (PS TPEs) are presented that can be used for simultaneous analysis of AA, DA, and UA without the need for surface modification. Different conductive carbon fillers were explored, and PS TPEs were optimized for conductivity, capacitance, and electrochemistry. Cyclic voltammetry (CV) was used to characterize the different TPE types, and square wave voltammetry (SWV) was used for quantitative simultaneous determination. Detection limits were determined to be 4, 0.9, and 4 μM for AA, DA, and UA respectively. As a proof of concept for use in real samples, electrodes were challenged with urine; excellent recoveries (90-110%) were seen for AA and UA. DA showed low recovery at the concentrations tested (82% for 10 μM and 47% for 5 μM), but in the future, higher

recoveries can likely be achieved through design considerations and more oxidized carbon fillers. Overall, these materials showed excellent promise for simultaneous analysis of AA, DA, and UA.

4.2 Introduction

Ascorbic acid (AA), uric acid (UA), and dopamine (DA) are small organic molecules that serve crucial roles in human metabolism and can be used as biomarkers for a variety of health conditions.[1] AA, DA, and UA coexist in bodily fluids and can also be found in pharmaceutical and food samples.[1] AA, also known as Vitamin C, is a vitamin and antioxidant; AA deficiencies can lead to neurodegenerative diseases, cardiovascular disease and scurvy, whereas excess AA can lead to kidney stones and stomach irritation.[2, 3] Dopamine is a neurotransmitter critical to the central nervous system and typically present at significantly lower concentrations than AA or UA.[4, 5] Irregular dopamine concentrations can be associated with neurodegenerative diseases, heart failure and addiction.[4, 6] UA is an antioxidant and the product of purine metabolism.[7] Irregular uric acid levels in bodily fluids have been linked to a variety of health conditions such as fatty liver disease, depression, and gout.[8-10]

As AA, DA, and UA are redox active, electroanalytical methods for direct detection are of particular interest. Unfortunately, AA, DA, and UA have similar oxidation potentials on most bare electrodes so further surface treatments and/or modifiers are typically necessary to resolve three peaks. In the past, this has been accomplished using metallic nanomaterials,[11-14] carbon nanomaterials,[11, 14-20] ionic liquids,[19, 21] conducting polymers,[22-25] and porous materials.[26, 27] Although effective at resolving the three oxidation peaks, surface modification introduces additional expense and complexity for sensor preparation. Also, electrodes with complex surface modifications could prove challenging to incorporate into different sensor configurations.

Therefore, it is beneficial to have inexpensive, easy to fabricate electrode materials that can resolve the oxidation peaks three molecules at bare electrodes.

Carbon electrodes are often used for redox biomolecule detection due to their low cost, biocompatibility, and excellent electrochemistry for organic redox molecules.[15, 28] Most common electrode materials, traditional and composites alike, are difficult to mold which also makes them more difficult to incorporate into various device geometries. Thermoplastic electrodes are a new class of materials that are highly moldable with excellent electrochemistry and tunable electrochemical properties.[29] TPEs are fabricated through a simple process of dissolving a thermoplastic binder in organic solvent, mixing in conductive carbon, drying the material, and then heat pressing into an electrode template.[29] Through the use of poly(methyl methacrylate) (PMMA),[29, 30] cyclic olefin copolymer (COC),[30-32] and polycaprolactone (PCL) binders, [30, 33-35] TPEs have achieved voltammetry similar to that of traditional electrode materials such as glassy carbon and noble metals. Their moldability has also allowed for the easy incorporation into plastic[33, 34] and paper-based[30, 31] fluidic devices as well as generating electrode arrays[29, 31] which could benefit simultaneous direct detection in the future.

In this work, using polystyrene (PS) as an aromatic thermoplastic binder, PS TPEs are introduced that can resolve AA, DA, and UA peaks for simultaneous analysis at bare electrode surfaces. Unmodified PS TPEs have similar behavior to that of nanomaterial-modified electrodes. Initially the conductive carbon filler was optimized, and electrodes characterized with conductivity and capacitance testing, voltammetry, and SEM. From the electrode characterization data, resolution between the three peaks likely stems from their 3D edge-plane rich morphology generated during the polishing process, similar to morphology achieved from carbon nanomaterial

modifications.[11, 14-20] Following characterization, PS TPEs were calibrated for AA, UA, and DA in the presence of the other two species as well as simultaneously and challenged in urine.

4.3 Experimental

Materials

Uric acid (99+%) was sourced from Sigma-Aldrich. Dopamine hydrochloride (99%) was sourced from Alfa Aesar. Ascorbic acid (99%) used in CV experiments was sourced from Sigma-Aldrich and sourced from EMD Millipore for SWV experiments. Sodium hydroxide (NaOH, 1M) was sourced from J.T. Baker. BupH™ Phosphate Buffered Saline Packs (PBS), hydrochloric acid, and methylene chloride (DCM) were sourced from Thermo Fisher Scientific. PBS buffer was prepared using the buffer packs to be 0.1 M sodium phosphate and 0.15 M NaCl; the pH was adjusted with NaOH or HCl for the pH 3.0, 4.0, 5.0, 6.0, 7.0, 7.4, and 8.0 to make PB buffers. For urine analysis, normal urine from pooled human donors was sourced from Lee BioSolutions Inc. The urine was filtered with a Millex® Nylon 0.45 µm syringe filter to remove solid particulates before use.

For the TPE binder, polystyrene (molecular weight 45,000) was sourced from Sigma-Aldrich. TC303 synthetic graphite, 3569 natural flake graphite, 3805 surface enhanced flake graphite (SEFG), and NANO 19 carbon nanoplatelets were sourced from Asbury Carbons. MG1599 was sourced from Great Lakes Graphite and acetylene carbon black (CB) was sourced from STREM Chemicals, Inc. The material properties of the conductive carbons are listed in Table 4.1. Particle diameters ranged from 0.05-180 µm and carbon types used were above 99% pure. Electrode templates were made from 3.175 mm thick Optix poly(methyl methacrylate) (PMMA) sheets sourced from Plaskolite.

Table 4.1. Type, size, and purity of conductive carbon types used in this work.

Carbon	Type	Particle diameter	Purity (%)
MG1599	Natural flake graphite	~ 15 µm	99.5–99.99
TC303	Synthetic graphite	16–30 µm	99.94
3805	Surface enhanced flake graphite	10–15 µm	99.12
3569	Natural flake graphite	44–180 µm	99.94
NANO 19	Carbon nanoplatelets	~5.48 µm	99.85
CB	Acetylene carbon black	~50 nm	99.33

Electrode Preparation

The graphic design program CorelDRAW was used to design electrode templates, and templates were cut with an Epilog CO_2 laser cutter (settings: speed=30% power=100% and frequency=5000 Hz) to have 2.5 mm diameter circular holes. PS TPE material was made by dissolving ~1 g of PS in ~15 mL DCM then mixing in the conductive carbon at a 2:1 carbon:PS mass ratio. For TPE materials, except those made with CB filler, electrode materials were fully dried prior to heat pressing into templates. CB powder was prone to clumping and therefore to create a homogenous material it was mixed with the dissolved PS overnight. CB TPE material was also too brittle to heat press dry, so instead was dried to a gum-like consistency and heat pressed with solvent still present and was left on the press for 2 h to fully dry. PS TPEs were heat pressed into templates at 80–90 °C and 300–500 psi with a hydraulic heated press. Once the TPEs were pressed, excess material was removed with 150 grit sandpaper and connections were made with silver paint, copper wires, and epoxy. TPEs were initially polished for 2 min with wet 150 grit sandpaper followed by 1 min with wet 600 grit sandpaper prior to the first use and polished for 10–30 s with wet 600 grit sandpaper for subsequent polishes. "Pressed electrodes" shown in Fig.

4.1 were heat pressed again following connections to re-melt material and gain insight into unpolished electrochemical behavior.

Electrochemical Measurements

Electrochemical measurements were performed on the 2.5 mm disk electrodes with a CHI 660b potentiostat from CH Instruments Inc. The counter electrode used was a 4 mm diameter disk electrode made from TPE material and sanded with 150 grit sandpaper for a high surface area. The reference electrode used for all the TPE disk experiments was a saturated calomel electrode (SCE) sourced from CH Instruments Inc. Electrical potential values given in this work are versus the SCE reference electrode. Separate electrodes were used for each replicate for a given data point and error bars shown in graphs represent the standard deviations.

Scanning Electron Microscopy (SEM)

For SEM sample preparation, MG1599 PS TPEs were heat pressed into flat ~ 2 mm thick sheets and ~6 mm squares were cut for analysis. Prior to analysis, one of the samples was left unpolished and the other was polished with 150 and 600 grit sandpaper. SEM was performed with a JSM6500F field emission scanning electron microscope (JEOL, Tokyo, Japan) at 15 kV acceleration voltage.

Conductivity and Capacitance Testing

Conductivity and capacitance tests were performed as described in previous TPE work on 2.5 mm disks ~3 mm in thickness.[29, 33] Resistance measurements to determine conductivity were performed prior to making the wire connections with a Fluke 187 multimeter (0.01 Ω accuracy). Capacitive current was measured with CV in 0.1 M KNO_3 at 100 mV/s, and current values taken at 0.2 V vs. SCE were used for capacitance calculations. Calculations were performed as described previously in the literature.[29, 33]

Voltammetry Experiments

The electrochemistry of AA, DA, and UA were each characterized separately with CV at 0.5 mM concentrations in PBS (pH 7.4). CVs were taken at v=100 mV/s from -0.2 to 0.6 V for AA and DA, and 0 to 0.7 V for UA. CVs of the species together in solution were taken in 0.5 mM AA, 0.1 mM DA, and 0.1 mM UA in PBS (pH 7.4) at v=20 mV/s scan rates from -0.2 to 0.5 V. Freshly polished (n=3) electrodes and freshly made solutions were used for all CV measurements.

For the SWV measurements, 10 mM stock solutions were made of each species: AA in pH 3 PB, DA in 0.01 M HCl, and UA in 0.01 M NaOH. Each SWV solution was made fresh with stock solutions and buffer prior to measurements. An SWV frequency of 5 Hz, amplitude of 30 mV, and increment voltage of 8 mV were used for all measurements. For pH optimization, measurements were taken from -0.2 to 0.7 mV for pH 3.0, 4.0, 5.0, 6.0, 7.0, 7.4, and 8 PB. SWV measurements were taken from -0.2 to 0.6 V in pH 5.0 PB on freshly polished electrodes for all subsequent experiments.

4.4 Results and Discussion

Fig. 4.1 presents an overview of PS TPE fabrication, morphology, and electrochemistry with MG1599 as the conductive carbon. The pressed PS TPE material SEM shows relatively flat surfaces with primarily basal plane graphite exposed as opposed to the polished PS TPE material which has more edge plane rich morphology (Fig. 4.1b). The different surface morphologies of pressed and polished PS TPE material correspond to unresolved and resolved AA, DA, and UA peaks in Fig. 4.1c. From the SEM and CV data shown, we hypothesize that the ability to resolve AA, DA, and UA peaks with this simple fabrication process (Fig. 4.1a) stems from the surface morphology generated during the polishing process. This agrees with the literature where similarly 3D and edge plane-rich electrode surface morphologies from carbon nanomaterial modifications

led to resolution of the three peaks which allowed simultaneous determination.[11, 14-20] PS TPEs also show sharper peaks voltammetry peaks for AA, DA, and UA (S4.1) and unique morphology relative to that of previously published PMMA and PCL TPE work.[29, 33] We hypothesize the superior properties of PS TPEs may be attributed to the more brittle nature of PS plastic and π-π interactions between PS, conductive carbon, and the redox active species.

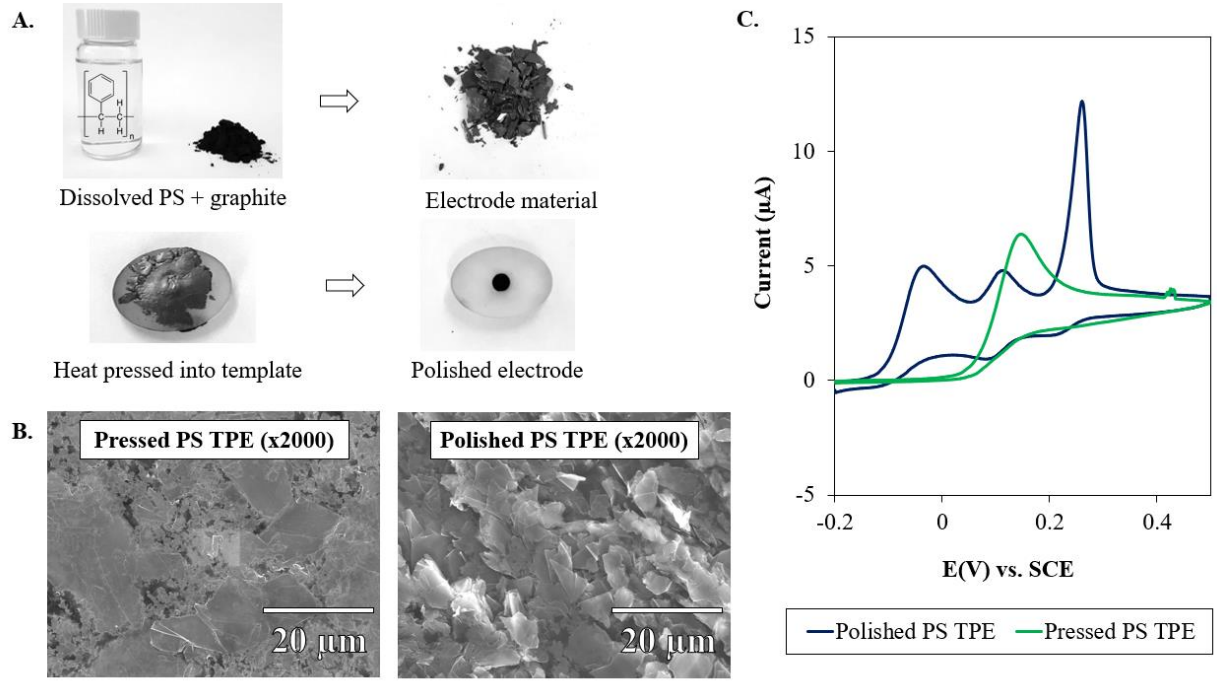

Fig. 4.1. A) Schematic for PS TPE fabrication, B) SEM images of heat pressed and polished MG1599 PS TPE material, and C) Cyclic voltammetry of 0.5 mM AA, 0.1 mM DA, and 0.1 mM UA in 0.1 M PBS (pH 7.4) for heat pressed and polished PS TPEs.

Conductivity/Capacitance

The conductivity and capacitance of PS TPEs made with different carbon types were compared. High conductivity is desired for electrodes to avoid Ohms law effects from cell resistance, and high conductivity often corresponds with higher electroactivity.[15] Low capacitance for electrochemical sensors leads to reduced background currents from non-faradaic processes.[15] Capacitance is also directly related to active surface area, but measured capacitance can be increased by background processes from metal contaminants and redox active surface oxides such

as quinones.[36] As shown in Fig. 4.2, conductivity and capacitance were greatly influenced by the conductive carbon type.

For conductivity, the differences between electrode materials with different fillers were dramatic, with TC303 synthetic graphite TPEs having the lowest conductivity at 57 ± 9 S/m and 3805 TPEs the highest at 2080 ± 90 S/m. The exceptional conductivity of 3805 SEFG TPEs may be due to the proprietary chemical treatment used to increase SEFG surface area.[37] Better wettability and distribution of graphite in a polymer matrix also improves composite conductivity.[38] The differences in conductivity did not relate to size or aspect ratio. Although quite different in size and shape, the carbon types MG1599, 3569, and CB did not have statistically different conductivities in PS TPEs. The three mid-sized graphite types MG1599, TC303, and 3805 had widely differing conductivities, with 3805 having 3× the conductivity of MG1599 and 36× the conductivity of TC303. These results suggest that surface structure and chemistry of the carbon filler is what influences conductivity of these PS TPEs most.

Capacitance for PS TPEs was comparable to traditional glassy carbon electrodes (24-318.0 $\mu F/cm^2$).[15, 39] Capacitance was lowest for MG1599 flake graphite TPEs at 90 ± 20 $\mu F/cm^2$ and the highest for 3805 SEFG at 214 ± 4 $\mu F/cm^2$. As capacitance is directly related to surface area, these results make sense; SEFG graphite is chemically treated to have double the surface area of flake graphite of the same particle size.[37] 3569 and CB had similar capacitance to MG1599, 110 ± 10 $\mu F/cm^2$ and 120 ± 20 $\mu F/cm^2$, respectively; therefore when low capacitance is needed material choice can be based on other considerations.

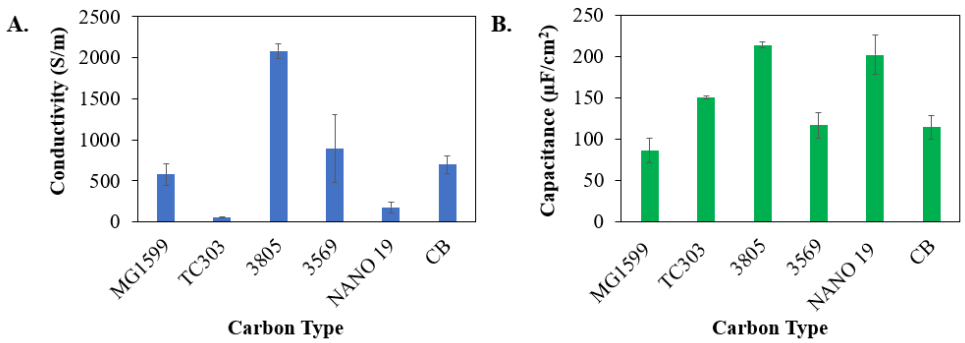

Fig. 4.2. Conductivity and capacitance measurements of PS TPEs made with different carbon types. A) Conductivity (n=4; n=5 CB) and B) capacitance (n=3).

Single Analyte CV data of PS TPEs

The voltammetry of each species was first examined separately with CV. The quantitative data is shown in Fig. 4.3, and CVs are shown in S4.1. For all PS TPEs, separation between average peak potentials for the three species were ≥150 mV which is promising for simultaneous determination at bare electrodes. The peak potential for AA ranged from -56 ± 2 mV for CB to -20 ± 10 mV for NANO 19, and peak currents from 7 ± 1 μA for MG1599 to 12 ± 1 μA for CB. Based on these results, AA oxidation is most favorable on CB TPEs. AA oxidation, unlike DA and UA, is an outer sphere process, so the amount of charge transferred should be more proportional to the active surface area.[15] Peak potential for DA ranged from 122 ± 1 mV for TC303 to 132 ± 3 mV for MG1599, and peak currents from 17 ± 2 μA for NANO 19 to 24 ± 2 μA for MG1599. The high peak currents and potentials for DA on MG1599 TPEs are promising for detection of DA in the presence of AA. Peak potential for UA ranged from 288 ± 1 mV for CB to 306 ± 3 mV for MG1599, and peak currents from 36 ± 3 μA for CB to 60 ± 3 μA for TC303. TC303 TPEs had high peak currents (24 ± 2, 11.4 ± 0.7, and 60 ± 3 μA) and relative standard deviation (RSD ≤ 8%) for all species tested. 3805, MG1599, and TC303 TPEs were chosen for further characterization as 3805 TPEs were the most conductive, MG1599 TPEs the least capacitive, and TC303 TPEs had the best overall voltammetry.

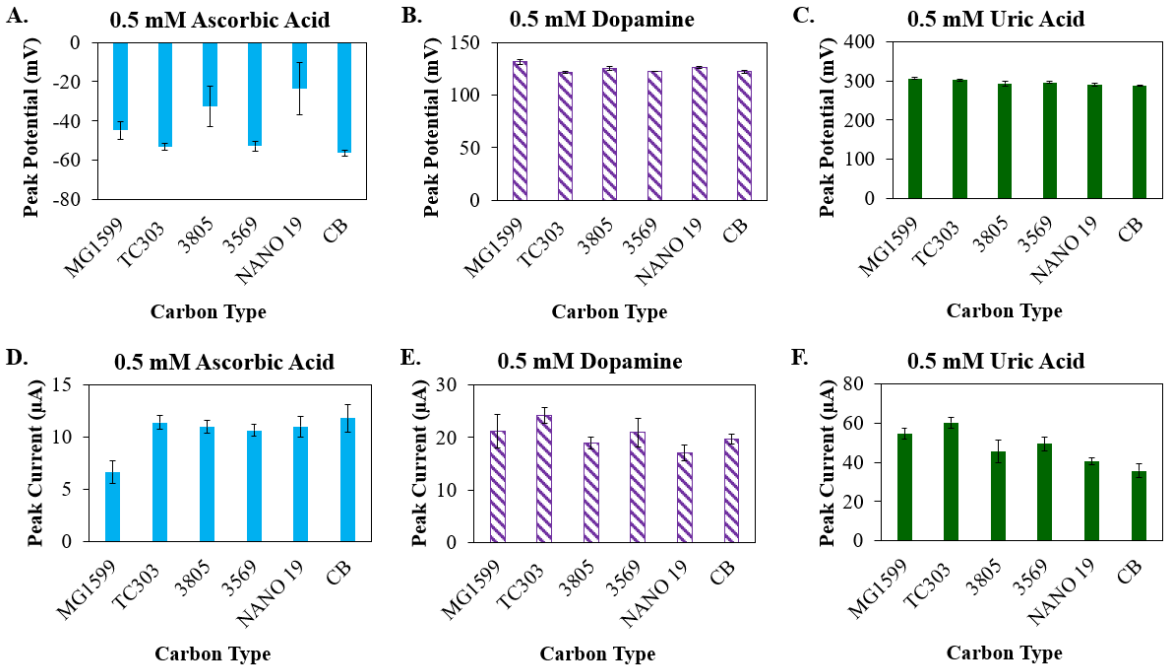

Fig. 4.3. Quantitative CV oxidation data for 0.5 mM AA (A, D), 0.5 mM of DA (B, E), or 0.5 mM UA (C,F) in 0.1 M PBS (pH 7.4) v=100 mV/s on 2.5 mm diameter disk TPEs made with different carbon filler types. A-C) Average oxidation peak potential (n=3), and D-F) average oxidation peak current (n=3).

Simultaneous Analysis CV Data

The three species were next tested in solution together by CV, with results shown in Fig. 4.4. The three oxidation peaks were well resolved on all three TPE types. For 3805 TPEs, the high capacitive background makes the three peaks appear less distinct than they do on the other two TPE types. AA, DA, and UA oxidation peak current values (~4, ~3.5, and ~10 µA, respectively) as well as DA-AA peak separation (~150 mV) were not statistically different between the TPE types. 3805 had the lowest DA-UA and AA-UA separations (146 ± 4 mV, 290 ± 20 mV, respectively) and highest RSD for peak currents (17, 19, 20% for AA, DA, and UA, respectively). TC303 had the lowest peak current RSDs (11, 9, 5% for AA, DA, and UA, respectively), and MG1599 had the second lowest overall peak current RSDs (10, 17, 7% for AA, DA, and UA, respectively). Peak separations were not statistically different between MG1599 and TC303, so

MG1599 was chosen for further experiments due to its lower capacitance and higher conductivity than TC303. However, in situations where sensitivity and reproducibility are more important than LOD, TC303 could be the most appropriate.

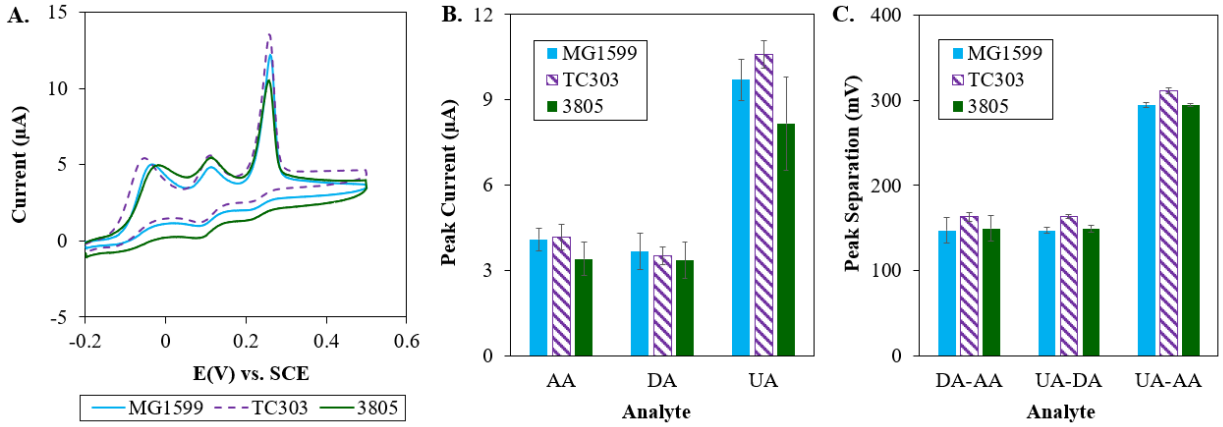

Fig. 4.4. CV data of 0.5 mM AA, 0.1 mM of DA, and 0.1 mM UA solution in 0.1 M PBS (pH 7.4) v=20 mV/s on 2.5 mm diameter disk TPEs made with MG1599, TC303, or 3805. A) Representative CVs of each TPE type, B) quantitative oxidation peak data, and C) potential separation between the different redox peaks (n=3).

pH Study

The influence of pH on signal was investigated with SWV for 100 µM AA, 10 µM DA, and 20 µM UA in buffers from pH 3–8. Quantitative data for the pH study is shown in Fig. 4.5. The relationships between peak potential and pH were linear for the three redox molecules tested: $E_{p(AA)}$ (mV) = 215 − 39.5 pH (R^2 = 0.9923), $E_{p(DA)}$ (mV) = 528 – 60.4 pH (R^2 = 0.9989), and $E_{p(UA)}$ (mV) = 688 – 62.3 pH (R^2 = 0.9978). DA and UA had slopes close to the theoretical slope as determined by the Nernst equation (59 mV), whereas AA a much lower pH slope of 39.5 mV/pH. AA's lower pH slope could be due to the oxidation reaction's high sensitivity to electrode surface oxide groups which also change with pH. Average oxidation peak current potentials were highest for AA at pH 3.0, DA at pH 5.0, and UA at pH 6.0. The widest separations between peaks were seen from pH 3–5, with pH 3.0 having the highest AA–DA separation at 243 mV and pH 5.0 having the highest AA–DA separation at 160 mV. At pH 5.0 the peak current RSD values for AA,

DA, and UA were 15, 9, and 3%, respectively, as opposed to pH 7.4 where the RSD values were 13, 12, and 31%. For further experiments pH 5.0 was used as it had relatively high peak currents and separations, as well as low RSD relative to that of physiological pH for all the species tested.

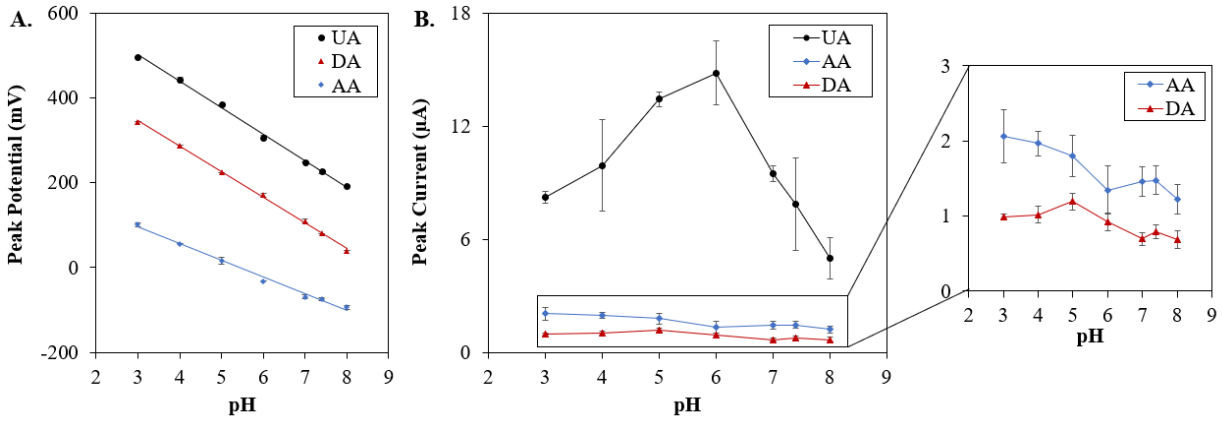

Fig. 4.5. Quantitative SWV data of 100 µM AA, 10 µM DA, and 20 µM UA solution in pH 3, 4, 5, 6, 7, 7.4, and 8 PB. A) Peak potentials, and B) peak currents for the three redox species (n=3).

Calibration Curves

To evaluate the performance of these PS TPE sensors, single analyte and simultaneous calibrations were performed. Linear regression data is summarized in Table 4.2. Calibration curves were first taken for each individual species in the presence of the other two species (Fig. 4.6) with 100 µM AA, 10 µM DA, and 20 µM UA background concentrations. The three species all showed linear responses in the presence of the other two species with linear ranges of 10–1000 µM for AA, 1–500 µM for DA, and two linear ranges for UA: 1-50 µM and 100-400 µM and R^2 values of 0.9970, 0.9988, 0.9944, and 0.9962 respectively. Sensitivities were 0.00203, 0.0057, and 0.0159 VA/M for AA, DA, and UA respectively.

AA had the lowest sensitivity and widest linear range of the three species, which is beneficial to simultaneous analysis as AA is often present in bodily fluids in high amounts and for a wide range of concentrations (34–9602 µM).[2, 3, 40, 41] However, at AA concentrations above 200 µM, AA shifted DA and UA peaks outward and their signals decreased by 11 and 22% respectively

when in the presence of 1000 µM AA. Therefore, at higher AA concentrations these sensors are less suitable for simultaneous determination, and dilutions may be required. DA had a wide linear range without interfering with AA or UA. Although this range is useful for pharmaceutical applications, additional measures to extend the lower linear range will be necessary for most biological applications (10 nM–1 µM DA typical in bodily fluids).[4, 21, 42] UA signal was the most sensitive of the three species and did not interfere with AA and DA signal from 1–50 µM. From 100–400 µM UA signal was also linear, but 3.6× less sensitive and suppressed AA and DA peaks. These sensors therefore are good for detection of higher UA concentrations in the presence of AA and DA, however, for simultaneous analysis UA concentrations need to be diluted to ≤50 µM. Healthy uric acid levels in the body are 89–387 µM with levels exceeding that indicating hyperuricemia,[43] and uric acid is excreted in urine at ~2 mM concentrations.[44]

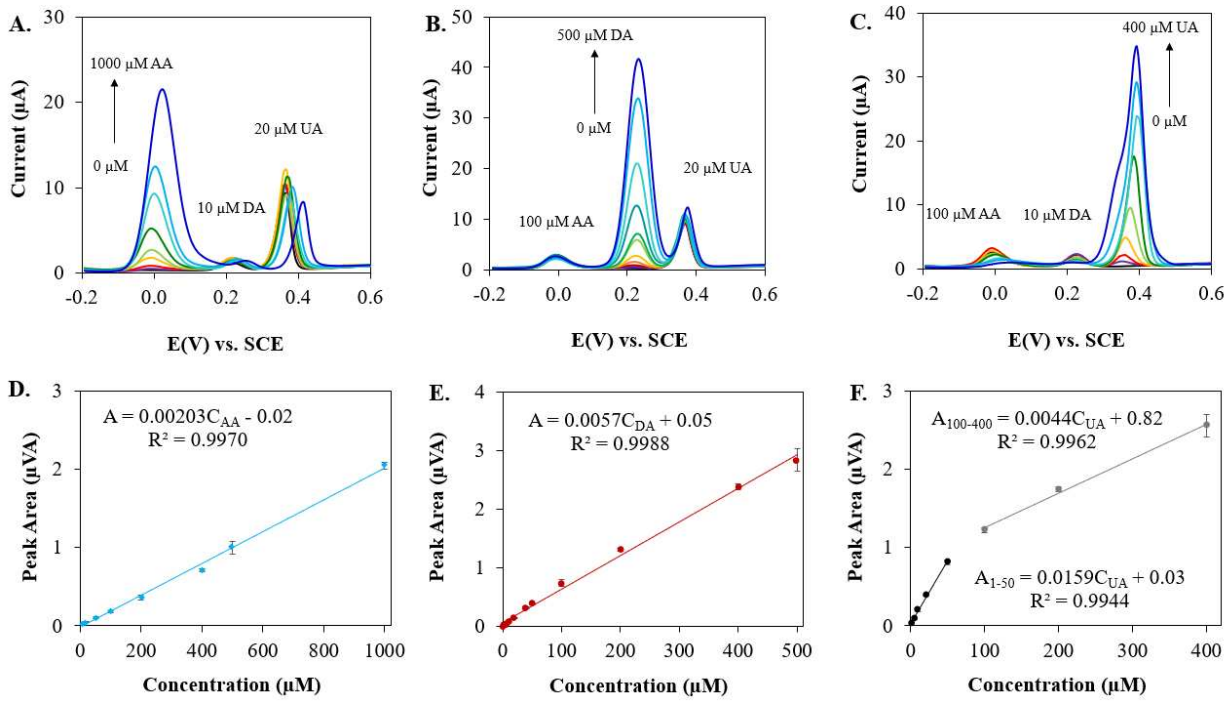

Fig. 4.6. AA, DA, and UA calibration curve data. A-C) Representative SWV of AA, DA, and UA calibration curves, respectively, in the presence of the other two species. D-E) Quantitative calibration curve SWV peak area data for AA, DA, and UA, respectively (n=3).

From the single analyte calibration data, concentration ranges were chosen for simultaneous calibration where the signal response was linear and there was no noticeable interference between the three analytes. For DA, the lower linear range was focused on as low DA concentrations are more relevant to analytical applications.[4] Simultaneous calibration data is shown in Fig. 4.7a-b, and all three species showed excellent linear responses with R^2 values of 0.9999, 0.9941, 0.9959 for AA, DA, and UA, respectively. Simultaneous calibration data showed similar sensitivities to that of single analyte calibrations, 0.001541, 0.0058, and 0.0159 VA/M for AA, DA, and UA respectively.

In Fig. 4.7c, the data from the single analyte calibration curves and simultaneous increase calibration curves were combined (n=6) to assess overall performance. The combined regressions are shown in Table 4.2. Combined regressions had the highest R^2 values, 0.9998, 0.9995, and 0.9952 for AA, DA, and UA, respectively. Sensitivities of 0.00165, 0.00683, and 0.159 VA/M for AA, DA, and UA, respectively therefore fit the overall data well. The detection limits of AA, DA and UA were determined from the combined calibration curves to be 4, 0.9, and 4 μM (S/N = 3), respectively. The results for these sensors are compared to that of other recently published literature in the field in Table 4.3. Although much simpler in electrode composition and fabrication, PS TPEs have comparable performance to that of porous, nanomaterial, and ionic liquid modified electrodes from recent literature.

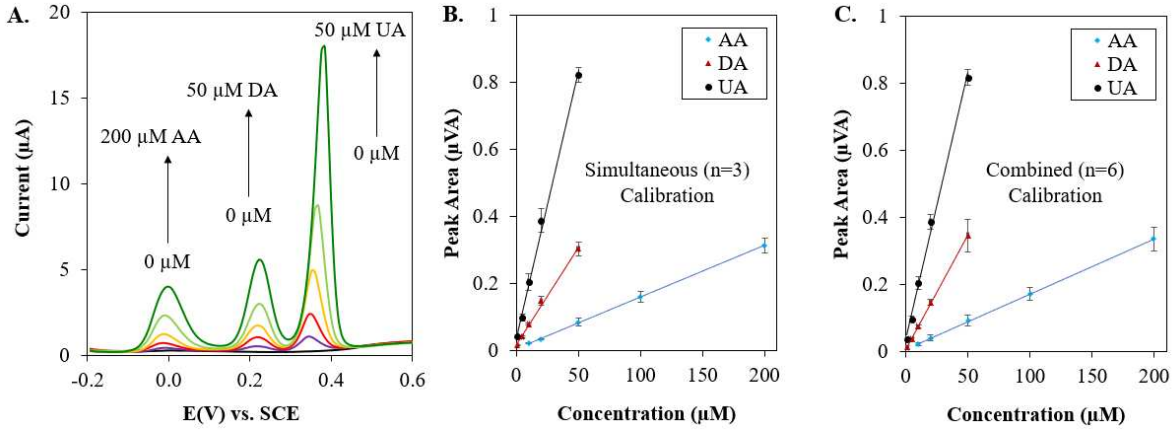

Fig. 4.7. Simultaneous calibration curve data. A) Representative SWV of AA, DA, and UA simultaneous calibration. B) Quantitative peak area data for simultaneous calibration experiment (n=3). C) Quantitative peak area data combined for simultaneous calibration and single analyte calibration experiments.

Table 4.2. Summary of linear regression data with coefficient uncertainty values for AA, DA, and UA calibration experiments.

Calibration	Species	Linear Equations y = mx + b	Range (µM)	R^2
Single	AA	A = (0.00203 ± 0.00005) C + (-0.02 ± 0.02)	10–1000	0.9970
Analyte	DA	A = (0.0057 ± 0.0001) C + (0.05 ± 0.03)	1–500	0.9988
(n=3)	UA	$A_{1\text{-}50}$ = (0.0159 ± 0.0006) C + (0.03 ± 0.02)	1–50	0.9944
		$A_{100\text{-}400}$ = (0.0044 ± 0.0003) C + (0.82 ± 0.07)	100–400	0.9962
Simultaneous	AA	A = (0.001541 ± 0.000009) C + (0.004 ±	10–200	0.9999
(n=3)	DA	0.001)	1–50	0.9941
	UA	A = (0.0058 ± 0.0003) C + (0.016 ± 0.006)	1–50	0.9959
		A = (0.0159 ± 0.0006) C + (0.04 ± 0.01)		
Combined	AA	A = (0.00165 ± 0.00001) C + (0.007 ± 0.002)	10–200	0.9998
(n=6)	DA	A = (0.00683 ± 0.00009) C + (0.005 ± 0.002)	1–50	0.9995
	UA	A = (0.0159 ± 0.0006) C + (0.03 ± 0.02)	1–50	0.9952

Table 4.3. Comparison of this work with recent literature.[a]

Sensor	Analyte	LOD (µM)	AA-DA (mV)	DA-UA (mV)	Reference
Holey nitrogen-doped graphene aerogel	AA DA UA	16.7 0.22 0.12	216	120	[27]
Porous graphitic C_3N_4 nanosheets and GO modified GCE	AA DA UA	3.7 0.07 0.43	150	340	[45]
N-Doped RGO/AuNPs modified GCE	AA DA UA	58 2.4 8.7	340	200	[14]
Graphene quantum dots/ionic liquid modified SPCE	AA DA UA	6.64 0.06 0.03	170	140	[21]
Bare PS TPE	AA DA UA	4 0.9 4	208	160	This work.

[a] *Graphene oxide (GO), glassy carbon electrode (GCE), reduced graphene oxide (RGO), and screen-printed carbon electrode (SPCE).*

Urine Analysis

For urine analysis, SWVs were taken for the pooled urine diluted 100-fold with pH 5.0 PB as well as urine diluted and spiked to final concentrations of 100 µM AA, 10 µM DA, and 20 µM UA (S4.1), and final concentrations of 200 µM AA, 5 µM DA, and 10 µM UA (S2). Results for the spiked samples are summarized in Table 4.4. The diluted urine sample was found to have 10 ± 2 µM UA (1.0 ± 0.2 mM undiluted), which agrees with typical UA concentrations in urine which are in the low mM range.[44] The recoveries ranged from 90–110% for AA and UA which were comparable to other recent literature in this field[27] and within error of 100%. For DA, there were lower recoveries in urine, 82% and 47% for 10 and 5 µM, respectively. For 10 µM, the recovery is within error of other published work;[46] however, additional considerations may be necessary for

DA determination in real samples. Fortunately, for the highly moldable and tunable PS TPEs, TPEs can be readily incorporated into fluidic devices or miniaturized to reduce background and lower LODs.[29, 31, 33] The use of more oxidized conductive carbons may also benefit DA detection due to electrostatics.

Table 4.4 SWV data and recoveries for spiked diluted urine (n=4).

Sample	Analyte	Detected (µM)	Spiked (µM)	Found (µM)	% Recovered	% RSD
1:100	AA	–	100	90 ± 10	90 ± 10	11
Urine	DA	–	10	8.2 ± 0.3	82 ± 3	4
(S1)	UA	10 ± 2	20	32 ± 3	110 ± 20	9
1:100	AA	–	200	220 ± 30	110 ± 20	14
Urine	DA	–	5	2.4 ± 0.2	47 ± 7	15
(S2)	UA	10 ± 2	10	21 ± 3	110 ± 20	14

4.5 Conclusions

PS TPEs were excellent electrodes for simultaneous analysis of AA, DA, and UA. The LODs and separation between peaks, and recoveries compared favorably with recent published literature while having simpler sensor preparation. Due to the tunable properties and excellent moldability of PS TPEs, in the future these materials can be incorporated small volume or fluidic devices to improve performance further. In addition, different conductive carbons that perform better for different analytes could be incorporated into an electrode array for lowered LODs and even better discrimination between multiple analytes. Thus, these materials show great promise for simultaneous direct detection for AA, DA, and UA.

REFERENCES

1. Kaya, S. I.; Kurbanoglu, S.; Ozkan, S. A., Nanomaterials-based nanosensors for the simultaneous electrochemical determination of biologically important compounds: ascorbic acid, uric acid, and dopamine. *Crit. Rev. Anal. Chem.* **2019,** *49* (2), 101-125.

2. Dhara, K.; Debiprosad, R. M., Review on nanomaterials-enabled electrochemical sensors for ascorbic acid detection. *Analytical biochemistry* **2019,** *586*, 113415.

3. Arrigoni, O.; De Tullio, M. C., Ascorbic acid: much more than just an antioxidant. *Biochimica et Biophysica Acta (BBA)-General Subjects* **2002,** *1569* (1-3), 1-9.

4. Liu, X.; Liu, J., Biosensors and sensors for dopamine detection. *View* **2021,** *2* (1), 20200102.

5. Iversen, S. D.; Iversen, L. L., Dopamine: 50 years in perspective. *Trends in neurosciences* **2007,** *30* (5), 188-193.

6. Reymond, M.; Speciale, S.; Porter, J., Dopamine in Plasma of Lateral and Medial Hypophysial Portal Vessels: Evidence for Regional Variation in the Release of Hypothalamic Dopamine into Hypophysial Portal Blood. *Obstetrical & Gynecological Survey* **1984,** *39* (4), 213-214.

7. Maiuolo, J.; Oppedisano, F.; Gratteri, S.; Muscoli, C.; Mollace, V., Regulation of uric acid metabolism and excretion. *International journal of cardiology* **2016,** *213*, 8-14.

8. Black, C. N.; Bot, M.; Scheffer, P. G.; Snieder, H.; Penninx, B. W., Uric acid in major depressive and anxiety disorders. *Journal of affective disorders* **2018,** *225*, 684-690.

9. Liu, J.; Xu, C.; Ying, L.; Zang, S.; Zhuang, Z.; Lv, H.; Yang, W.; Luo, Y.; Ma, X.; Wang, L., Relationship of serum uric acid level with non-alcoholic fatty liver disease and its inflammation progression in non-obese adults. *Hepatology Research* **2017,** *47* (3), E104-E112.

10. Perez-Ruiz, F.; Dalbeth, N.; Bardin, T., A review of uric acid, crystal deposition disease, and gout. *Advances in therapy* **2015,** *32* (1), 31-41.

11. Rahman, M. M.; Lopa, N. S.; Ju, M. J.; Lee, J.-J., Highly sensitive and simultaneous detection of dopamine and uric acid at graphene nanoplatelet-modified fluorine-doped tin oxide electrode in the presence of ascorbic acid. *Journal of Electroanalytical Chemistry* **2017,** *792*, 54-60.

12. Krishnan, S.; Tong, L.; Liu, S.; Xing, R., A mesoporous silver-doped TiO 2-SnO 2 nanocomposite on gC 3 N 4 nanosheets and decorated with a hierarchical core− shell metal-organic framework for simultaneous voltammetric determination of ascorbic acid, dopamine and uric acid. *Microchim. Acta* **2020,** *187* (1), 1-9.

13. Salahandish, R.; Ghaffarinejad, A.; Naghib, S. M.; Niyazi, A.; Majidzadeh-A, K.; Janmaleki, M.; Sanati-Nezhad, A., Sandwich-structured nanoparticles-grafted functionalized graphene based 3D nanocomposites for high-performance biosensors to detect ascorbic acid biomolecule. *Scientific reports* **2019,** *9* (1), 1-11.

14. Minta, D.; González, Z.; Wiench, P.; Gryglewicz, S.; Gryglewicz, G., N-Doped Reduced Graphene Oxide/Gold Nanoparticles Composite as an Improved Sensing Platform for Simultaneous Detection of Dopamine, Ascorbic Acid, and Uric Acid. *Sensors* **2020,** *20* (16), 4427.

15. McCreery, R. L., Advanced carbon electrode materials for molecular electrochemistry. *Chem. Rev.* **2008,** *108* (7), 2646-2687.

16. Ping, J.; Wu, J.; Wang, Y.; Ying, Y., Simultaneous determination of ascorbic acid, dopamine and uric acid using high-performance screen-printed graphene electrode. *Biosensors and Bioelectronics* **2012,** *34* (1), 70-76.

17. Zhu, S.; Li, H.; Niu, W.; Xu, G., Simultaneous electrochemical determination of uric acid, dopamine, and ascorbic acid at single-walled carbon nanohorn modified glassy carbon electrode. *Biosensors and Bioelectronics* **2009,** *25* (4), 940-943.

18. Yang, B.; Wang, H.; Du, J.; Fu, Y.; Yang, P.; Du, Y., Direct electrodeposition of reduced graphene oxide on carbon fiber electrode for simultaneous determination of ascorbic acid, dopamine and uric acid. *Colloids and Surfaces A: Physicochemical and Engineering Aspects* **2014,** *456*, 146-152.

19. Nagles, E.; García-Beltrán, O.; Calderón, J. A., Evaluation of the usefulness of a novel electrochemical sensor in detecting uric acid and dopamine in the presence of ascorbic acid using a screen-printed carbon electrode modified with single walled carbon nanotubes and ionic liquids. *Electrochimica Acta* **2017,** *258*, 512-523.

20. Taleb, M.; Ivanov, R.; Bereznev, S.; Kazemi, S. H.; Hussainova, I., Ultra-sensitive voltammetric simultaneous determination of dopamine, uric acid and ascorbic acid based on a graphene-coated alumina electrode. *Microchim. Acta* **2017,** *184* (12), 4603-4610.

21. Kunpatee, K.; Traipop, S.; Chailapakul, O.; Chuanuwatanakul, S., Simultaneous determination of ascorbic acid, dopamine, and uric acid using graphene quantum dots/ionic liquid modified screen-printed carbon electrode. *Sensors and Actuators B: Chemical* **2020,** *314*, 128059.

22. Hsine, Z.; Blili, S.; Milka, R.; Dorizon, H.; Said, A. H.; Korri-Youssoufi, H., Sensor based on redox conjugated poly (para-phenylene) for the simultaneous detection of dopamine, ascorbic acid, and uric acid in human serum sample. *Anal. Bioanal. Chem.* **2020,** *412*, 4433-4446.

23. Hung, P.-S.; Wang, G.-R.; Chung, W.-A.; Chiang, T.-T.; Wu, P.-W., Green synthesis of ni@ PEDOT and ni@ PEDOT/au (Core@ shell) inverse opals for simultaneous detection of ascorbic acid, dopamine, and uric acid. *Nanomaterials* **2020,** *10* (9), 1722.

24. Zhang, K.; Zhang, N.; Zhang, L.; Wang, H.; Shi, H.; Liu, Q., Simultaneous voltammetric detection of dopamine, ascorbic acid and uric acid using a poly (2-(N-morpholine) ethane sulfonic acid)/RGO modified electrode. *RSC advances* **2018,** *8* (10), 5280-5285.

25. Ensafi, A. A.; Taei, M.; Khayamian, T.; Arabzadeh, A., Highly selective determination of ascorbic acid, dopamine, and uric acid by differential pulse voltammetry using poly (sulfonazo III) modified glassy carbon electrode. *Sensors and Actuators B: Chemical* **2010,** *147* (1), 213-221.

26. Zhang, W.; Liu, L.; Li, Y.; Wang, D.; Ma, H.; Ren, H.; Shi, Y.; Han, Y.; Ye, B.-C., Electrochemical sensing platform based on the biomass-derived microporous carbons for simultaneous determination of ascorbic acid, dopamine, and uric acid. *Biosensors and Bioelectronics* **2018,** *121*, 96-103.

27. Feng, S.; Yu, L.; Yan, M.; Ye, J.; Huang, J.; Yang, X., Holey nitrogen-doped graphene aerogel for simultaneously electrochemical determination of ascorbic acid, dopamine and uric acid. *Talanta* **2021,** *224*, 121851.

28. Zhang, W.; Zhu, S.; Luque, R.; Han, S.; Hu, L.; Xu, G., Recent development of carbon electrode materials and their bioanalytical and environmental applications. *Chem. Soc. Rev.* **2016,** *45* (3), 715-752.

29. Klunder, K. J.; Nilsson, Z.; Sambur, J. B.; Henry, C. S., Patternable Solvent-Processed Thermoplastic Graphite Electrodes. *J. Am. Chem. Soc.* **2017,** *139* (36), 12623-12631.

30. Pradela-Filho, L. A.; Noviana, E.; Araujo, D.; Takeuchi, R.; Santos, A.; Henry, C. S., Rapid Analysis in Continuous Flow Electrochemical Paper-Based Analytical Devices. *ACS Sens.* **2020**.

31. Noviana, E.; Klunder, K. J.; Channon, R. B.; Henry, C. S., Thermoplastic Electrode Arrays in Electrochemical Paper-Based Analytical Devices. *Analytical Chemistry* **2019,** *91* (3), 2431-2438.

32. Berg, K. E.; Leroux, Y. R.; Hapiot, P.; Henry, C. S., Increasing Applications of Graphite Thermoplastic Electrodes with Aryl Diazonium Grafting. *ChemElectroChem* **2019,** *6* (18), 4811-4816.

33. Klunder, K. J.; Clark, K. M.; McCord, C.; Berg, K. E.; Minteer, S. D.; Henry, C. S., Polycaprolactone-enabled sealing and carbon composite electrode integration into electrochemical microfluidics. *Lab Chip* **2019,** *19* (15), 2589-2597.

34. Berg, K. E.; Clark, K. M.; Li, X.; Carter, E. M.; Volckens, J.; Henry, C. S., High-throughput, semi-automated dithiothreitol (DTT) assays for oxidative potential of fine particulate matter. *Atmospheric Environment* **2020,** *222*, 117132.

35. Ozer, T.; McCord, C.; Geiss, B. J.; Dandy, D.; Henry, C. S., Thermoplastic Electrodes for Detection of Escherichia coli. *Journal of The Electrochemical Society* **2021,** *168* (4), 047509.

36. Brousse, T.; Belanger, D.; Long, J. W., To Be or Not To Be Pseudocapacitive? *Journal of the Electrochemical Society* **2015,** *162* (5), A5185-A5189.

37. Tamashausky, A. V. In *Surface enhanced flake graphite and its utility as a functional extender for molybdenum disulfide*, NLGI Spokesman-Including NLGI Annual Meeting-National Lubricating Grease Institute, [Kansas City, Mo.] National Lubricating Grease Institute.: 2006; pp 8-16.

38. Boyaci San, F. G.; Tekin, G., A review of thermoplastic composites for bipolar plate applications. *Int. J. Energy Res.* **2013,** *37* (4), 283-309.

39. Antiochia, R.; Lavagnini, I.; Magno, F.; Valentini, T.; Palleschi, G., Single-wall carbon nanotube paste electrodes: a comparison with carbon paste, platinum and glassy carbon electrodes via cyclic voltammetric data. *Electroanalysis* **2004,** *16* (17), 1451-1458.

40. Tallaksen, C.; Bøhmer, T.; Bell, H., Concentrations of the water-soluble vitamins thiamin, ascorbic acid, and folic acid in serum and cerebrospinal fluid of healthy individuals. *The American journal of clinical nutrition* **1992,** *56* (3), 559-564.

41. Brigden, M. L.; Edgell, D.; McPherson, M.; Leadbeater, A.; Hoag, G., High incidence of significant urinary ascorbic acid concentrations in a west coast population—implications for routine urinalysis. *Clin. Chem.* **1992,** *38* (3), 426-431.

42. Iranmanesh, T.; Foroughi, M. M.; Jahani, S.; Zandi, M. S.; Nadiki, H. H., Green and facile microwave solvent-free synthesis of CeO2 nanoparticle-decorated CNTs as a quadruplet electrochemical platform for ultrasensitive and simultaneous detection of ascorbic acid, dopamine, uric acid and acetaminophen. *Talanta* **2020,** *207*, 120318.

43. KUMAR, A. N.; ARUNA, P.; NAİDU, J. N.; KUMAR, R.; SRİVASTAVA, A. K., Review of concepts and controversies of uric acid as antioxidant and pro-oxidant. *Arşiv kaynak tarama dergisi* **2015,** *24* (1), 19-40.

44. Lakshmi, D.; Whitcombe, M. J.; Davis, F.; Sharma, P. S.; Prasad, B. B., Electrochemical detection of uric acid in mixed and clinical samples: a review. *Electroanalysis* **2011,** *23* (2), 305-320.

45. Zhang, L.; Liu, C.; Wang, Q.; Wang, X.; Wang, S., Electrochemical sensor based on an electrode modified with porous graphitic carbon nitride nanosheets (C 3 N 4) embedded in

graphene oxide for simultaneous determination of ascorbic acid, dopamine and uric acid. *Microchim. Acta* **2020,** *187* (2), 1-10.

46. Wang, L.; Yang, R.; Qu, L.; Harrington, P. d. B., Electrostatic repulsion strategy for high-sensitive and selective determination of dopamine in the presence of uric acid and ascorbic acid. *Talanta* **2020,** *210*, 120626.

CHAPTER 5: CONCLUSIONS AND FUTURE DIRECTIONS

Detection of biomarkers is essential to understanding and monitoring health, however, many laboratory-based methods for biomarker detection can be lengthy, costly, and inaccessible in resource limited settings.[1, 2] The ability to detect biomarkers at the point of care can improve health outcomes.[2, 3] Developing new electrochemical sensors for biomarker detection is of interest as electrochemical detection methods have fast measurement times and low-cost portable instrumentation.[3, 4] Electrochemical sensors are widely used for glucose detection; however, challenges remain for developing viable electrochemical sensors for a wider variety of analytes.[3, 5] Important challenges in this field include developing high-performance inexpensive electrode materials, as well as improving ease of fabrication, stability, and simplicity of electrochemical sensors.[3, 5] This thesis contributes to solving these challenges through successfully utilizing a new class of inexpensive and moldable carbon composite electrode materials, called thermoplastic electrodes (TPEs) to develop electrochemical sensors for detection of protein and small molecule biomarkers.[6] TPE immunosensors were first developed for C-reactive protein (CRP) using novel diazonium tosylate functionalization methods, new PS TPEs were developed and characterized as the first TPEs with aromatic binders, and unmodified PS TPEs were then used successfully for simultaneous determination of ascorbic acid (AA), uric acid (UA), and dopamine (DA).

Inexpensive electrodes with fast redox kinetics, and simple stable methods of electrode functionalization are important for electrochemical immunosensors.[5, 7] However, many inexpensive and easy to fabricate electrodes suffer from poor electrochemical properties, and functionalization can often be difficult and/or unstable.[8, 9] In Chapter 2 these issues are addressed through the development of TPE immunosensors which are functionalized using diazonium

tosylates. TPE materials have excellent electrochemical properties relative to other inexpensive composites and are easy to mold into different sensor configurations.[6, 10] TPE material for these immunosensors was made with polymethyl methacrylate (PMMA) mixed with polycaprolactone (PCL) binder. In this thesis, the first TPE immunosensors were developed using a sandwich enzyme-linked immunosorbent assay (ELISA) format and square wave voltammetry (SWV) detection. The use of TPE materials enabled small volume electrode arrays with excellent electrochemistry. In Chapter 2, diazonium tosylates were synthesized in-situ through a simple 6 min process and used to spontaneously modify TPEs in 5 min. TPEs were amine functionalized either directly through grafting of p-aminophenyl diazonium salt or indirectly through grafting p-nitrophenyl diazonium salt followed by electrochemical reduction to an amine. Diazonium salts are particularly stable and soluble salts that can be useful for electrode functionalization but had not been used for immunosensor modification previously.[11, 12] Amine functionalized electrodes were then conjugated to antibodies and applied for ELISA detection of CRP, a cardiovascular disease (CVD) biomarker.[13] These immunosensors showed clinically relevant detection limits (2 ng/mL in buffer, 10 ng/mL in serum) and retained sensitivity in serum.

In the future, to further simplify fabrication and detection for these TPE immunosensors, bulk modification and label-free detection methods can be explored. For bulk modification, diazonium tosylates would be mixed directly with graphite prior to incorporation into TPEs. The modified graphite would be washed and then used as the conductive TPE filler. If successful, this would create bulk modified TPE materials with renewable amine functionalized surfaces. Label-free detection would simplify the assay by removing the need for additional assay steps following sample incubation. For label-free assays antibody-antigen binding can be quantified through

increase in resistance to charge transfer at the electrode surface.[14] If label-free detection methods fail, additional assay steps could be automated using microfluidics.[15]

These low-cost and robust TPE immunosensors can also be easily adapted for other analytes as and used for multiplexed detection. One potential future application for this platform is multiplexed detection of CVD biomarkers in saliva. Blood serum is typically used for the detection of CVD biomarkers; however, less invasive sample matrices like saliva would be beneficial for widespread biomarker screening.[16] CRP, galectin-3, and s100A7 are promising salivary biomarkers of CVD, and monitoring multiple CVD biomarkers can provide a more complete picture of a patients state of health.[16-19] The selective TPE immunosensors developed in this thesis can be multiplexed through functionalizing different working electrodes with different antibodies for each analyte. Based on the CRP results in Chapter 2, additional sensor optimization will be needed for determination in saliva where healthy CRP levels average around 289 pg/mL and cardiovascular disease patients average just below the TPE sensor detection limit (2 ng/mL) at 1680 pg/mL.[16] However, determination in saliva could likely be achieved with further optimization of assay steps, sensor design, and use of the more electroactive and less capacitive PS TPEs. Saliva as a matrix may pose some challenges, but TPEs can be easily incorporated into fluidic devices, so saliva can be pre-processed in sensor devices if needed.[20-22]

Although TPEs made with PCL and PMMA performed well in Chapter 2, TPE binders up to this point had only contained aliphatic hydrocarbons. Thus, we investigated how aromatic binder functionalities would impact TPE properties, and whether aromatic binders could improve performance for biomarker detection. In Chapter 3 different PS molecular weights, expanded polystyrene (EPS) waste, and PS-PCL blends were explored as the first TPE binders containing aromatic functionalities; previously developed PCL TPEs were used for comparison.

Conductivity, capacitance, morphology, and voltammetry were characterized for the various TPE compositions. Even small additions of PS to PCL TPEs were found to substantially lower capacitance, which is important for electrochemical detection as capacitance contributes to background current. PS-PCL binder blends were found to increase conductivity. Surface morphology was characterized with scanning electron microscopy (SEM) and optical profilometry (OP) and PS TPEs were found to have more edge-plane rich 3D microscale surface structures but lower overall surface roughness than PCL TPEs. Cyclic voltammetry (CV) was taken of the different PS TPE materials using various common and biologically relevant redox probes. PS TPE voltammetry had sharp peaks and low peak potentials for many redox species relative to other unmodified carbon electrode materials. The voltammetry and morphology of unmodified PS TPEs was like that of carbon nanomaterial modified electrodes, making these materials an exciting new development with many potential applications for electrochemical detection.

In Chapter 4 unmodified PS TPEs are used for simultaneous detection of AA, DA, and UA biomarkers. AA, DA, and UA are important biomolecules that coexist in bodily fluids but their oxidation peaks are poorly resolved at most bare electrode materials.[23] Electrode modifiers such as metal or carbon nanomaterials are often needed for simultaneous analysis, unfortunately, surface modifications add cost and complexity to sensor fabrication.[23, 24] The development of inexpensive PS TPEs that can perform simultaneous analysis of AA, DA, and UA unmodified is therefore a useful achievement. PS TPEs were optimized for conductivity, capacitance, and electrochemistry using different conductive carbon fillers. Different PS TPE materials were characterized with CV and following optimization SWV was used for quantitative simultaneous determination. Detection limits and separation between AA, DA, and UA oxidation peaks on PS TPEs overall compared favorably with recent literature electrodes that utilized multiple surface

modifiers. [25-27] As a proof of concept for use in biological samples, PS TPEs were challenged in urine and PS TPEs showed excellent AA and UA signal recoveries. Although comparable to some literature values, the detection limit for DA with these sensors is not sufficient yet for bioanalysis, and signal recovery for DA in urine was low.[26, 28] However, overall PS TPEs were promising materials for simultaneous analysis, and additional work can be done to improve DA detection in the future.

For future PS TPE work, additional characterization experiments could help elucidate the relationships between TPE binders, surface morphology, and electrochemistry. Scanning electrochemical microscopy (SECM) is a powerful tool for measuring localized electrochemical behavior at an electrode interface and has been used previously to characterize TPEs with non-aromatic binders.[29] SECM can be used to measure localized electrochemistry of different PS and PS-PCL TPEs and correlate surface features with electrode kinetics for redox molecules of interest.[29] To better understand the impacts of the different conductive carbon fillers on PS TPEs further characterization should also be performed on the conductive carbons and TPEs used in this thesis. X-ray photoelectron spectroscopy (XPS) can be used to characterize surface oxides and Raman spectroscopy can probe the disorder and exfoliation of graphite for carbon electrode materials.[6, 30] The different conductive carbon particles can also be imaged with SEM by themselves and imaged incorporated into TPEs.

In addition to further characterization of PS TPE materials, surface pre-treatments can be characterized as well to determine their impact on PS TPEs. In this thesis, 600 grit sandpaper polishing was the only surface pre-treatment used for PS TPEs. However, characterizing other polishing methods, such as lower grit sandpaper or micro-fiber polishing pads could provide insights into how morphology impacts performance, which could be useful to further improve

detection of biomarkers.[6, 31] Anodic and cathodic surface treatments could also impact the surface chemistry and morphology, and be used to enhance voltammetry for biomarker detection.[32-34] To improve DA detection in the presence of AA and UA specifically, more surface oxides could prove beneficial for electrostatic reasons as DA is positively charged at physiological pH.[35] More surface oxides can be achieved through the conductive carbon filler or surface treatment used. As PS TPEs have proven useful for simultaneous determination, in the future they can be applied to other redox active analytes as well.

Due to the excellent moldability of TPEs, in the future the materials and sensors discussed in this work can be incorporated small volume and/or fluidic devices to improve sensor performance further. Electrode dimensions can also be reduced to improve detection limits for both direct and immunoassay detection of biomarkers. Electrochemical detection in small volumes with microelectrodes can exhibit improved sensitivity compared to large electrode / volume measurements.[7] Fluidic devices can be used to increase analyte transport to electrode surfaces, to pre-process difficult sample matrices, or to automate assay steps, so the ease of incorporation of TPEs into fluidic devices is extremely beneficial. [15, 20-22, 36]

In summary, this thesis focused on electrochemical detection of biomarkers and contributes to the field through the development and characterization of new TPE materials and modifications for detection of protein and small molecule biomarkers. Firstly, synthesis and grafting of diazonium tosylates was optimized for TPEs and used as a novel functionalization method for the first TPE immunosensors. Then PS plastics were explored as the first aromatic binders for TPEs. PS TPEs exhibited unique edge-plane rich morphology and exceptional voltammetry for biologically relevant redox molecules. Lastly, unmodified PS TPEs were used successfully for simultaneous direct detection of important small molecule biomarkers: AA, DA, and UA. Overall,

this thesis has furthered knowledge related to TPE composite materials and how binder choice, conductive carbon type, and surface modifications can impact detection of biomarkers. The TPE immunosensors, and electrode materials developed in this thesis are also quite versatile and can easily be adapted for a wider range of biomarkers and applications.

REFERENCES

1. Bernabé-Ortiz, A.; Zafra-Tanaka, J. H.; Moscoso-Porras, M.; Sampath, R.; Vetter, B.; Miranda, J. J.; Beran, D., Diagnostics and monitoring tools for noncommunicable diseases: a missing component in the global response. *Globalization and Health* **2021,** *17* (1), 1-5.

2. Kumar, S.; Nehra, M.; Khurana, S.; Dilbaghi, N.; Kumar, V.; Kaushik, A.; Kim, K.-H., Aspects of point-of-care diagnostics for personalized health wellness. *International journal of nanomedicine* **2021,** *16*, 383.

3. Campuzano, S.; Pedrero, M.; Yáñez-Sedeño, P.; Pingarrón, J. M., New challenges in Point of Care electrochemical detection of clinical biomarkers. *Sensors and Actuators B: Chemical* **2021**, 130349.

4. Morais, A. L.; Rijo, P.; Batanero Hernan, M. B.; Nicolai, M., Biomolecules and Electrochemical Tools in Chronic Non-Communicable Disease Surveillance: A Systematic Review. *Biosensors* **2020,** *10* (9), 121.

5. Noviana, E.; McCord, C. P.; Clark, K. M.; Jang, I.; Henry, C. S., Correction: Electrochemical paper-based devices: sensing approaches and progress toward practical applications. *Lab Chip* **2020,** *20* (1), 185-185.

6. Klunder, K. J.; Nilsson, Z.; Sambur, J. B.; Henry, C. S., Patternable Solvent-Processed Thermoplastic Graphite Electrodes. *J. Am. Chem. Soc.* **2017,** *139* (36), 12623-12631.

7. Ricci, F.; Adornetto, G.; Palleschi, G., A review of experimental aspects of electrochemical immunosensors. *Electrochimica Acta* **2012,** *84*, 74-83.

8. Cao, M.; Fu, A.; Wang, Z.; Liu, J.; Kong, N.; Zong, X.; Liu, H.; Gooding, J. J., Electrochemical and theoretical study of π–π stacking interactions between graphitic surfaces and pyrene derivatives. *The Journal of Physical Chemistry C* **2014,** *118* (5), 2650-2659.

9. Srisombat, L.; Jamison, A. C.; Lee, T. R., Stability: A key issue for self-assembled monolayers on gold as thin-film coatings and nanoparticle protectants. *Colloids and Surfaces A: Physicochemical and Engineering Aspects* **2011,** *390* (1-3), 1-19.

10. Klunder, K. J.; Clark, K. M.; McCord, C.; Berg, K. E.; Minteer, S. D.; Henry, C. S., Polycaprolactone-enabled sealing and carbon composite electrode integration into electrochemical microfluidics. *Lab Chip* **2019,** *19* (15), 2589-2597.

11. Via, G. G.; Shugart, C. L.; Melnyk, S. L.; Hupman, S. R.; Cline, K. K., One-step Solvent-free Synthesis and Grafting of Diazonium Ions at Glassy Carbon Electrodes. *Electroanalysis* **2018,** *30* (10), 2421-2426.

12. Filimonov, V. D.; Trusova, M.; Postnikov, P.; Krasnokutskaya, E. A.; Lee, Y. M.; Hwang, H. Y.; Kim, H.; Chi, K.-W., Unusually stable, versatile, and pure arenediazonium tosylates: their preparation, structures, and synthetic applicability. *Organic letters* **2008,** *10* (18), 3961-3964.

13. Huang, Y.; Gulshan, K.; Nguyen, T.; Wu, Y. P., Biomarkers of Cardiovascular Disease. *Dis. Markers* **2017**, 2.

14. Daniels, J. S.; Pourmand, N., Label-free impedance biosensors: Opportunities and challenges. *Electroanalysis* **2007,** *19* (12), 1239-1257.

15. Dong, H.; Li, C.-M.; Zhang, Y.-F.; Cao, X.-D.; Gan, Y., Screen-printed microfluidic device for electrochemical immunoassay. *Lab Chip* **2007,** *7* (12), 1752-1758.

16. Punyadeera, C.; Dimeski, G.; Kostner, K.; Beyerlein, P.; Cooper-White, J., One-step homogeneous C-reactive protein assay for saliva. *Journal of Immunological Methods* **2011,** *373* (1-2), 19-25.

17. Zhang, X.; Karunathilaka, N.; Senanayake, S.; Subramaniam, V. N.; Chan, W.; Kostner, K.; Fraser, J.; Atherton, J. J.; Punyadeera, C., The potential prognostic utility of salivary galectin-3 concentrations in heart failure. *Clin Res Cardiol* **2020,** *109* (6), 685-692.

18. Zhang, X.; Broszczak, D.; Kostner, K.; Guppy-Coles, K. B.; Atherton, J. J.; Punyadeera, C., Salivary Protein Panel to Diagnose Systolic Heart Failure. *Biomolecules* **2019,** *9* (12), 766.

19. Pedrero, M.; Campuzano, S.; Pingarron, J. M., Electrochemical Biosensors for the Determination of Cardiovascular Markers: a Review. *Electroanalysis* **2014,** *26* (6), 1132-1153.

20. Noiphung, J.; Nguyen, M. P.; Punyadeera, C.; Wan, Y.; Laiwattanapaisal, W.; Henry, C. S., Development of Paper-Based Analytical Devices for Minimizing the Viscosity Effect in Human Saliva. *Theranostics* **2018,** *8* (14), 3797-3807.

21. Noviana, E.; Klunder, K. J.; Channon, R. B.; Henry, C. S., Thermoplastic Electrode Arrays in Electrochemical Paper-Based Analytical Devices. *Analytical Chemistry* **2019,** *91* (3), 2431-2438.

22. Pradela-Filho, L. A.; Noviana, E.; Araujo, D.; Takeuchi, R.; Santos, A.; Henry, C. S., Rapid Analysis in Continuous Flow Electrochemical Paper-Based Analytical Devices. *ACS Sens.* **2020**.

23. Kaya, S. I.; Kurbanoglu, S.; Ozkan, S. A., Nanomaterials-based nanosensors for the simultaneous electrochemical determination of biologically important compounds: ascorbic acid, uric acid, and dopamine. *Crit. Rev. Anal. Chem.* **2019,** *49* (2), 101-125.

24. Baig, N.; Rana, A.; Kawde, A. N., Modified electrodes for selective voltammetric detection of biomolecules. *Electroanalysis* **2018,** *30* (11), 2551-2574.

25. Zhang, L.; Liu, C.; Wang, Q.; Wang, X.; Wang, S., Electrochemical sensor based on an electrode modified with porous graphitic carbon nitride nanosheets (C 3 N 4) embedded in graphene oxide for simultaneous determination of ascorbic acid, dopamine and uric acid. *Microchim. Acta* **2020,** *187* (2), 1-10.

26. Minta, D.; González, Z.; Wiench, P.; Gryglewicz, S.; Gryglewicz, G., N-Doped Reduced Graphene Oxide/Gold Nanoparticles Composite as an Improved Sensing Platform for Simultaneous Detection of Dopamine, Ascorbic Acid, and Uric Acid. *Sensors* **2020,** *20* (16), 4427.

27. Kunpatee, K.; Traipop, S.; Chailapakul, O.; Chuanuwatanakul, S., Simultaneous determination of ascorbic acid, dopamine, and uric acid using graphene quantum dots/ionic liquid modified screen-printed carbon electrode. *Sensors and Actuators B: Chemical* **2020,** *314*, 128059.

28. Liu, X.; Liu, J., Biosensors and sensors for dopamine detection. *View* **2021,** *2* (1), 20200102.

29. Berg, K. E.; Leroux, Y. R.; Hapiot, P.; Henry, C. S., SECM Investigation of Carbon Composite Thermoplastic Electrodes. *Analytical Chemistry* **2020,** *93* (3), 1304-1309.

30. McCreery, R. L., Advanced carbon electrode materials for molecular electrochemistry. *Chem. Rev.* **2008,** *108* (7), 2646-2687.

31. Kamau, G., Surface preparation of glassy carbon electrodes. *Anal. Chim. Acta* **1988,** *207*, 1-16.

32. Musameh, M.; Lawrence, N. S.; Wang, J., Electrochemical activation of carbon nanotubes. *Electrochemistry Communications* **2005,** *7* (1), 14-18.

33. Rice, M. E.; Galus, Z.; Adams, R. N., GRAPHITE PASTE ELECTRODES - EFFECTS OF PASTE COMPOSITION AND SURFACE-STATES ON ELECTRON-TRANSFER RATES. *Journal of Electroanalytical Chemistry* **1983,** *143* (1-2), 89-102.

34. Gyan, I. O.; Wojcik, P. M.; Aston, D. E.; McIlroy, D. N.; Cheng, I. F., A Study of the Electrochemical Properties of a New Graphitic Material: GUITAR. *Chemelectrochem* **2015,** *2* (5), 700-706.

35. Wang, L.; Yang, R.; Qu, L.; Harrington, P. d. B., Electrostatic repulsion strategy for high-sensitive and selective determination of dopamine in the presence of uric acid and ascorbic acid. *Talanta* **2020,** *210*, 120626.

36. Channon, R. B.; Yang, Y. Y.; Feibelman, K. M.; Geiss, B. J.; Dandy, D. S.; Henry, C. S., Development of an Electrochemical Paper-Based Analytical Device for Trace Detection of Virus Particles. *Analytical Chemistry* **2018,** *90* (12), 7777-7783.

APPENDIX 1: CHARACTERIZATION OF PCL-PMMA TPEs

Prior to performing the work described in Chapter 2, the properties of TPEs with different binder material compositions were tested. The goal was to improve PCL TPE properties while still being able to heat press material dry. PMMA TPEs have higher conductivity and lower capacitance than PCL TPEs which are beneficial properties for electrochemical sensors, however PMMA needs to be solvent processed due to its higher melting point whereas PCL can be processed dry.[1-2] Solvent processing TPE materials can lead to issues when too much or too little organic solvent is still present, such as the formation of gaps or cracks in the material.[1] Thus blending the two polymers was investigated to see if adding PMMA to PCL TPEs could improve properties while maintaining the ability to dry press materials.

All TPEs in this appendix were 2.5 mm disks made as described in Chapter 2 with MG1599 graphite but with different binder compositions (PCL, 2:1 PCL:PMMA, and 1:1 PCL:PMMA). Conductivity and capacitance tests were performed as described in Chapter 3 and 4. 5 mM ferri/ferrocyanide ($Fe(CN)6^{3-/4}$) was made in 0.1 M KNO_3 and rate constants (k_0) for ferri/ferrocyanide were determined using the Nicholson method, and higher k_0 corresponds to faster charge transfer at the electrode surface.[3] Data for the three experiments is shown in Fig. S1.1. Conductivity increased as PMMA content increased, the k_0 values were similar for the three TPE types but slightly higher for 2:1 PCL:PMMA, and capacitance decreased when PMMA content increased. For Chapter 2, 2:1 PCL:PMMA was used as the TPE binder. Although 1:1 had higher conductivity, 1:1 was significantly harder to heat press dry, had a lower rate constant, and higher variability for capacitance.

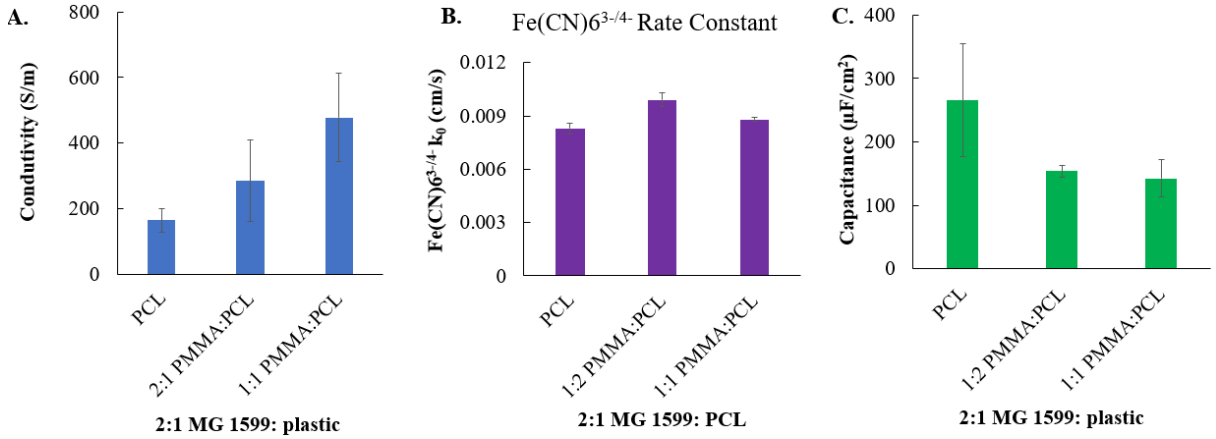

Fig S1.1. Characterization of 2:1 MG1599 graphite: plastic with PCL, 2:1 PCL:PMMA, and 1:1 PCL:PMMA TPE binders. A) Conductivity data, B) k_0 rate constant data, and C) capacitance data.

REFERENCES

1. Klunder, K. J.; Clark, K. M.; McCord, C.; Berg, K. E.; Minteer, S. D.; Henry, C. S., Polycaprolactone-enabled sealing and carbon composite electrode integration into electrochemical microfluidics. *Lab Chip* **2019,** *19* (15), 2589-2597.

2. Klunder, K. J.; Nilsson, Z.; Sambur, J. B.; Henry, C. S., Patternable Solvent-Processed Thermoplastic Graphite Electrodes. *J. Am. Chem. Soc.* **2017,** *139* (36), 12623-12631.

3. Nicholson, R. S., Theory and application of cyclic voltammetry for measurement of electrode reaction kinetics. *Analytical chemistry* **1965,** *37* (11), 1351-1355.

APPENDIX 2: SUPPLEMENTARY INFORMATION FOR CHAPTER 2

S2.1 Impact of pre-ground p-nitroaniline modified electrode voltammetry

Diazonium pastes used to modify the 1 mm diameter array electrodes were synthesized with un-ground p-nitroaniline crystals and with p-nitroaniline pre-ground to a fine powder with a mortar and pestle. Cyclic voltammograms were taken before and after modification.

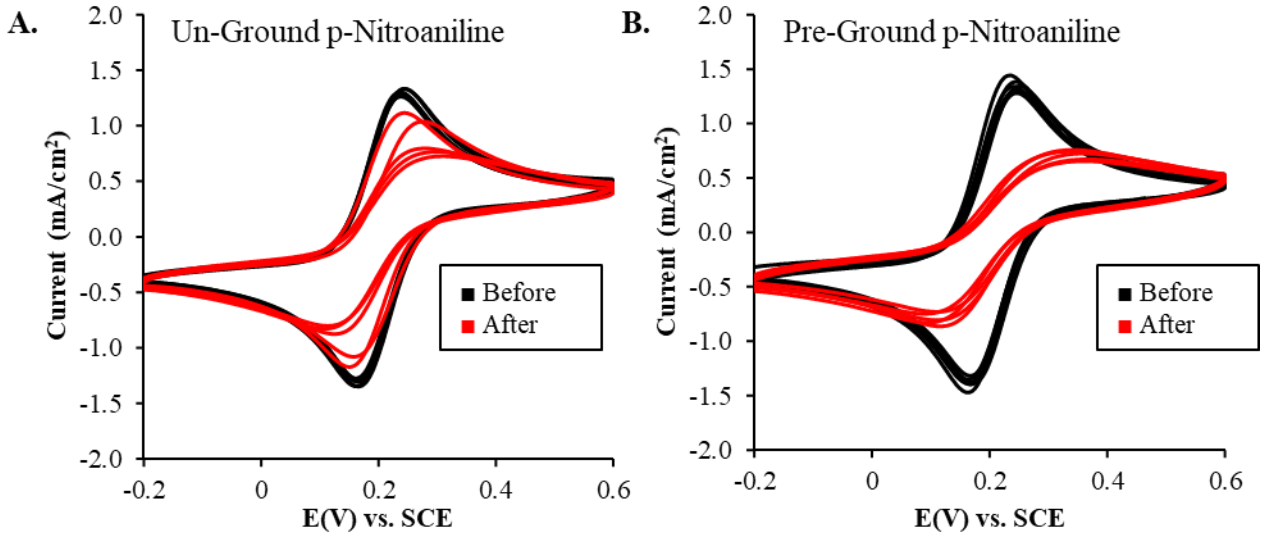

Figure S2.1. Cyclic voltammetry for 5 mM ferri/ferrocyanide in PBS on 1 mm diameter electrode arrays v=100 mV/s before and after modification with p-aminophenyl diazonium paste.

S2.2 Cyclic voltammetry of the different electrode pre-treatments

Cathodic pre-treatments were performed at -1.5 V vs. SCE for 30 seconds in 0.1 M sulfuric acid to reduce electrode surfaces. Anodic pre-treatments were performed at +1.5 V vs. SCE for 30 seconds in 0.1 M sodium hydroxide to oxidize electrode surfaces. Sanded electrodes were modified as is following 600 grit sandpaper. Cyclic voltammetry of the modified electrodes is shown in Fig. S2.3.

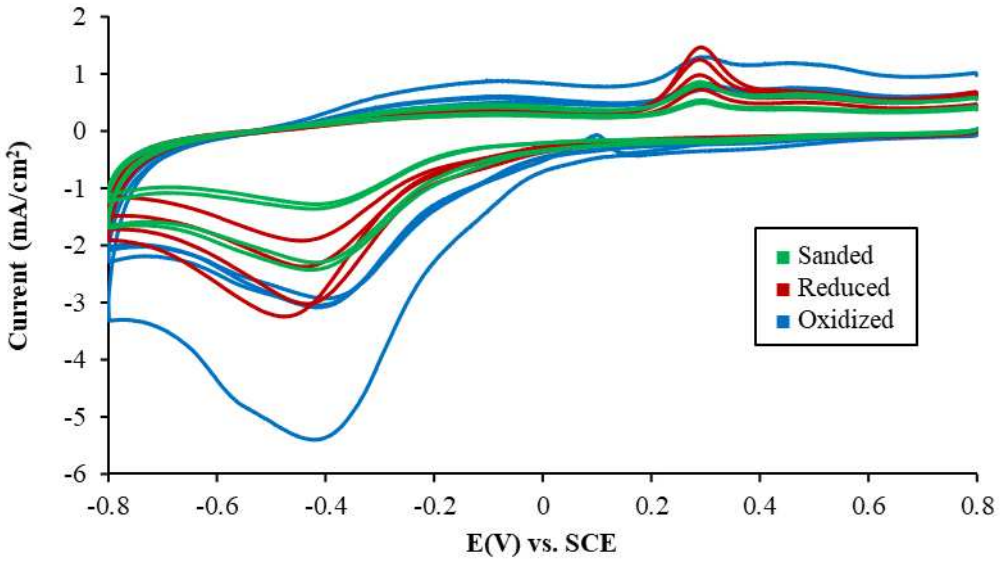

Figure S2.2. Cyclic voltammetry for N_2 degassed 0.1 M H_2SO_4 on p-nitrophenyl diazonium salt modified 2.5 mm diameter disk electrodes v=100 mV/s.

S2.3 Coverage and capacitance data for p-nitrophenyl modified electrodes

2.5 mm diameter disk electrodes and 1 mm diameter array electrodes were modified with p-aminophenyl diazonium salt using either single recipe 0.2 mmol p-nitroaniline (PN) paste or triple recipe 0.6 mmol paste with un-ground or pre-ground PN. Before and after modification, capacitance measurements were taken with cyclic voltammetry from 0.15 to 0 V vs. SCE v=100 mV/s in N_2 degassed 0.1 M H_2SO_4. The capacitance was calculated using the following equation:

$$C = \left(\frac{|I_a|+|I_c|}{(2v)A}\right)$$

where C is the geometric area-normalized capacitance, v is the scan rate (V/s), I_a is the anodic current and I_c is the cahodic current at 0.1 V vs. SCE, and A is the geometric surface area of the electrode. Following capacitance measurements, cyclic voltammograms were taken of the modified electrodes from 0.8 to -0.8 V vs. SCE v=100 mV/s in N_2 degassed 0.1 M H_2SO_4 to calculate surface nitrophenyl coverage.

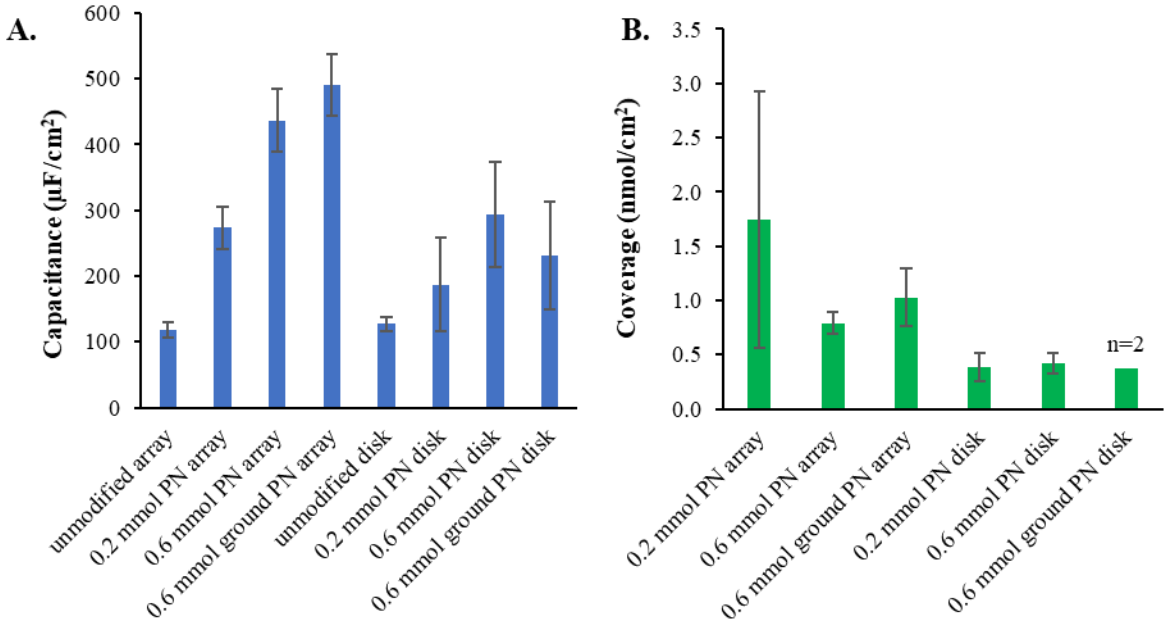

Figure S2.3. Data for unmodified and p-nitrophenyl diazonium salt modified electrodes for A) capacitance (n=4), and B) nitrophenyl coverage (n=4).

S2.4 Cyclic voltammetry of p-aminophenyl and p-nitrophenyl diazonium salt modified electrodes

p-Aminophenyl diazonium salt pastes were synthesized with both 1:1 and 3:2 p-phenylenediamine sodium nitrite ratios and used to modify 2.5 mm diameter disk electrodes. The voltammetry of the aminophenyl modified electrodes were compared to that of p-nitrophenyl diazonium salt modified electrodes as shown in Fig. S2.5.

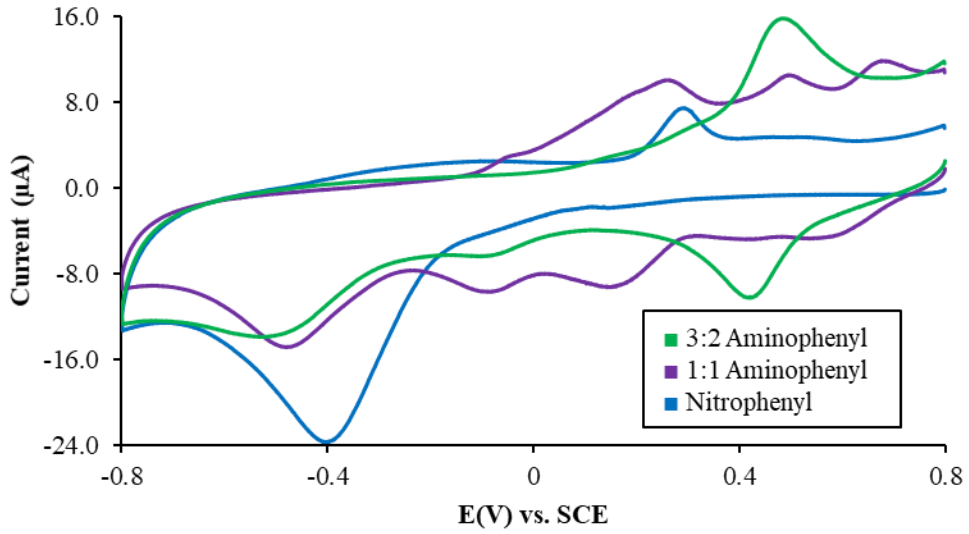

Fig. S2.4. Cyclic voltammetry for N_2 degassed 0.1 M H_2SO_4 on p-nitrophenyl and p-aminophenyl diazonium salt modified 2.5 mm diameter disk electrodes v=100 mV/s.

S2.5 Four-Parameter Logistic (4-PL) Regressions

To fit the CRP ELISA data, 4-PL logistic fits were calculated using MATLAB 2020a using L4P and L4Pinv code sourced from Giuseppe Cardillo:

Cardillo G. (2012) Four parameters logistic regression - There and back again https://it.mathworks.com/matlabcentral/fileexchange/38122

The 4-PL fits for PN, PPD, and PPD in serum are listed below:

General model: cf(x) = D+(A-D)/(1+(x/C)^B)

PN 4-PL: 0.1-10000 ng/mL

Coefficients (with 95% confidence bounds):

A = 16.19 (1.801, 30.57)

B = 0.6628 (0.2096, 1.116)

C = 120.2 (-7.422, 247.8)

D = 131.9 (106.5, 157.3)

R^2=0.9978

PPD 4-PL: 0.1-10000 ng/mL

Coefficients (with 95% confidence bounds):

A = 39.07 (1.408, 76.73)

B = 0.8874 (-0.02673, 1.802)

C = 52.53 (-14.9, 120)

D = 227 (184.1, 269.9)

R^2=0.9943

PPD 4-PL: 0-1000 ng/mL

Coefficients (with 95% confidence bounds):

A = 52.12 (20.73, 83.5)

B = 0.9139 (-0.3075, 2.135)

C = 32.61 (-28.99, 94.2)

D = 181.1 (124, 238.1)

R^2=0.9993

APPENDIX 3: SUPPLEMENTARY INFORMATION FOR CHAPTER 3

S3.1 OP data for all TPE types

Table S3.1. Quantitative OP roughness data for TPEs.

Binder	RMS Roughness (nm)	Roughness Ratio (Binder/45K PS)
45K PS	578.501	1
PS-PCL	848.45	1.466635
PCL	1464.35	2.531283
192K PS	450.718	0.779114
350K PS	580.247	1.003018
EPS	553.69	0.957112

S3.2 SEM data for different PS binders: 192K PS, 350K PS, and EPS

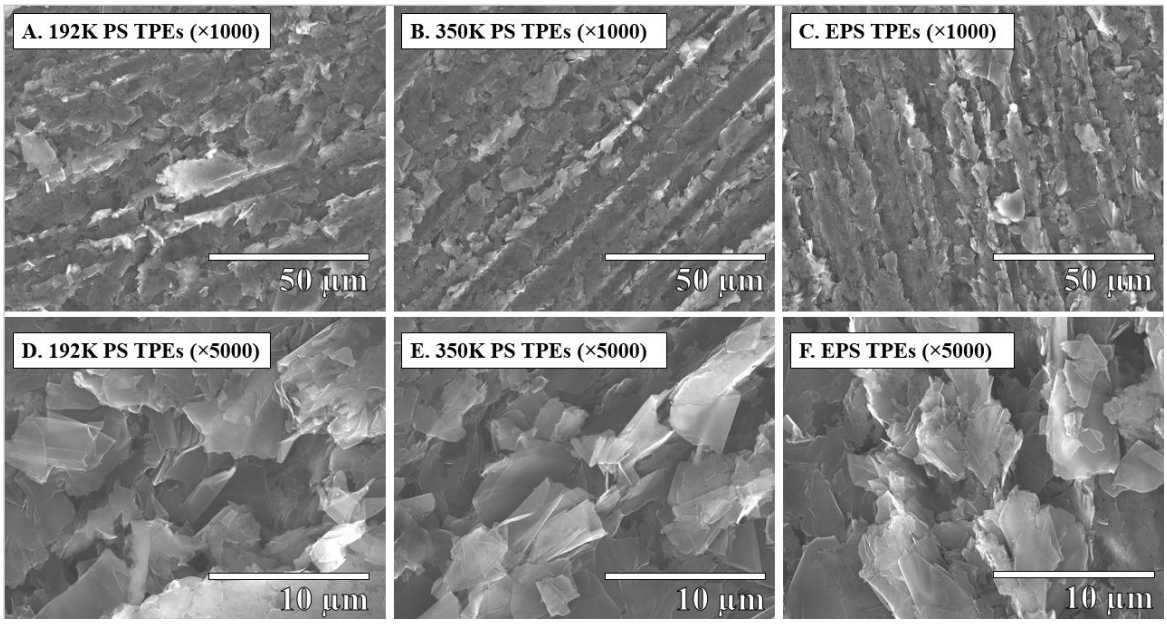

Fig. S3.2. 15.0 kV SEM images of 2:1 graphite: plastic TPEs at ×1000 for A) 192K PS, B) 350K PS, and C) EPS binders; ×5000 for D) 192K PS, E) 350K PS, and F) EPS.

S3.3 Quantitative cyclic voltammetry data for p-aminophenol at pH 5, 7.4, and 9

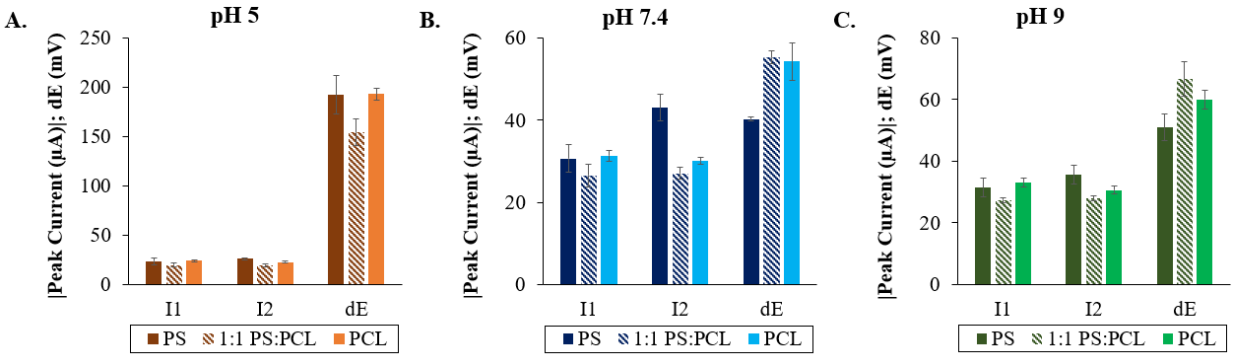

Fig. S3.3. Quantitative pH study CV data of 1 mM p-aminophenol v=100 mV/s on 45K PS, 1:1 PS:PCL, and PCL TPEs (n=3) in A) B) 0.1 M MES buffer pH=5, C) 0.1 M PBS buffer pH=7.4, and D) 0.1 M Tris-HCl pH=9.

S3.4 Uric acid voltammetry for PS, PS-PCL, and PCL TPEs

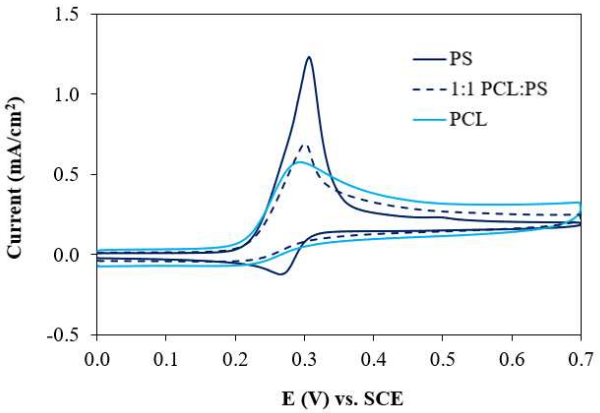

Fig. S3.4. Averaged CVs of 1 mM uric acid in PBS (n=3) v=100 mV/s on 45K PS, 1:1 PS:PCL, and PCL TPEs

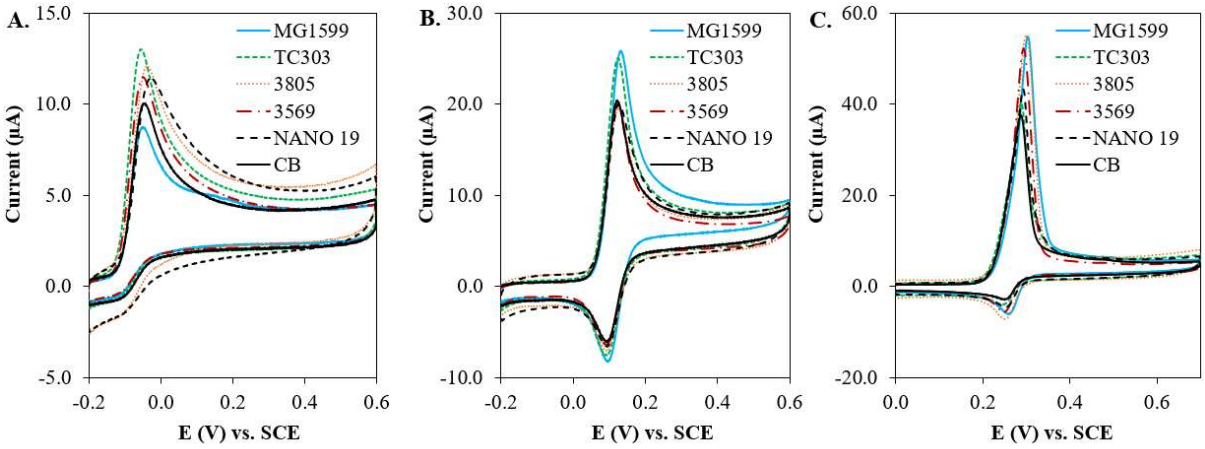

Fig. S4.1. Single analyte CV (v=100 mV/s) of AA, DA, and UA on different carbon types in PBS. A) 0.5 mM AA, B) 0.5 mM DA, and C) 0.5 mM UA.